

Frequency domain based performance optimization of systems with static nonlinearities

Citation for published version (APA):

Rijlaarsdam, D. J. (2012). *Frequency domain based performance optimization of systems with static nonlinearities*. [Phd Thesis 1 (Research TU/e / Graduation TU/e), Mechanical Engineering]. Technische Universiteit Eindhoven. <https://doi.org/10.6100/IR732581>

DOI:

[10.6100/IR732581](https://doi.org/10.6100/IR732581)

Document status and date:

Published: 01/01/2012

Document Version:

Publisher's PDF, also known as Version of Record (includes final page, issue and volume numbers)

Please check the document version of this publication:

- A submitted manuscript is the version of the article upon submission and before peer-review. There can be important differences between the submitted version and the official published version of record. People interested in the research are advised to contact the author for the final version of the publication, or visit the DOI to the publisher's website.
- The final author version and the galley proof are versions of the publication after peer review.
- The final published version features the final layout of the paper including the volume, issue and page numbers.

[Link to publication](#)

General rights

Copyright and moral rights for the publications made accessible in the public portal are retained by the authors and/or other copyright owners and it is a condition of accessing publications that users recognise and abide by the legal requirements associated with these rights.

- Users may download and print one copy of any publication from the public portal for the purpose of private study or research.
- You may not further distribute the material or use it for any profit-making activity or commercial gain
- You may freely distribute the URL identifying the publication in the public portal.

If the publication is distributed under the terms of Article 25fa of the Dutch Copyright Act, indicated by the "Taverne" license above, please follow below link for the End User Agreement:

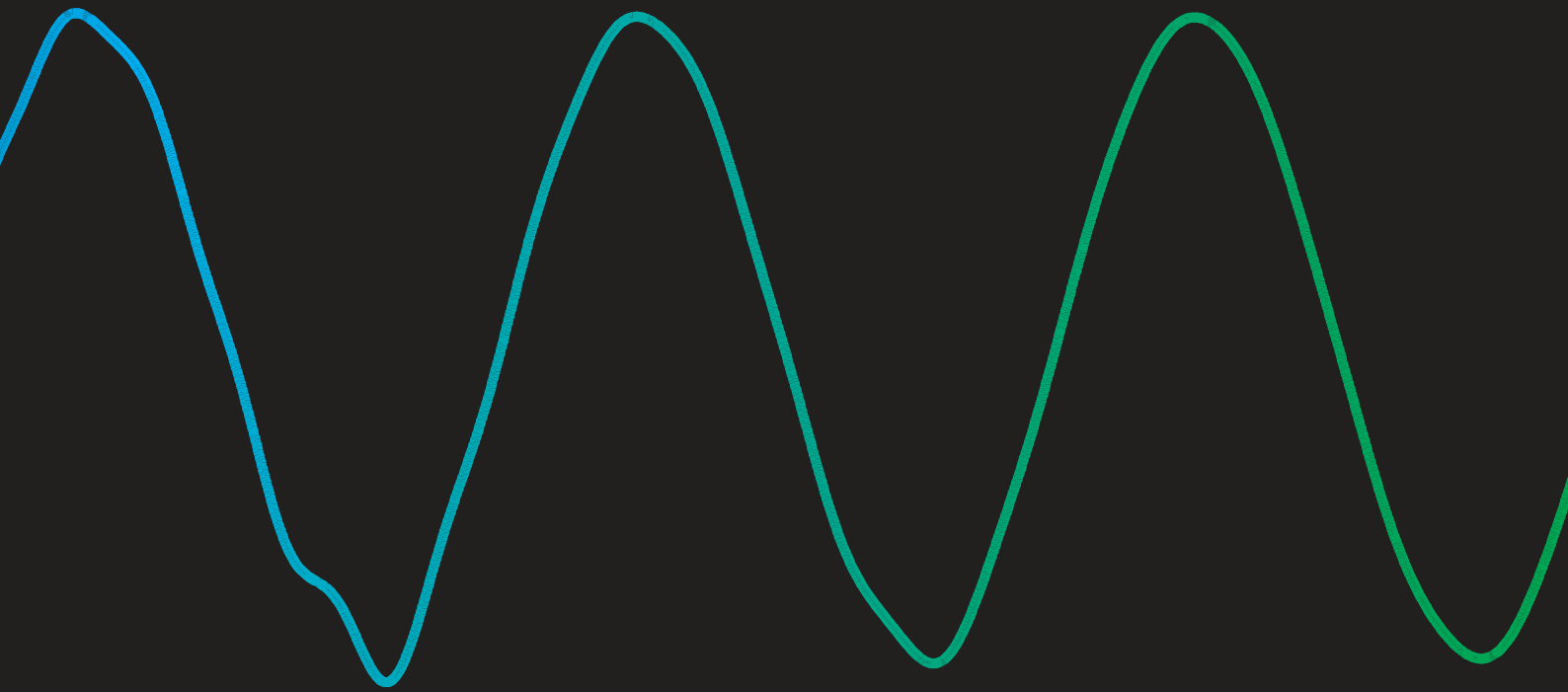
www.tue.nl/taverne

Take down policy

If you believe that this document breaches copyright please contact us at:

openaccess@tue.nl

providing details and we will investigate your claim.



frequency domain based performance
optimization of systems with
static nonlinearities

David Rijlaarsdam

Frequency Domain Based Performance
Optimization of Systems with
Static Nonlinearities



The research reported in this thesis is carried out as part of the Condor project, a project under the supervision of the Embedded Systems Institute (ESI) with FEI Company as the industrial partner. This project is partially supported by the Dutch Ministry of Economic Affairs under the BSIK program. This work was supported in part by the Fund for Scientific Research (FWO-Vlaanderen), by the Flemish Government (Methusalem), and by the Belgian Government through the Interuniversity Poles of Attraction (IAP VI/4) Program.



The research reported in this thesis is part of a dual PhD program, a cooperation between the Eindhoven University of Technology (department of Mechanical Engineering), Eindhoven, The Netherlands and the Vrije Universiteit Brussel (department of Fundamental Electricity and Instrumentation), Brussels, Belgium.

disc

The research reported in this thesis is part of the research program of the Dutch Institute of Systems and Control (DISC). The author has successfully completed the educational program of the Graduate School DISC.

Frequency Domain Based Performance Optimization of Systems with Static Nonlinearities
by David Rijlaarsdam – Eindhoven University of Technology, 2012 – PhD thesis.

A catalogue record is available from the Eindhoven University of Technology Library.
ISBN: 978-90-386-3149-3

Reproduction: Ipskamp Drukkers B.V., Enschede, The Netherlands.
Cover design: Sonja van der Meer and Djoya Hattu.

Copyright ©2012 by D.J. Rijlaarsdam. All rights reserved.

Frequency Domain Based Performance Optimization of Systems with Static Nonlinearities

PROEFSCHRIFT

ter verkrijging van de graad van doctor
aan de Technische Universiteit Eindhoven,
op gezag van de rector magnificus, prof.dr.ir. C.J. van Duijn,
voor een commissie aangewezen door het College voor Promoties
in het openbaar te verdedigen
op donderdag 21 juni om 16.00 uur

door

David Jan Rijlaarsdam

geboren te Leiden

Dit proefschrift is goedgekeurd door de promotoren:

prof.dr.ir. M. Steinbuch

en

prof.dr.ir. J. Schoukens

Copromotor:

dr.ir. P.W.J.M. Nuij

Contents

| | | |
|----------|--|-----------|
| 1 | Introduction and preliminaries | 1 |
| 1.1 | Introduction | 1 |
| 1.2 | Nomenclature and preliminaries | 7 |
| 2 | Frequency domain methods for nonlinear systems | 11 |
| 2.1 | Volterra series based approaches | 13 |
| 2.2 | Nonlinear frequency response function and Bode plot | 16 |
| 2.3 | Describing functions | 19 |
| 2.4 | Linear approximation in the presence of nonlinearities | 24 |
| 2.5 | Comparison | 30 |
| 3 | Frequency domain analysis of block structured nonlinear systems | 37 |
| 3.1 | Frequency domain analysis of polynomial nonlinearities | 38 |
| 3.2 | Connecting different frequency domain representations | 45 |
| 4 | Frequency domain based nonlinearity detection and compensation | 53 |
| 4.1 | Frequency domain performance | 54 |
| 4.2 | Numerical examples | 60 |
| 4.3 | Conclusions | 66 |
| 5 | Frequency domain based feed forward friction compensation | 69 |
| 5.1 | From analysis to application | 70 |
| 5.2 | Friction compensation in a TEM | 76 |
| 5.3 | Frequency domain based performance in practice | 80 |
| 5.4 | Conclusions | 82 |
| 6 | Conclusions and recommendations | 85 |
| 6.1 | Conclusions | 85 |
| 6.2 | Recommendations | 87 |

| | |
|--|------------|
| Appendix | 89 |
| A Proofs | 91 |
| A.1 Proofs in Chapter 3 | 91 |
| A.2 Proofs in Chapter 4 | 92 |
| B Additional results | 95 |
| B.1 Computation of the BLA and signal processing | 95 |
| B.2 Statistics | 96 |
| Bibliography | 99 |
| Summary | 107 |
| Samenvatting | 109 |
| Dankwoord | 111 |
| List of Publications | 113 |
| Curriculum Vitae | 115 |

Abbreviations

| abbreviation | description | reference |
|---------------------|---|------------------|
| BLA | Best Linear Approximation | p. 25 |
| DF | Describing Function | p. 19 |
| FRF | Frequency Response Function | p. 11 |
| GDF | Generalized Describing Function | p. 19 |
| GFRF | Generalized Frequency Response Function | p. 14 |
| HOSIDF | Higher Order Sinusoidal Input Describing Function | p. 22 |
| LTI | Linear and Time Invariant | p. 2 |
| N(O/S)FRF | Nonlinear (Output / State) Freq. Resp. Function | p. 16 |
| SIDF | Sinusoidal Input Describing Function | p. 19 |

List of Symbols

| symbol | definition | reference |
|------------------------------|--|-----------|
| α | vector of polynomial coefficients $\alpha = [\alpha_1, \alpha_2, \dots, \alpha_p]^T$ | p. 39 |
| Γ | input gain matrix | p. 39 |
| γ | amplitude of sinusoidal signal | p. 9 |
| δ | Dirac delta function | p. 39 |
| ϵ | time domain based performance measure | p. 73 |
| ζ | frequency domain based performance measure | p. 74 |
| κ | set of controller parameters | p. 58 |
| Λ | expansion matrix | p. 47 |
| ξ | frequency (in Hz) | p. 8 |
| ξ_0 | frequency of sinusoidal signal | p. 9 |
| ϖ_p | set of frequencies $\varpi = \{\xi_1, \xi_2, \dots, \xi_p\}$ | p. 46 |
| ϖ_P | collection of frequency sets $\varpi_P = \{\varpi_1, \varpi_2, \dots, \varpi_P\}$ | p. 47 |
| $\Upsilon, \check{\Upsilon}$ | gain compensation matrix | p. 42 |
| $\Phi, \check{\Phi}$ | input phase matrix | p. 39 |
| ϕ | static nonlinear mapping | p. 55 |
| φ_0 | phase of sinusoidal signal | p. 9 |
| χ | static nonlinear compensator | p. 59 |
| $\Omega, \check{\Omega}$ | inter-harmonic gain matrix | p. 39 |
| | <i>continued on next page</i> | |

| symbol | definition | reference |
|---------------------------|--|-----------|
| \mathbb{B}_p | space of piecewise continuous, bounded functions | p. 7 |
| \mathfrak{B}_u | best linear approximation | p. 25 |
| $\overline{\mathcal{CS}}$ | class of uniformly convergent systems | p. 16 |
| \mathfrak{D}_S | sinusoidal input describing function | p. 21 |
| \mathfrak{D}_G | generalized describing function | p. 21 |
| \mathfrak{F}_p | fundamental HOSIDF of order p | p. 42 |
| \mathfrak{G} | nonlinear Bode plot | p. 18 |
| \mathbf{G} | set of Gaussian signals | p. 8 |
| \mathbf{G}_{eq} | set of Gaussian equivalent signals | p. 26 |
| \mathfrak{H}_k | higher order sinusoidal input describing function of order k | p. 22 |
| h_p | Volterra kernel of order p | p. 14 |
| \mathbf{M} | set of multisine signals | p. 9 |
| \mathcal{N}_F | Fourier transform of stochastic output distortion | p. 25 |
| \aleph | frequency domain based performance measure | p. 58 |
| $\mathfrak{N}_{S/O}$ | nonlinear output / state frequency response function | p. 17 |
| \mathcal{S}_{Fu} | Fourier transform of distortion due to nonlinearities | p. 8 |
| S_u | power density spectrum of u | p. 8 |
| $\mathbf{S}_{(\xi_0)}$ | set of sinusoidal signals (with frequency ξ_0) | p. 9 |
| \mathfrak{T}_p | generalized frequency response function of order p | p. 14 |
| u | input signal | p. 38 |
| $\overline{\mathbf{VS}}$ | class of Volterra systems | p. 14 |
| $\overline{\mathbf{WS}}$ | class of special Wiener systems | p. 26 |
| w | input signal | p. 7 |
| x | state vector | p. 7 |
| x_w | solution corresponding to input w | p. 7 |
| \bar{x}_w | limit / steady state solution corresponding to input w | p. 7 |
| y | output signal | p. 7 |
| \bar{y}_w | output corresponding to limit / steady state solution | p. 7 |
| \mathcal{Y}_F | Fourier transform of y | p. 8 |
| \mathcal{Y} | single sided spectrum of y | p. 8 |
| Y | vector containing spectral components $Y[\ell] = \mathcal{Y}((\ell - 1)\xi_0)$ | p. 39 |

Chapter 1

Introduction and Preliminaries

1.1 Introduction

Increasing performance requirements on high performance (motion) systems require novel techniques to deal with performance degrading effects. In contrast to the large amount of results and methods that deal with linear effects, this thesis focuses on the detection, analysis and optimal compensation of performance degrading nonlinear effects. Although systems may be specifically designed to minimize nonlinear effects (e.g. waferscanners), nonlinearities such as magnetic fields may be inherently present in the design. In particular, some applications require the presence of nonlinear effects such as friction in the motion stage of an electron microscope.

Whether performance is measured by speed, accuracy, reproducibility, smoothness, or other performance measures, the effects of nonlinearities become increasingly important in high precision applications. To accurately detect, analyze and compensate performance degrading effects in controlled nonlinear dynamical systems, practically applicable tools are required. The research presented in this thesis contributes to this field by introducing new frequency domain based analysis, modeling and performance optimization techniques for nonlinear systems. By extending frequency domain techniques used for the analysis and control of linear systems, a new, well defined notion of performance for a class of nonlinear systems is presented. This yields novel methods to analyze, visualize and optimally compensate performance degrading nonlinear effects in dynamical systems. The results are accompanied by an industrial case study of optimal friction compensation in a transmission electron microscope moving at 20 billionths of a meter per second (a speed at which it would take you over 1.5 years to slide over to the seat next to you).

In the following, the motivation for the application of frequency domain methods to nonlinear systems is discussed first. Specifically, the concepts which make frequency domain methods so successful for linear systems are used to illustrate the issues arising when such methods are extended to nonlinear systems. Based on this

motivation the research objectives and corresponding main contributions of the thesis are presented. Finally, the organizational scope of the project is discussed and an overview of the content of the thesis is presented.

A Frequency Domain Perspective on Nonlinear Systems

Frequency domain methods are widely accepted and have been an impetus for the development of modeling and control design techniques for Linear and Time Invariant (LTI) systems (Bode, 1945). Although the linearity assumption can rarely be satisfied in practice, linear models and analysis often suffice when systems are operated around a given working point. However, in cases where nonlinearities play a prominent role, it is required to assess the validity of a linear model and tools and methodologies are required to detect and compensate performance degrading nonlinear effects. Given the widespread acceptance and success of frequency domain methods for LTI systems, several approaches exist that extend frequency domain methods towards nonlinear systems. Chapter 2 provides an overview and comparison of such methods, which are therefore not further discussed here. Instead, the discussion is limited to what makes frequency domain methods so successful for LTI systems and why their extension towards nonlinear systems is nontrivial.

Why Frequency Domain Analysis Works for Linear Systems

The success and popularity of frequency domain methods for LTI systems is largely due to the combination of Fourier analysis and the fact that a sine wave in an eigenfunction of LTI systems, which satisfy the properties of superposition and homogeneity. To further understand this, consider a deterministic system described by a time invariant operator \mathcal{N} which maps an input¹ $u(t) \in \mathbb{R}$ to an output $y(t) \in \mathbb{R}$. Such a system is linear if the properties of superposition and homogeneity are satisfied (Zhou et al., 1996). Hence, \mathcal{N} is linear if for any admissible inputs u_1, u_2 and corresponding steady state outputs y_1, y_2 the following holds:

$$\alpha y_1 + \beta y_2 = \mathcal{N}\{\alpha u_1 + \beta u_2\} \quad \forall \alpha, \beta \in \mathbb{C} \quad (1.1)$$

Now, note that using Fourier analysis (Philips et al., 2008) almost any input signal can be described (in mean square sense) as a sum of sinusoidal signals, i.e.

$$u(t) = \sum_{k=0}^{\infty} c_k \cos(2\pi k \xi_k t) \quad c_k \in \mathbb{C}, \xi_k \in \mathbb{R} \quad (1.2)$$

This allows to combine (1.1) and (1.2), which illustrates the process of frequency domain analysis of LTI systems, i.e.

$$y = \mathcal{N}\{u\} \xrightarrow{\text{Fourier}} \mathcal{N} \left\{ \sum_{k=0}^{\infty} c_k \cos(2\pi k \xi_k t) \right\} \xrightarrow[\text{homogeneity}]{\text{superposition}} \sum_{k=0}^{\infty} c_k \underbrace{\mathcal{N}\{\cos(2\pi k \xi_k t)\}}_{\text{frequency domain model}}$$

¹The scalar case is considered here for simplicity.

In a nutshell this summarizes why frequency domain methods are so successful when applied to LTI systems, i.e.

1. Using Fourier analysis, almost any input can be represented by a sum of sinusoidal signals, i.e. a spectral or frequency domain representation of the signal.
2. A frequency domain model can then be used to describe the response to each individual spectral component of the input signal.
3. Using the principles of superposition and homogeneity, the response to an arbitrary input can be computed from the response to the individual spectral components, which follow from the frequency domain model in step 2.

Hence, the key properties of LTI systems: superposition, homogeneity and the fact that a sine wave is an eigenfunction of LTI systems, allow for frequency domain modeling of the dynamics of such systems. When these properties are not satisfied, frequency domain analysis becomes more involved, which is discussed in the next section.

What is Lost and What is Gained for Nonlinear Systems

When considering nonlinear systems, the properties of superposition and homogeneity are not satisfied and a sine wave is generally not an eigenfunction of the system. Hence, the response of a nonlinear system to an arbitrary input cannot straightforwardly be computed from the response to sinusoidal components in the input signal. This diminishes the prospect of finding a 'conventional' frequency domain model that captures the complete nonlinear dynamics. In literature, several approaches are presented which succeed in deriving frequency domain models for a specific class of nonlinear systems. However, such models differ significantly from the intuitive models that exist for LTI systems and generally capture only a subset of the systems dynamics. A detailed discussion on results available in this area is presented in Chapter 2. In general, the application of frequency domain methods to nonlinear systems is nontrivial and has a number of disadvantages. The main drawbacks observed in this work are summarized below.

- **RESTRICTED SIGNAL TYPE:** Excitation signals are generally harmonic (Definition 1.4), which limits online application during regular operation of the system (see Chapter 4).
- **INCOMPLETE MODEL:** The complete nonlinear dynamics are generally not captured in the frequency domain. Capturing the relevant effects can be difficult (see Chapters 2 and 5).
- **EXPERT USER LEVEL:** Application of frequency domain methods to nonlinear systems requires a high level of understanding of the user (see Chapters 2 and 4).

So, what can be gained by applying frequency domain methods to nonlinear systems? Can useful properties of nonlinear systems still be captured in the frequency domain and when / how can they be obtained? These questions are addressed in the remainder of this thesis. The research presented in the following indicates that the increased

richness of the response of a class of nonlinear systems can be utilized to optimize the performance of such systems using frequency domain methods. Specifically, the following advantages are noted in relation to the research presented in this thesis:

- **NONLINEARITY DETECTION:** Frequency domain analysis provides means to quickly detect nonlinear effects from output measurements (see Chapter 4).
- **PERFORMANCE DEFINITION AND OPTIMIZATION:** Frequency domain analysis allows to define and optimize the performance of nonlinear systems and to assess the best performance obtainable using a given controller structure (see Chapters 4 and 5).
- **SEPARATION OF (NON-)LINEAR EFFECTS:** Linear and nonlinear effects are separable in the frequency domain (see Chapter 5).
- **QUALIFICATION OF NONLINEARITY:** The nature of the nonlinearity can be qualified in the frequency domain, yielding valuable information for the selection of nonlinear compensators (see Chapter 4).
- **QUANTIFICATION OF NONLINEARITY:** Nonlinear effects are quantifiable in the frequency domain, allowing assessment of the validity of a linear approximation (see Chapter 2).

Research Objectives and Contributions

The research presented in this thesis aims to contribute to the unification of frequency domain techniques and nonlinear dynamical systems. Specifically, the following research objectives are addressed in the following:

- O₁** : Investigate the application of frequency domain techniques to the modeling and analysis of nonlinear systems.
- O₂** : Develop theoretical concepts and practically applicable methods for performance optimization of nonlinear systems, based on frequency domain analysis.

The first objective is addressed by a comparative literature study and frequency domain analysis of systems with static polynomial nonlinearities. This yields a novel overview and comparison of existing frequency domain methods for nonlinear systems. Specifically, the signal / system classes for which each model is defined is discussed and an overview of the type of nonlinear effects captured in each model is provided. Moreover, new analytical results are derived that allow spectral analysis of block structured nonlinear systems with polynomial nonlinearities.

The second objective is based on the premise that the observed nonlinear effects negatively influence the performance of the system. By developing frequency domain based methods that allow quantification of nonlinear effects, a new frequency domain based performance measure is defined. This yields a methodology to design optimized static compensators that minimize performance degrading nonlinear effects. This method is then utilized to optimize the performance of an industrial transmission electron microscope. Summarizing, the results presented in the sequel yield the following main contributions:

- C₁** Overview and comparison of different frequency domain based methods for the modeling and analysis of nonlinear systems (Chapters 2, 3 and (Rijlaarsdam et al., 2012b)),
- C₂** Analytical results that allow analysis and numerically efficient computation of the effects of polynomial nonlinearities in the frequency domain (Chapter 3 and (Rijlaarsdam et al., 2011)),
- C₃** Theoretical results and practically applicable methodologies that allow optimization of the performance of nonlinear systems by means of novel frequency domain based detection and compensation techniques (Chapter 4, 5 and (Rijlaarsdam et al., 2012a)).

Scope of the Project

The research presented in this thesis is part of the Condor project, a joint project between academia and industry. The carrying industrial partner of the project and owner of the industrial problem is FEI Company, which develops and produces high end electron microscope systems. The second industrial partner is Technolution, a company specializing in embedded systems and technical automation. In addition, four academic partners are involved in the project: Catholic University of Leuven, University of Antwerp, Delft University of Technology and Eindhoven University of Technology. Finally, the project is coordinated by the Embedded Systems Institute which carries responsibility for the overall project management and knowledge dissemination.

The overall goal of the Condor project is to improve performance and increase evolvability of the electron microscope system. The project aims to improve the accuracy, productivity and image quality of the system as well as the adaptability with respect to different use cases. Within that scope, the work presented in this thesis focuses on the analysis and optimal control of the mechanics of the motion stage in the electron microscope. These results contribute to the project by supplying a new, improved methodology to assess and optimize the performance of the system by minimizing performance degrading nonlinear effects such as friction (Rijlaarsdam et al., 2012a). Moreover, the project yielded scientific contributions in several other fields such as: image sharpness analysis (Rudnaya et al., 2010, 2011), characterization of atomic scale using STEM (van den Broek et al., 2010, 2011) and system and software architecture (Langsweirdt et al., 2010; Muhammad et al., 2010). Finally, results on image based defocus control and control of electromagnetic lenses are presented in Tejada and den Dekker (2011); Tejada et al. (2011); van Bree et al. (2010a,b).

The work presented in the sequel is also part of a dual PhD program, a cooperation between the Eindhoven University of Technology and the Vrije Universiteit Brussel. The dual PhD program intends to increase international cooperation and offers the opportunity to gain research and cultural experience by spending time at a foreign institute. At the point of publication of this thesis, this collaboration resulted in three joint journal articles, with a fourth currently under review and four joint contributions to international conferences (for a full list of publication see page 113).

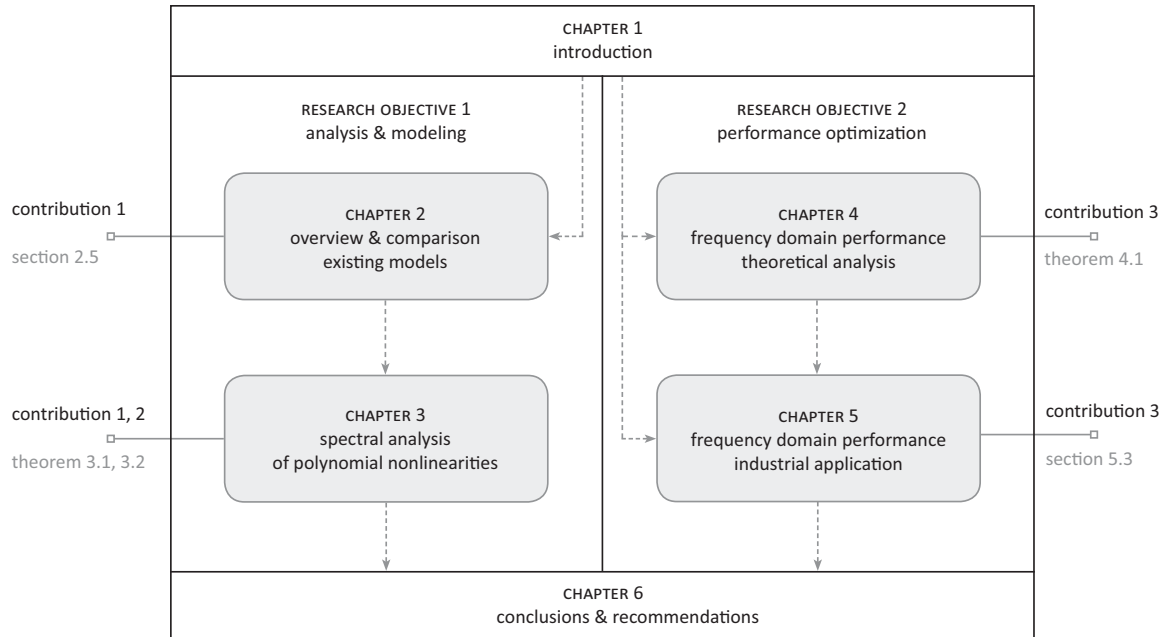


Figure 1.1: Overview of the thesis, main research objectives and contributions (dashed lines indicate the suggested order of reading).

Outline of the Thesis

The work presented in this thesis splits into two main parts: the analysis / modeling of nonlinear systems in the frequency domain and the optimization of the performance of such systems. Figure 1.1 presents an overview of the thesis with respect to the different research objectives and contributions along with the suggested order of reading.

Chapters 2 and 3 deal with the analysis and modeling of nonlinear systems in the frequency domain. First, an overview and comparison of the different frequency domain models for nonlinear systems as well as a discussion on relevant literature is provided in Chapter 2. Next, in Chapter 3 novel analytical results for the analysis and computation of the effects of polynomial nonlinearities are presented. These results are utilized to connect different frequency domain models for nonlinear systems and the reader is therefore suggested to read Chapter 2 prior to Chapter 3.

The results provided in chapters 2 and 3 are a stepping stone towards the results presented in Chapters 4 and 5 as they provide an overview of existing results and the relevant theoretical concepts and yield an increased understanding of the application of frequency domain methods to nonlinear systems. This leads to a further analysis of the performance of nonlinear systems using frequency domain based methods in the second part of the thesis.

Chapters 4 and 5 present a new, frequency domain based methodology to assess and optimize the performance of nonlinear systems and may be read independently. In Chapter 4 a theoretical analysis of the assessment and optimization of the performance

of nonlinear systems in the frequency domain is discussed. Next, in Chapter 5, these results are applied to optimize the performance of the high precision motion stage in a transmission electron microscope by minimizing the performance degrading effects of friction. Finally, conclusions and recommendations are provided in Chapter 6.

1.2 Nomenclature and Preliminaries

The following concludes this chapter by introducing the nomenclature used in this thesis. First, the notation used in the sequel is introduced. Next, the class of nonlinear systems considered in the thesis is defined. Finally, the analysis presented in the following makes frequent use of various signal classes which are introduced in this section as well.

Notation

In the sequel, signals are real-valued, scalar and denoted by non-capitalized roman letters, e.g. $u(t)$. Frequency domain representations of time domain signals, such as the Fourier transform and other spectra are denoted by corresponding capitalized calligraphic font, e.g. $\mathcal{U}(\xi) \in \mathbf{C}$. Furthermore, transfer functions are denoted by Fraktur font, e.g. $\mathfrak{H}(\xi) \in \mathbf{C}$ (unless specified otherwise) and matrices are denoted by capitalized Greek characters. Frequent use is made of vectors containing specific spectral components $U[\ell] = \mathcal{U}((\ell - 1)\xi_0)$, denoted in capitalized roman letters, such that $U[\ell] \in \mathbf{C}$ contains the spectral component at the $k = (\ell - 1)^{\text{th}}$ harmonic $k\xi_0$ of some frequency ξ_0 . Moreover, signal classes are denoted by single blackboard bold capital letter, e.g. \mathbf{S} and system classes by multiple, overlined blackboard bold capital letter, e.g. $\overline{\mathbf{S}}$. The sets of real, natural and complex numbers are denoted as usual by \mathbb{R} , \mathbb{N} and \mathbf{C} respectively and finally, differentiation with respect to time is denoted by $\dot{\cdot}$, i.e. $\dot{x}(t) = \frac{d}{dt}x(t)$.

System Class

Let \mathbb{B}_p denote the space of piecewise continuous, bounded functions² $\mathbb{R}_{\geq t_0} \mapsto \mathbb{R}$, $t_0 \in \mathbb{R}$. In the following all systems³ considered are continuous time, causal, time invariant and are assumed to have a realization of the form:

$$\begin{aligned} \dot{x}(t) &= f(x(t), w(t)) & x(t_0) &= x_0 \\ y(t) &= g(x(t), w(t)) \end{aligned} \tag{1.3}$$

where $x(t) \in \overline{\mathbb{R}^n}$ are the states, $y(t) \in \mathbb{R}^m$ the outputs, $w \in \mathbb{B}_p$ the input of the system and $f : \mathbb{R}^n \times \mathbb{R} \mapsto \mathbb{R}^n$ and $g : \mathbb{R}^n \times \mathbb{R} \mapsto \mathbb{R}^m$. A solution of (1.3), corresponding to an input $w(t)$, is denoted by $x_w(t)$. The corresponding limit solution (if it exists)

²Where $\mathbb{R}_{\geq t_0} = \{t \in \mathbb{R} | t \geq t_0\}$.

³In the sequel only single input, multi output systems are considered.

is denoted by $\bar{x}_w(t)$, such that $\lim_{t \rightarrow \infty} \|\bar{x}_w(t) - x_w(t)\| = 0 \forall x_0 \in \mathbb{R}^n$. Furthermore, the output corresponding to the limit solution is denoted by $\bar{y}_w(t) = g(\bar{x}_w(t), w(t))$. Finally, a system (1.3) is called Linear and Time Invariant (LTI) if it satisfies the principles of superposition and homogeneity (Zhou et al., 1996).

Signal Classes

The analysis presented in the sequel makes use of several signal classes and transforms. Hence, consider a real valued signal $z(t) \in \mathbb{R}$ and define the corresponding Fourier transform as follows:

Definition 1.1 ($\mathcal{Z}_F(\xi)$: Fourier transform).

Consider a signal $z(t)$. Then its Fourier transform $\mathcal{Z}_F(\xi)$ is given by:

$$\mathcal{Z}_F(\xi) = \int_{-\infty}^{\infty} z(t)e^{-2\pi i \xi t} dt \quad (1.4)$$

with $\xi \in \mathbb{R}$ the frequency in [Hz], $i = \sqrt{-1}$ and the corresponding scaling of the transform equal to one. The corresponding inverse Fourier transform is then given by:

$$z(t) = \int_{-\infty}^{\infty} \mathcal{Z}_F(\xi)e^{2\pi i \xi t} d\xi \quad (1.5)$$

Moreover, for real valued signals, all information available in the Fourier transform is fully captured in the single sided spectrum, i.e.

Definition 1.2 ($\mathcal{Z}(\xi)$: single sided spectrum).

Consider a signal $z(t) \in \mathbb{R}$ and its Fourier transform $\mathcal{Z}_F(\xi)$. Then, the single sided spectrum $\mathcal{Z}(\xi)$, equals:

$$\mathcal{Z}(\xi) = \begin{cases} 2\mathcal{Z}_F(\xi) & \xi > 0 \\ \mathcal{Z}_F(\xi) & \xi = 0 \\ 0 & \xi < 0 \end{cases}$$

In the following, several signal classes are used extensively. The classes of Gaussian, multisine and sinusoidal signals are of particular importance and are therefore defined below. First consider the sequence $z(t_k)$, which equals a Gaussian signal if it is defined as follows:

Definition 1.3 (**G**: Gaussian signal).

Let **G** denote the set of Gaussian signals. A discrete time signal $z(t_k)$ is Gaussian if it is a discrete random sequence drawn from a zero mean, normally distributed process with a user defined power density spectrum $S_z(\xi) = \mathcal{R}_F(\xi)$. Here $\mathcal{R}_F(\xi)$ denotes the Fourier transform of the autocorrelation function of $z(t)$.

Next, consider a real valued signal $z(t)$ which is composed of a finite number of sinusoidal components. In general such signal is referred to as a multisine and in the special case where the sinusoidal components are harmonically related, the resulting signal is called harmonic, i.e.

Definition 1.4 (**M**: multisine).

Let \mathbf{M} denote the set of multisine signals. A signal $z(t)$ is a multisine if $z(t) = \sum_{k=1}^K \gamma_k \cos(2\pi\xi_k t + \varphi_k)$, $t \in \mathbb{R}$, for some $\xi_k, \gamma_k \in \mathbb{R}_{>0}$, and $\varphi_k \in \mathbb{R}$. Furthermore, a signal $z(t)$ is called harmonic if it is a multisine and $\xi_k = k\xi_0$, $k \in \mathbb{N}$ for some $\xi_0 \in \mathbb{R}_{>0}$.

Finally, a special type of multisine signal is the single sine or sinusoidal signal, which is defined as follows:

Definition 1.5 (**S**: sinusoidal signal).

Let $\mathbf{S} \subset \mathbf{M}$ denote the set of sinusoidal signals. A signal $z(t)$ is sinusoidal if $z(t) = \gamma \cos(2\pi\xi_0 t + \varphi_0)$, $t \in \mathbb{R}$, for some $\gamma, \xi_0 \in \mathbb{R}_{>0}$, $\varphi_0 \in \mathbb{R}$. Finally, $\mathbf{S}_{\xi_0} \subset \mathbf{S}$ denotes the subset of sinusoidal signals with frequency ξ_0 .

Chapter 2

Frequency Domain Methods for Nonlinear Systems

For linear and time invariant (LTI) systems, frequency domain techniques resulted in a widespread acceptance in the engineering community for analysis, modeling and controller design (Bode, 1945). Correspondingly, the Frequency Response Function (FRF) and representations such as the Bode, Nyquist and Nichols plot have become standard engineering tools. However, the linearity assumption can only be satisfied to a certain extent for physical systems and increasing performance requirements force systems into regimes where nonlinear effects can no longer be neglected. Hence, the widespread acceptance of frequency domain techniques for LTI systems has been an impetus for the extension of these methodologies towards nonlinear systems.

A fundamental property of LTI systems is that the response to a sinusoidal input with a particular frequency is again sinusoidal with the same frequency as the input signal. The phase shift and gain relating the input and output are characterized by the FRF at that particular frequency and as superposition holds for LTI systems, the response to more general input signals is fully captured by the FRF as well. However, for nonlinear systems the superposition principle does not hold and the response to even a simple sinusoid can be a complex, multi harmonic signal. Hence, classical frequency domain approaches for LTI systems cannot be straightforwardly applied when nonlinearities are present and additional analysis is required to investigate if, when and how similar methodologies can be used when analyzing nonlinear systems.

In the frequency domain, nonlinear effects manifest themselves in different ways. The gain of a nonlinear system may, for example, depend on the amplitude of the input and the output may contain harmonics of the input frequency. Moreover, when a nonlinear system is subject to a multisine input, input frequencies may combine producing new frequencies which are not present in the input signal and spectral components at a given frequency in the output may depend on other frequencies in the input. These effects are summarized in Table 2.1 and they are used in the following to

| effect | description |
|------------------------------|---|
| gain compression / expansion | variation in gain for changing input amplitude |
| desensitization | dependence of the response at one frequency on the input at another frequency |
| intermodulation | frequencies combine to produce new frequencies |
| harmonics | generation of components at multiples of the fundamental input frequency |

Table 2.1: Effects of nonlinearities in the frequency domain.

discuss different frequency domain models for nonlinear systems. To further illustrate the effects listed in Table 2.1, consider the following example.

Example 2.1 (effects of nonlinearities in the frequency domain).

To illustrate the effects of nonlinearities in the frequency domain summarized in Table 2.1, consider the following harmonic signal with nonzero spectral contributions at 1 [Hz] and 5 [Hz].

$$u(t) = a \cos(1 \cdot 2\pi t) + b \cos(5 \cdot 2\pi t)$$

Now consider a static nonlinear mapping $y(t) = 4u^3(t)$, which yields:

$$\begin{aligned}
 y(t) = & \underbrace{(3a^3 + 6ab^2) \cos(1 \cdot 2\pi t)}_{\text{gain comp. / exp. } \& \text{ desensitization}} + \underbrace{(a^3 + 3a^2b) \cos(3 \cdot 2\pi t)}_{\text{harmonics } \& \text{ intermodulation}} + \underbrace{(6a^2b + 3b^3) \cos(5 \cdot 2\pi t)}_{\text{gain comp. / exp. } \& \text{ desensitization}} \\
 & + \underbrace{3a^2b \cos(7 \cdot 2\pi t)}_{\text{intermodulation}} + \underbrace{3ab^2 \cos(9 \cdot 2\pi t)}_{\text{intermodulation}} + \underbrace{3ab^2 \cos(11 \cdot 2\pi t)}_{\text{intermodulation}} + \underbrace{b^3 \cos(15 \cdot 2\pi t)}_{\text{harmonics}} \quad (2.1)
 \end{aligned}$$

The expression in (2.1) clearly shows the different effects indicated in Table 2.1. First of all, multiples of the input frequencies 1 [Hz] and 5 [Hz] appear at 3 [Hz] and 15 [Hz] (harmonics). Moreover, the 1 [Hz] and 5 [Hz] components in (2.1) depend nonlinearly on the input amplitude (gain compression / expansion) and depend on the input at other frequencies as well (desensitization). Finally, the nonlinear mapping combines input frequencies and their sum and difference frequencies to new frequencies at 3, 7, 9 and 11 [Hz] (intermodulation).

These effects are visualized in Figure 2.1 where the nonlinear deformation of the signal $u(t)$ is depicted for $a = 2$ and $b = 3$. Figure 2.1a,b show the deformation of the signal in the time domain. The corresponding frequency domain representations are depicted in Figures 2.1c,d and show the effects described in (2.1) and Table 2.1.

Although different approaches have been independently developed to analyze and model nonlinear systems in the frequency domain, differences and equivalences between alternative methods have been minorly addressed. In this chapter an overview and comparison of the following four well established approaches is presented:

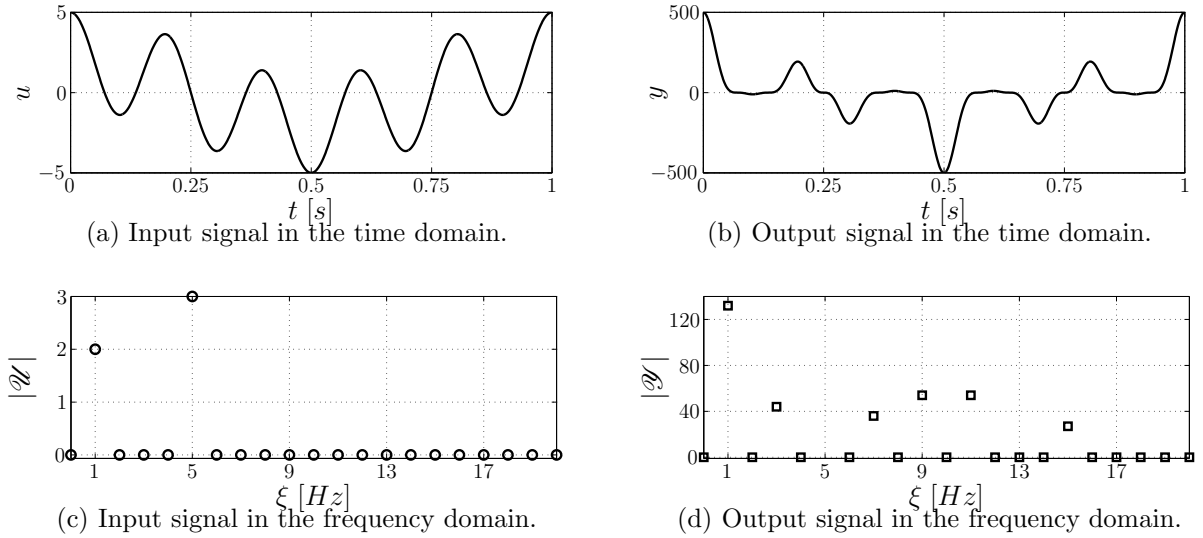


Figure 2.1: Time and frequency domain representation of a nonlinearly deformed harmonic signal.

- Volterra series based approaches (Section 2.1)
- frequency response function and Bode plot for nonlinear systems (Section 2.2)
- describing functions (Section 2.3)
- linear approximations in the presence of nonlinearities (Section 2.4)

Each method / model type is formally introduced in the following sections, including a definition of the system and signal class for which it is defined. The notation and terminology used in the different sections is consistent, which allows comparison between different approaches. A brief overview of relevant literature is provided for each method and each section is concluded by either an analytical example or an experimental case study, illustrating the introduced approach. Finally, in Section 2.5 a comparison of the properties of the different model types is provided as well as an overview of relevant literature.

2.1 Volterra Series Based Approaches

Modeling of nonlinear phenomena is often achieved by identifying a local approximation of the behavior by an approximative series. In case of continuous functions, a polynomial or Taylor approximation is often used and the existence and convergence of such series is analyzed in the Stone-Weierstrass theorem (Weierstrass, 1985; Stone, 1948a,b). An extension of the series approximation for nonlinear dynamical systems is based on the work of Vito Volterra (Volterra, 1887, 1959) which was further developed by Norbert Wiener during World War II (Wiener, 1942). This series approximation is referred to as the Volterra series (Schetzen, 1980; Rugh, 1981). In this section, the frequency domain representation of the Volterra series developed in the 1950s (George, 1959) is discussed, which is referred to as the generalized frequency response function.

The Volterra series approximation generalizes the polynomial approximation of 'static functions' over a given interval, to the approximation of dynamical systems around a given working point. This series expansion captures the input-output dynamics of a (nonlinear) dynamical system in a set of Volterra kernels that are a generalization of the impulse response of LTI systems. Provided that a Volterra series exists and can be identified (Lesiak and Krener, 1978; Sandberg, 1983; Boyd et al., 1983), the response up to order \wp , i.e. $y_\wp(t) \in \mathbb{R}$ of such system to an input $u(t) \in \mathbb{R}$ is given by:

$$y_p(t) = \int_{-\infty}^{\infty} \cdots \int_{-\infty}^{\infty} h_p(\tau_1, \tau_2, \dots, \tau_p) \prod_{m=1}^p u(t - \tau_m) d\tau_m \quad (2.2)$$

$$y_\wp(t) = \sum_{p=1}^{\wp} y_p(t)$$

where $h_p(\tau_1, \tau_2, \dots, \tau_p) : \mathbb{R}^p \mapsto \mathbb{R}$ is the p^{th} order Volterra kernel and $y_p(t)$ is referred to as the corresponding p^{th} order output. The Volterra series model (2.2) is defined for the class of Volterra systems, which is defined as follows.

Definition 2.1 ($\overline{\text{VS}}$: Volterra system).

A dynamical system is called a Volterra system if there exists a Volterra series representation (2.2) that converges uniformly around a given working point, with probability 1 to $y(t)$ for all bounded inputs $u \in \mathbf{G}$, i.e.

$$\lim_{\wp \rightarrow \infty} \int_0^\tau \mathbb{E} \{|y(t) - y_\wp(t)|\} = 0 \quad \forall \tau \in \mathbb{R}_{\geq 0}$$

where the expected value $\mathbb{E}\{\cdot\}$ is the ensemble average over the considered class of random inputs.

(see: Schetzen (1980); Schoukens et al. (2005))

The frequency domain representation corresponding to (2.2) is obtained by applying the multiple Fourier transform to the p^{th} order Volterra kernel. This yields the definition of the p^{th} order Generalized Frequency Response Function (GFRF).

Definition 2.2 ($\mathfrak{F}_p(\varpi_p)$: generalized frequency response function (GFRF)).

Consider a Volterra system according to Definition 2.1. Then, its p^{th} order GFRF is denoted $\mathfrak{F}_p(\varpi_p) : \mathbb{R}^p \mapsto \mathbb{C}$, with $\varpi_p = (\xi_1, \xi_2, \dots, \xi_p) \in \mathbb{R}^p$. The GFRF is defined as the p -dimensional Fourier transform of the p^{th} order Volterra kernel in (2.2), i.e.

$$\mathfrak{F}_p(\varpi_p) = \int_{-\infty}^{\infty} \cdots \int_{-\infty}^{\infty} h_p(\tau_1, \dots, \tau_p) \prod_{m=1}^p e^{-2\pi i \xi_m \tau_m} d\tau_m \quad (2.3)$$

(see: George (1959); Eykhoff (1974); Schetzen (1980); Billings and Tsang (1989a))

The concept of the GFRF was first introduced in George (1959) as a frequency domain equivalent of the Volterra kernel, and represents a generalization of the FRF for LTI systems. Although identification of the FRF for LTI systems is well understood, identification of the GFRF is nontrivial. Nevertheless, several approaches exist to obtain the GFRF for different classes of nonlinear systems. First of all, for some nonlinear models the GFRF can be computed analytically. Examples of such approaches are: rational nonlinear models (Zhang et al., 1995), nonlinear, autoregressive moving average models with exogenous inputs (NARMAX) (Peyton Jones and Billings, 1989) and nonlinear integro-differential equations (Billings and Peyton Jones, 1990). Moreover, the GFRF of a known NARMAX model may also be obtained by application of the probing method as (Billings and Tsang, 1989a; Billings et al., 1990; Bedrosian and Rice, 1971) and more complex dynamical systems may be modeled by a series of piecewise valid GFRFs (Li and Billings, 2012). Finally, the GFRF of quadratic and cubic nonlinear systems can be obtained in a numerically efficient manner by application of a symbolic expression of the output of such system as discussed in Li and Billings (2011a).

In general, a parametric representation is often used to analyze the GFRF. For example, in Jing et al. (2006), a parameter extraction operator is discussed that allows to study the influence of the parameters of a nonlinear model on the GFRFs. This operator is applied to analyze the relationship between different order GFRFs (Jing et al., 2008a) and to distinguish between input and output nonlinearities in a class nonlinear models (Jing et al., 2009a). Moreover, it is used to characterize and efficiently compute the generalized output frequency response function as discussed in Jing et al. (2008b, 2009b). Where the GFRF describes the relation between the input and output of Volterra systems, the generalized output frequency response function relates the parameters of a nonlinear model to the output spectrum of the nonlinear system (Lang and Billings, 1996, 2000; Lang et al., 2007).

For Volterra systems, the GFRF allows for spectral analysis of the nonlinear dynamics. In Lang and Billings (1997), it is shown that it is possible to predict the output frequency range for an arbitrary input signal using the GFRF. Moreover, a spectral analysis of block structured dynamical systems in terms of the GFRF is presented in Jing (2011) and the GFRF can be used to attain a user defined frequency domain performance for a nonlinear system as shown in Jing et al. (2008c, 2010). Finally, application of the GFRF allows to compute bounds on the output of Volterra systems (Billings and Lang, 1996a,b) and assess convergence of the corresponding Volterra series (Li and Billings, 2011b).

Although the GFRF allows for detailed spectral analysis of the behavior of Volterra systems their interpretation is nontrivial. In Yue et al. (2005a) an interpretation of the nonlinear effects in Table 2.1 in terms of the GFRF is presented. Moreover, techniques to visualize the GFRFs up to order three are introduced in Billings and Tsang (1989b); Yue et al. (2005b). Finally, to illustrate the derivation of the GFRF the following example, taken from Billings and Peyton Jones (1990), presents the computation of the GFRF for the Duffing oscillator.

Example 2.2 (GFRF of the Duffing oscillator (Billings and Peyton Jones, 1990)).

The GFRFs can be analytically computed for nonlinear systems described by nonlinear integro-differential equations. A well known example of such nonlinear system is the Duffing oscillator which dynamics are given by:

$$\ddot{y}(t) + 2\zeta\omega_n\dot{y} + \omega_n^2 y(t) + \omega_n^2 \varepsilon y^3(t) = u(t) \quad (2.4)$$

with $\zeta, \omega_n, \varepsilon \in \mathbb{R}$ and the input and output are denoted by $u(t)$ and $y(t)$ respectively. As shown in Billings and Peyton Jones (1990) the GFRFs of the system in (2.4) equal:

$$\begin{aligned} \mathfrak{T}_1(\xi_1) &= \frac{1}{\omega_n^2 + 4\pi\zeta\omega_n i\xi_1 - 4\pi^2\xi_1^2} \\ \mathfrak{T}_2(\xi_1, \xi_2) &= 0 \\ \mathfrak{T}_3(\xi_1, \xi_2, \xi_3) &= -\varepsilon\omega_n^2 \mathfrak{T}_1\left(\sum_{\ell=1}^3 \xi_\ell\right) \prod_{m=1}^3 \mathfrak{T}_1(\xi_m) \\ \mathfrak{T}_p(\xi_1, \xi_2, \dots, \xi_p) &= 0 \quad \forall p > 3 \end{aligned}$$

where $\mathfrak{T}_1(\xi_1)$ relates to the linear part of the dynamics in (2.4) and the cubic nonlinearity appears in $\mathfrak{T}_3(\xi_1, \xi_2, \xi_3)$. As the nonlinearity is odd, no even components arise in the description of the dynamics and $\mathfrak{T}_2(\xi_1, \xi_2) = 0$.

2.2 Nonlinear Frequency Response Function and Bode plot

In this section a class of frequency response functions for nonlinear systems is introduced that is based on the concept of convergent systems. The idea of convergent systems originates from Russian literature (Demidovich, 1967) and relates to the existence of stable and unique limit solutions of nonlinear systems. The notion of convergent systems is introduced in Pavlov et al. (2004, 2006) as follows:

Definition 2.3 ($\overline{\text{CS}}$: uniformly convergent systems).

A time invariant system (1.3) is said to be uniformly convergent for a class of input signals \mathfrak{W} if for every $w \in \mathfrak{W}$:

1. all solutions $x_w(t)$ are well-defined for all $t \in [t_0, \infty)$ and all initial conditions $x_0 \in \mathbb{R}^n$;
2. there exists a unique solution $\bar{x}_w(t)$ defined and bounded for all $t \in (-\infty, +\infty)$;
3. the solution $\bar{x}_w(t)$ is uniformly globally asymptotically stable.

To emphasize the dependence on the input $w(t)$, the limit solution is denoted by $\bar{x}_w(t)$.

(see: Pavlov et al. (2004, 2006))

In Pavlov et al. (2005, 2007a) convergence is discussed for interconnected and piecewise affine systems, which allows to analyze tracking and synchronization in this type

of nonlinear system (van de Wouw and Pavlov, 2008). For uniformly convergent nonlinear systems, it is possible to relate a sinusoidal input signal to the corresponding steady-state solution and output of the system. These mappings are referred to as the nonlinear state and output frequency response function (NSFRF and NOFRF) and are collectively referred to as the nonlinear frequency response function (NFRF). The NFRF was first introduced in Pavlov et al. (2007b) and is defined as follows:

Definition 2.4 ($\mathfrak{N}_{S/O}(\gamma \sin(\omega t), \gamma \cos(\omega t), \omega)$: nonlinear state and output FRF (NFRF)).

Consider the system (1.3) subject to a sinusoidal input¹ $w(t) = \gamma \sin \omega t$ with frequency $\xi = \omega/2\pi$ and amplitude γ and assume that:

1. $f(x, w)$ is locally Lipschitz with respect to x ;
2. the system is uniformly convergent for the class of bounded continuous input signals;
3. the system is input to state stable.

Then, there exist a continuous function $\mathfrak{N}_S(\gamma \sin(\omega t), \gamma \cos(\omega t), \omega) : \mathbb{R}^3 \mapsto \mathbb{R}^n$, called the Nonlinear State Frequency Response Function (NSFRF), such that for any sinusoidal input the steady state solution of (1.3) is given by:

$$\bar{x}_w(t) = \mathfrak{N}_S(\gamma \sin(\omega t), \gamma \cos(\omega t), \omega) \quad (2.5)$$

Furthermore, the Nonlinear Output Frequency Response Function (NOFRF) is denoted by $\mathfrak{N}_O(\gamma \sin(\omega t), \gamma \cos(\omega t), \omega) : \mathbb{R}^3 \mapsto \mathbb{R}^m$ and relates a sinusoidal input to the corresponding steady state output. Using the definition of the NSFRF in (2.5), the NOFRF is defined as:

$$\mathfrak{N}_O(\gamma \sin(\omega t), \gamma \cos(\omega t), \omega) = g(\mathfrak{N}_S(\gamma \sin(\omega t), \gamma \cos(\omega t), \omega))$$

(see: Pavlov et al. (2007b))

Remark. As any sinusoidal signal $w(t) = \gamma \sin(\omega\tau + \varphi)$ can be written as $w(t) = \gamma \sin \omega t$, with $t = \tau + \frac{\varphi}{\omega}$, Definition 2.4 holds for all $w \in \mathbf{S}$.

Remark. Both the NSFRF and NOFRF depend on the sinusoidal signals $\gamma \sin(\omega t)$, $\gamma \cos(\omega t)$ and frequency ω which are related to the corresponding response and outputs respectively. This notation is adapted from Pavlov et al. (2007c).

Numerically efficient methods are required to compute the periodic solutions required to derive the NFRF. In Pavlov and van de Wouw (2008); Alcorta-García et al. (2010) examples of such methods are presented. When using the NFRF, a method for visualization of the dynamics is required for analysis and controller design. For LTI

¹In the remainder of this section the angular frequency $\omega = 2\pi\xi$ is used for ease of notation.

systems, the Bode plot visualizes the FRF and is widely applied in both analysis and controller design. Using the NOFRF, the concept of the Bode plot is extended to nonlinear systems in Pavlov et al. (2007b). Therefore, consider the following definition of the nonlinear Bode plot.

Definition 2.5 ($\mathfrak{G}(\omega, \gamma)$: nonlinear Bode plot).

Consider the system (1.3), with scalar output $y(t) \in \mathbb{R}$ and subject to a sinusoidal input $w \in \mathbf{S}$ with frequency $\xi = \omega/2\pi$ and assume conditions 1-3 in Definition 2.4 are satisfied. Then, the nonlinear Bode plot $\mathfrak{G}(\omega, \gamma) : \mathbb{R}^2 \mapsto \mathbb{R}$ is defined as:

$$\mathfrak{G}(\omega, \gamma) = \frac{1}{\gamma} \left(\sup_{t \in [-\frac{\pi}{\omega}, \frac{\pi}{\omega})} |\mathfrak{N}_O(\gamma \sin(\omega t), \gamma \cos(\omega t), \omega)| \right)$$

where $\mathfrak{N}_O(\cdot)$ is the NOFRF as in Definition 2.4.

(see: Pavlov et al. (2007b))

The definition of the nonlinear Bode plot in Definition 2.5, although based on the norm of a time domain signal, relates directly to the gain of the FRF as visualized in the classical Bode plot for LTI systems. However, where the classical Bode plot provides information about the phase shift as well, such phase information cannot be defined for nonlinear systems. Moreover, where system norms can be computed from the FRF and Bode plot for LTI systems, this is generally not possible for nonlinear systems based on the NFRF and nonlinear Bode plot. The concept of the nonlinear Bode plot is used to extend the notion of the sensitivity function to nonlinear systems in Pavlov et al. (2007c). These generalized sensitivity functions have been applied for the design of variable gain control for optical storage drives (van de Wouw et al., 2008) and feed forward design for wafer scanners (Heertjes et al., 2010). Finally, the following example is taken from (Pavlov et al., 2007b) and concludes this section by illustrating the computation of the NFRF for a given nonlinear system.

Example 2.3 (nonlinear state and output FRF (Pavlov et al., 2007b)).

Consider the following dynamical system, subject to a sinusoidal input $u(t) = \gamma \sin(\omega t)$ with frequency $\xi = \omega/2\pi$ and amplitude γ .

$$\begin{aligned} \dot{x}_1 &= -x_1 + x_2^2 & y &= x_1 \\ \dot{x}_2 &= -x_2 + u \end{aligned} \tag{2.6}$$

As shown in Pavlov et al. (2007b), condition 1-3 in Definition 2.4 are satisfied for this system. Hence, the NSFRF exists and is unique. Next, using the results from Pavlov et al. (2007b) and denoting $v(t) = [\sin(\omega t) \cos(\omega t)]^T$, the NSFRF, which describes the steady state solution $\bar{x}_u(t) = [\bar{x}_{1,u}(t) \bar{x}_{2,u}(t)]^T$ of (2.6), equals:

$$\begin{aligned} \mathfrak{N}_S(\gamma \sin(\omega t), \gamma \cos(\omega t), \omega) &= \gamma \begin{bmatrix} \gamma v^T(t) \Psi_1(\omega) v(t) \\ \Psi_2(\omega) v(t) \end{bmatrix} \\ \Psi_1(\omega) &= (1 + \omega^2)^{-2} (1 + 4\omega^2)^{-1} \begin{bmatrix} 2\omega^4 + 1 & \omega^3 - 2\omega \\ \omega^3 - 2\omega & 2\omega^4 + 5\omega^2 \end{bmatrix} \\ \Psi_2(\omega) &= (1 + \omega^2)^{-1} \begin{bmatrix} 1 & -\omega \end{bmatrix} \end{aligned}$$

Using these results, and as $y(t) = g(x(t)) = x_1(t)$, the corresponding NOFRF, which describes the output corresponding to the steady state solution $\bar{y}_u(t) = \bar{x}_{1,u}(t)$ of (2.6), equals:

$$\mathfrak{N}_O(\gamma \sin(\omega t), \gamma \cos(\omega t), \omega) = \gamma^2 v^T(t) \Psi_1(\omega) v(t)$$

Finally, the nonlinear Bode plot is obtained by (numerically) computing:

$$\mathfrak{G}(\omega, \gamma) = \frac{1}{\gamma} \left(\sup_{t \in [-\frac{\pi}{\omega}, \frac{\pi}{\omega})} |\gamma^2 v^T(t) \Psi_1(\omega) v(t)| \right) \quad (2.7)$$

and the result is depicted in Figure 2.2. Hence, the NSFRF relates any sinusoidal input to the corresponding steady state solution and the NOFRF yields the corresponding steady state output. Finally, the nonlinear Bode plot yields the maximum gain of the nonlinear system for a sinusoidal input with a given amplitude and excitation frequency.

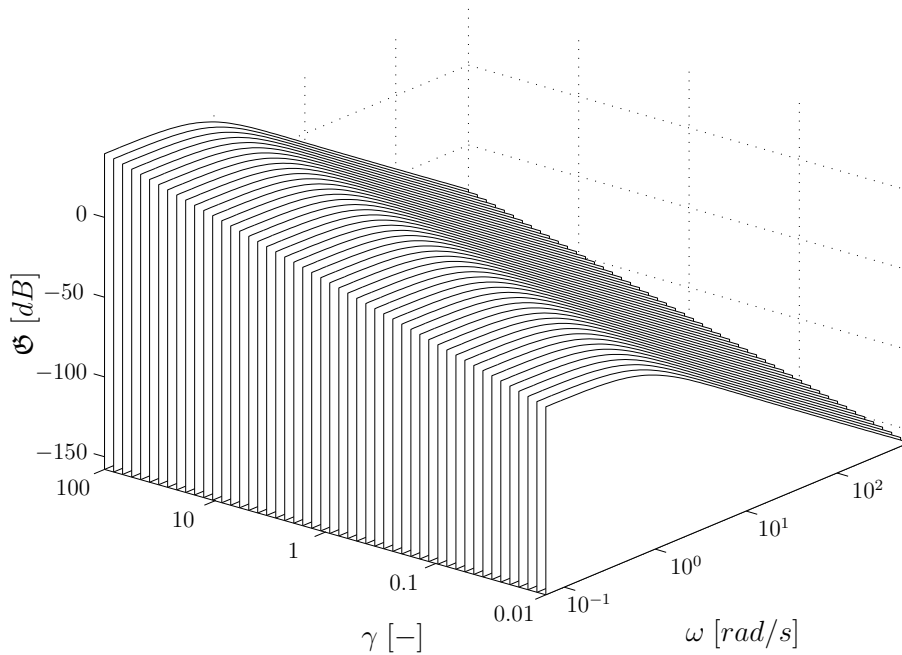


Figure 2.2: Nonlinear Bode plot (2.7) of system (2.6).

2.3 Describing Functions

For LTI systems the FRF fully captures the systems dynamics as the response to a single sinusoid can be extended to arbitrary inputs using the principle of superposition. For nonlinear systems superposition does not hold and the FRF fails to capture the full dynamics. Hence, an alternative approach is required to extend the concept of the FRF to nonlinear systems. Describing Functions (DF) aim to do so by describing the response to a given type of input signal based on some frequency domain mapping

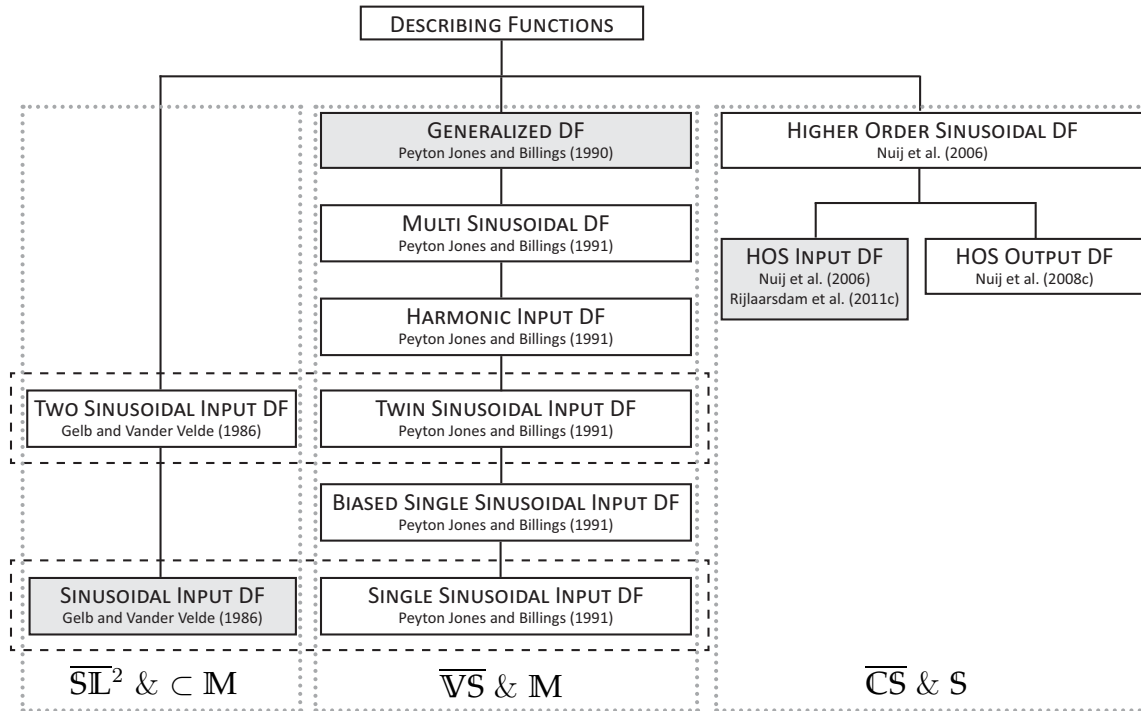


Figure 2.3: Overview of a selection of different describing functions. The signal and system classes refer to the definitions used by the authors in the corresponding references.

from input to output. Although different types of describing functions exist (Figure 2.3), their definition is generally similar to that of the FRF for LTI systems. The main difference between different describing functions originates from the signal and system class for which they are defined and the type of nonlinear effects captured. In this section a selection of describing functions is introduced, compared and an experimental example is provided illustrating the identification of one of the describing functions.

In Figure 2.3, three classes of describing functions are depicted: the sinusoidal describing function, the generalized describing function and the higher order sinusoidal describing function. The different branches represent different subclasses of DF such that for any two consecutive DF, the lower one is always a special case of the upper one. The classical (two) sinusoidal input describing function (SIDF) models the response to (two) sinusoidal inputs at the corresponding excitation frequencies. The Generalized Describing Function (GDF) on the other hand, is based on the Volterra series approximation of nonlinear systems and allows to model the response to multisine inputs. Finally, the Higher Order Sinusoidal Describing Functions (HOSDF) model the response to sinusoidal signals at both the fundamental excitation frequency and higher harmonics of this frequency. These describing functions are defined for different classes of input signals and nonlinear systems and capture a different subset of nonlinear effects. In this section three describing functions are introduced in detail: the SIDF, GDF and the Higher Order Sinusoidal Input Describing Function (HOSIDF).

First, consider the SIDF, which is defined for sinusoidal input signals and is defined as follows:

Definition 2.6 ($\mathfrak{D}_S(\xi, \gamma)$: sinusoidal input describing function (SIDF)).

Consider a nonlinear system² (1.3), with $y(t) \in \mathbb{R}$, subject to a sinusoidal input $u \in \mathbb{S}$ with frequency ξ_0 and amplitude γ and define the systems steady state output $y(t)$ and Fourier transforms of the input and output $\mathcal{U}_F(\xi), \mathcal{Y}_F(\xi) \in \mathbb{C}$. Then the sinusoidal input describing function $\mathfrak{D}_S(\xi, \gamma) : \mathbb{R}_{>0} \times \mathbb{R} \mapsto \mathbb{C}$ is defined as:

$$\mathfrak{D}_S(\xi_0, \gamma) = \frac{\mathcal{Y}_F(\xi_0, \gamma)}{\mathcal{U}_F(\xi_0, \gamma)}$$

(see: Gelb and Vander Velde (1968))

The SIDF models the response to a sinusoidal input by relating the spectral components in the input and output at the fundamental excitation frequency. Hence, the SIDF captures gain compression / expansion (see Table 2.1), but fails to model desensitization as the input is a single sinusoid. Moreover, intermodulation is not captured for the same reason and generation of harmonic components is not detected as only the response at the excitation frequency is considered.

The GDF, on the other hand, captures a wider range of nonlinear phenomena and allows for a broader class of input signals, but is defined only for Volterra systems. Consider the following definition of the GDF:

Definition 2.7 ($\mathfrak{D}_G(\xi, \varsigma)$: generalized describing function (GDF)).

Consider a Volterra system (1.3) subject to multisine input (wave form) $u \in \mathbb{M}$ scaled by a factor ς and output $y(t)$. Moreover, define the corresponding Fourier transforms of the input and output $\mathcal{U}_F(\xi), \mathcal{Y}_F(\xi) \in \mathbb{C}$. Then, the generalized describing function $\mathfrak{D}_G(\xi, \varsigma) : \mathbb{R}^2 \mapsto \mathbb{C}$ is defined as:

$$\mathfrak{D}_G(\xi', \varsigma) = \frac{\sum_{p=1}^{\infty} \varsigma^{p-1} \mathcal{Y}_{F_p}(\xi')}{\mathcal{U}_F(\xi')}$$

where the GDF is defined for all $\xi' \in \{\xi \in \mathbb{R} \mid |\mathcal{U}_F(\xi)| \neq 0\}$ and the uni-dimensional spectrum $\mathcal{Y}_{F_p}(\xi')$ is related to the output generated by the order p^{th} order GFRF, $\mathfrak{T}_p(\tau_p)$ by:

$$\mathcal{Y}_{F_p}(\xi') = \int_{-\infty}^{\infty} \dots \int_{-\infty}^{\infty} \mathfrak{T}_p \left(\xi_1, \dots, \xi_{p-1}, \xi' - \sum_{m=1}^{p-1} \xi_m \right) \mathcal{U}_F \left(\xi' - \sum_{m=1}^{p-1} \xi_m \right) \prod_{\ell=1}^{p-1} \mathcal{U}_F(\xi_\ell) d\xi_1 \dots d\xi_{p-1}$$

(see: Peyton Jones and Billings (1991))

²The authors in Gelb and Vander Velde (1968) define these describing functions for systems that 'have a single loop configuration with separable linear and nonlinear elements', here denoted by $\overline{\text{SL}}$. However, this describing function can be computed for all system classes considered in this chapter.

The GDF allows to model the response of Volterra systems to multisine input signals (Peyton Jones and Billings, 1990, 1991). However, it is specific to the selected input signal, which limits the validity of the model to the excitation signal used. As the GDF allows for broadband input signals, both gain compression / expansion and desensitization are captured by the GDF. However, intermodulation and the generation of harmonics are not modeled as the GDF only models the response at frequencies present in the input signal.

Finally, the Higher Order Sinusoidal Input Describing Functions model the response of uniformly convergent nonlinear systems to a sinusoidal input at harmonics of the excitation frequency and are defined as follows:

Definition 2.8 ($\mathfrak{H}_k(\xi, \gamma)$): higher order sinusoidal input describing function (HOSIDF)).

Consider a uniformly convergent, time invariant nonlinear system (1.3) subject to a sinusoidal input $u \in \mathcal{S}$ with frequency ξ_0 and amplitude γ . Next, define the systems steady state output $y(t)$ and single sided spectra of the input and output $\mathcal{U}(\xi)$, $\mathcal{Y}(\xi) \in \mathbb{C}$. Then, the k^{th} higher order sinusoidal input describing function $\mathfrak{H}_k(\xi, \gamma) : \mathbb{R}_{>0} \times \mathbb{R} \mapsto \mathbb{C}$, $k = 0, 1, 2, \dots$ is defined as:

$$\mathfrak{H}_k(\xi_0, \gamma) = \frac{\mathcal{Y}(k\xi_0, \gamma)}{\mathcal{U}^k(\xi_0, \gamma)} \quad (2.8)$$

where $\mathcal{U}^k(\xi_0, \gamma) = \prod_{\ell=1}^k \mathcal{U}(\xi_0, \gamma)$.

(see: Nuij et al. (2006); Rijlaarsdam et al. (2011))

Remark. Note that $\mathfrak{H}_1(\xi_0, \gamma) = \mathfrak{D}_S(\xi_0, \gamma) \forall \xi_0 > 0$.

Remark. Compared to the original definition in Nuij et al. (2006), the amplitude dependency $|\mathfrak{F}_k| \propto \gamma^k$ inherent to the original HOSIDF model structure is removed in Rijlaarsdam et al. (2011) such that the HOSIDFs reveal only system characteristics.

The HOSIDFs model the response to a sinusoidal input signal at harmonics of the fundamental input frequency. Therefore both gain compression / expansion and the generation of harmonics are captured in this describing function. However, as the excitation signal is a single sinusoid, both desensitization and intermodulation are not captured by the HOSIDFs. The HOSIDFs yield valuable information about nonlinearities that can be used for modeling and control purposes (Nuij et al., 2008a,b; Rijlaarsdam et al., 2012a, 2011). Finally, related studies as presented in Nuij et al. (2008c) use the concept of the HOSIDF to find an input signal that yields a sinusoidal output signal, similar to Volterra based approaches presented in Jing et al. (2008c, 2010).

A comparison of the describing functions discussed in this section is provided in Tables 2.3 and 2.5, which are presented in Section 2.5. Finally, this section is concluded by an example that illustrates the identification of the HOSIDFs in practice.

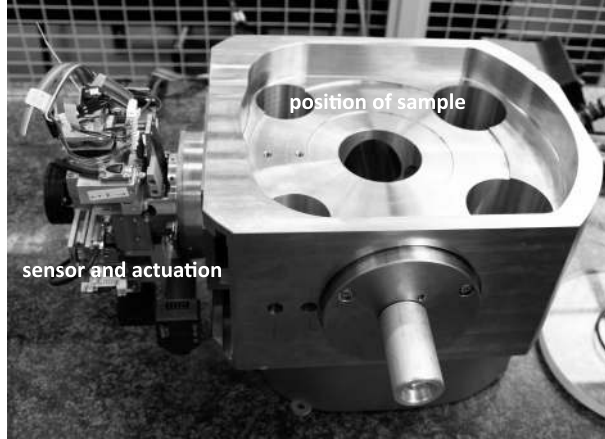


Figure 2.4: Industrial high precision stage used in a transmission electron microscope.

Example 2.4 (experimental identification of the HOSIDFs).

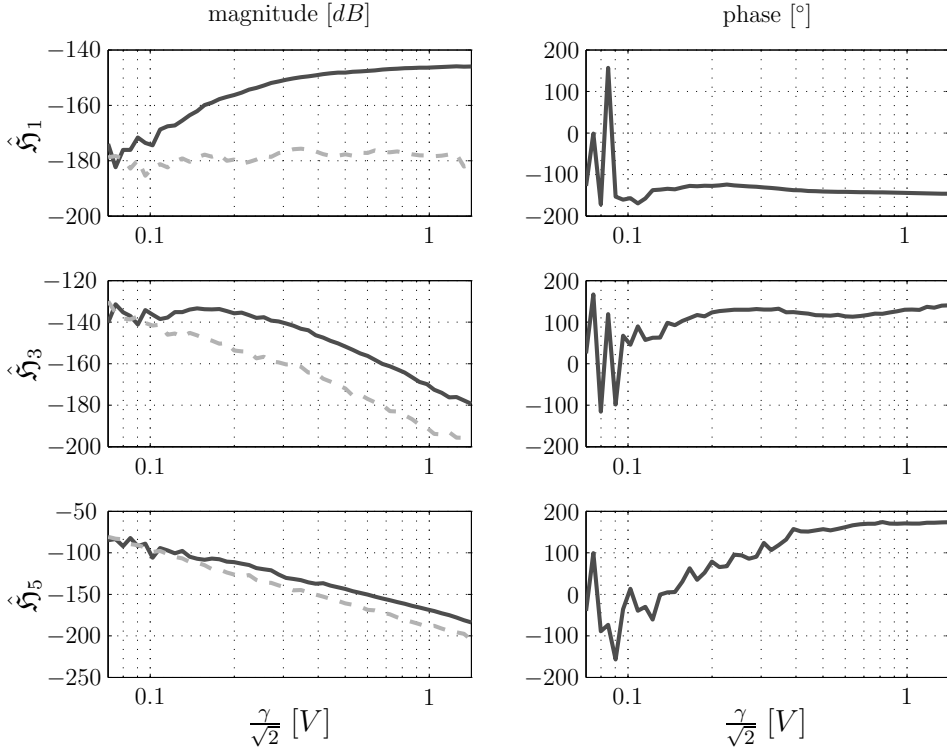
In this section the identification of the HOSIDFs of a nonlinear dynamical system in practice is presented. The system under test in this study is an industrial high precision stage (Figure 5.2) used in a Transmission Electron Microscope (TEM). At the high resolution and reproducibility that is required in a TEM, nonlinear effects start to effect the performance of the system significantly. This motivated the measurements presented in this section. The motion stage is a single input, single output system with the voltage to the current amplifier as the input and the position of the stage as its output. The identification is performed in open loop as in Nuij et al. (2006).

The system is excited with a sinusoidal input and the response is measured using a SigLab 20-42 dynamic signal analyzer. To measure the response of the system an encoder system is used that allows high resolution position measurements over the entire stroke of the set-up. To measure a single HOSIDF $\mathfrak{H}_k(\xi_0, \gamma)$ for a given frequency / amplitude combination, a sinusoidal input signal $u \in \mathbf{S}$ is applied. Next, the single sided spectra of the input and output are computed using standard DFT algorithms and Definition 2.8 is applied. Finally, repeating the experiment multiple times yields the average HOSIDF and variance on the average which are denoted by $\hat{\mathfrak{H}}_k(\xi_0, \gamma)$ and $\varsigma^2(\xi_0, \gamma)$ respectively.

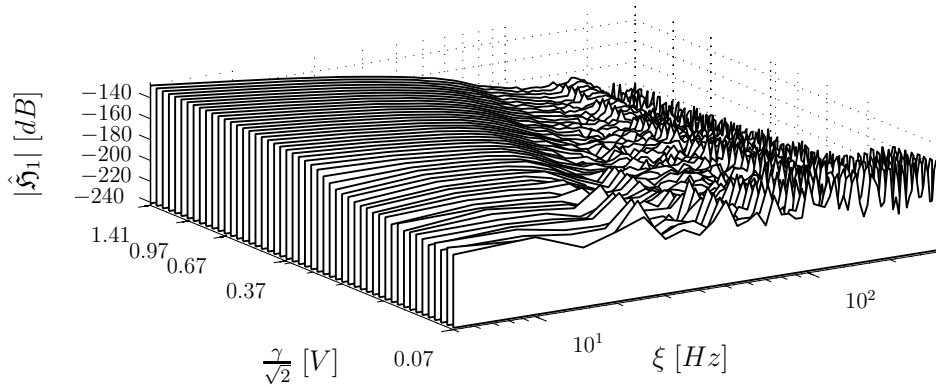
By repeating each experiment ten times with frequencies ranging from 5 [Hz] to 300 [Hz] in steps of 5 [Hz] and input signal powers $\gamma/\sqrt{2}$, ranging from 0.07 [V] to 1.41 [V] (logarithmically spaced) the HOSIDFs are identified. All measurements have been performed with a sampling frequency of 5120 [Hz] and a block length of 2048 points, resulting in leakage free measurements.

A typical series of HOSIDFs is depicted in Figure 2.5a. Given the odd nature of the friction nonlinearity in this case, the even HOSIDFs are very low, hence only the odd HOSIDFs are considered. Figure 2.5a hints that the system behaves more linearly for increasing value of γ . This can be observed from the combination of a

decreasing gradient $\partial \hat{\mathfrak{H}}_1 / \partial \gamma$ and a decreasing value of $\hat{\mathfrak{H}}_k(\xi, \gamma) \forall k > 1$ for all measured frequencies. Finally, in Figure 2.5b $|\hat{\mathfrak{H}}_1|$ is depicted as a function of input power and frequency.



(a) The first three odd HOSIDFs as a function of input amplitude γ , for one frequency $\xi_0 = 20$ Hz.: (—) \mathfrak{H}_k , (---) ς (with ς^2 the variance on the average).



(b) The first HOSIDF as a function of input amplitude γ and frequency ξ .

Figure 2.5: Measured HOSIDF of the motion stage in a TEM.

2.4 Linear Approximation in the Presence of Nonlinearities

In many applications, the use of LTI models is common practice, mainly because methods to identify and interpret such models are well developed (Ljung, 1999) and many tools exist that allow controller design and synthesis based on LTI models

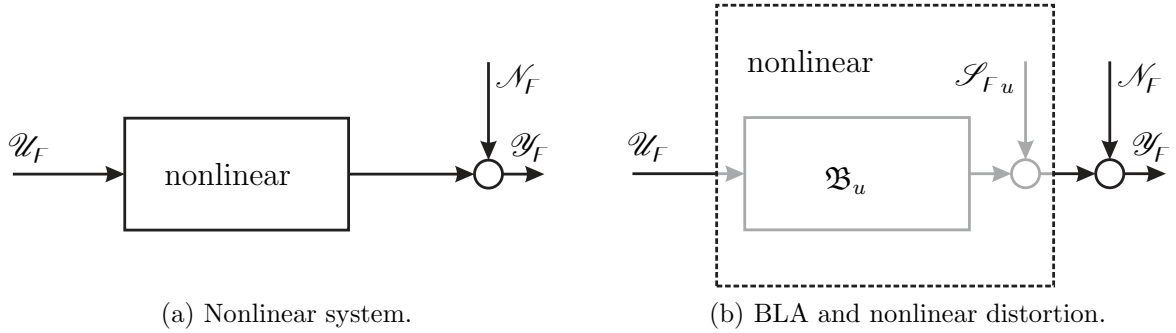


Figure 2.6: Equivalent representations of a nonlinear system.

(Skogestad and Postlethwaite, 2005). However, most real life systems are not linear and it is therefore required to assess the validity of a linear approximation (see for example Schoukens and Dobrowiecki (1998); Pintelon and Schoukens (2012); Schoukens et al. (2005, 2009)). In this section, the estimation of a linear model in the presence of nonlinearities is addressed.

Consider a nonlinear system as depicted in Figure 2.6a and assume the system can be transformed to a structure as in Figure 2.6b. In Figure 2.6b, the output $\mathcal{Y}_F(\xi)$ is assumed to exist of a component that is generated by an LTI system $\mathfrak{B}_u(\xi)$, a distortion $\mathcal{S}_{Fu}(\xi)$ due to nonlinearities and an output disturbance $\mathcal{N}_F(\xi)$. Note that the transformation in Figure 2.6 is nontrivial and a (unique) transformation may not exist. In the sequel, the existence and invariance of this transformation is addressed. However, for now, consider the representation in Figure 2.6b and note that the nonlinear system is represented by the combination of an LTI model $\mathfrak{B}_u(\xi)$ and a nonlinear disturbance $\mathcal{S}_{Fu}(\xi)$, both of which depend on the power spectrum of the input signal.

In literature, $\mathfrak{B}_u(\xi)$ is referred to as the Best Linear Approximation (BLA) (Schoukens et al., 2005, 2009). A BLA can be computed for a large class of input signals and nonlinear systems, but additional assumptions are required to assure invariance of the approximation with respect to a given class of input signals. In this section the BLA is therefore introduced in two steps. First, the formal definition of the BLA is provided and then sufficient conditions are provided for a class of nonlinear systems and input signals for which the BLA exists and is invariant.

The transformation in Figure 2.6 is defined by the pair $(\mathfrak{B}_u, \mathcal{S}_{Fu})$, which is defined along the lines of Enqvist and Ljung (2005); Schoukens et al. (2005).

Definition 2.9 ($(\mathfrak{B}_u, \mathcal{S}_{Fu})$: Best Linear Approximation).

Consider a nonlinear system (1.3), with $y(t) \in \mathbb{R}$ and assume the transformation in Figure 2.6 exists, such that:

$$\mathcal{Y}_F(\xi) = \mathfrak{B}_u(\xi)\mathcal{U}_F(\xi) + \mathcal{S}_{Fu}(\xi) + \mathcal{N}_F(\xi)$$

then, the Best Linear Approximation (BLA) is defined by the pair $(\mathfrak{B}_u, \mathcal{S}_{Fu})$, such that:

$$\mathfrak{B}_u(\xi) = \arg \min_{\mathfrak{B}(\xi)} E\{(y(t) - \mathfrak{B}(\xi)u(t))^2\} \quad (2.9)$$

where the expected value $E\{\cdot\}$ is the ensemble average over the considered class of inputs.

(see: Enqvist and Ljung (2005))

Definition 2.9 does not assure the existence of the BLA, i.e. of the minimizer in (2.9). Moreover, although it is clear that the BLA depends on the power spectrum of the input signal, invariance of the BLA with respect to a class of input signals needs to be addressed as well. Therefore, consider the following class of excitation signals.

Definition 2.10 (\mathbf{G}_{eq} : Gaussian Riemann equivalent signals).

Consider a power density spectrum $S_u(\xi)$, which is piecewise continuous and has a finite number of discontinuities and consider an excitation signal $u(t)$ that equals:

1. a Gaussian noise excitation \mathbf{G} with power density spectrum $S_u(\xi)$, or
2. a periodic, real valued signal $u(t) \in \mathbb{R}$ such that $\mathcal{W}_F(\pm\xi_k) = A_k e^{\pm i\varphi_k}$, $k \in \mathbb{N}_{>1}$, $\xi_k \in \mathbb{R}_{>0}$ and $\mathcal{W}_F(\xi) = 0$ otherwise. Moreover, A_k and φ_k are random and mutually independent, $E\{e^{i\varphi_k}\} = 0$ and either $E\{A_k^2\} = f_A^2(\xi_k)$ or $A_k^2 = f_A^2(\xi_k)$ with $f_A(\xi)$ a piecewise continuous function with a finite number of discontinuities.

Then, the sets of signals 1 and 2 are Gaussian Riemann equivalent if:

$$\sum_{k \in \mathbb{K}} E\{|\mathcal{W}_F(\xi_k)|^2\} = \int_{\zeta_1}^{\zeta_2} S_u(\xi) d\xi + O(N_{\mathbb{K}}^{-1}) \quad \forall \zeta_i \in \mathbb{R}_{>0}$$

with $\mathbb{K} = \{k \in \mathbb{N}_{>1} | \zeta_1 < \xi_k < \zeta_2\}$, $N_{\mathbb{K}}$ the number of elements in \mathbb{K} , $0 < \zeta_1 < \zeta_2$ and where $E\{\cdot\}$ denotes the expected value.

(proof: (Schoukens et al., 2005))

To assure that the minimizer in (2.9) and thus the BLA exists, the class of nonlinear systems is restricted as follows (along the lines of Schoukens et al. (2009)):

Definition 2.11 ($\overline{\mathbf{WS}}$: special Wiener system).

System (1.3) is called a special Wiener system if there exists a Volterra series representation (2.2), with continuous multidimensional Fourier transforms (2.3), that converges in mean square sense, with probability 1 to $y(t)$ for all bounded inputs $u \in \mathbf{G}_{eq}$, i.e.

$$\lim_{\varphi \rightarrow \infty} \frac{1}{\tau} \int_0^{\tau} E\{|y(t) - y_{\varphi}(t)|^2\} = 0 \quad \forall \tau \in \mathbb{R}_{\geq 0}$$

where the expected value $E\{\cdot\}$ is the ensemble average over the considered class of random inputs.

Remark. This class of systems is referred to as special Wiener systems as it is closely related to the classical Wiener systems (Schetzen, 1980) for which the requirement on continuity of the Fourier transforms is not imposed and which considers only Gaussian inputs $\mathbf{G} \subset \mathbf{G}_{eq}$ in the convergence criterium.

Using Definitions 2.10 and 2.11, the following sufficient conditions for the existence and invariance of the BLA are derived in Schoukens et al. (2009).

Lemma 2.1 (invariance and existence of the BLA).

Consider a nonlinear system (1.3). If the system:

1. *belongs to the class of special Wiener systems $\overline{\text{WS}}$;*
2. *is subject to Gaussian Riemann equivalent input signals, i.e. $u \in \mathbf{G}_{eq}$,*

then, the best linear approximation (Definition 2.9) exists and the pair $(\mathfrak{B}_u, \mathcal{S}_{F_u})$ is asymptotically invariant under inputs in the equivalence class \mathbf{G}_{eq} . Moreover, if condition 1-2 are satisfied, the BLA equals:

$$\mathfrak{B}_u(\xi) = \frac{\mathbb{E}\{\mathcal{Y}_F(\xi)\mathcal{U}_F^*(\xi)\}}{\mathbb{E}\{\mathcal{U}_F(\xi)\mathcal{U}_F^*(\xi)\}} \quad (2.10)$$

where $$ indicates the complex conjugate and the expected value $\mathbb{E}\{\cdot\}$ is the ensemble average over the considered class of inputs which includes averaging over the effect of the measurement noise \mathcal{N}_F .*

(proof: see³ Schoukens et al. (2009))

Remark. Although Lemma 2.1 assures invariance of the BLA, the BLA still specific to the fixed power spectrum of the set of input signals that is used.

Remark. In the sequel, the BLA is considered under the conditions in Lemma 2.1 which assures both invariance and existence of the linear approximation but does not provide any condition about the quality of the approximation.

Experimental identification of the BLA and the detection of nonlinear effects in the frequency domain requires careful design of the excitation signal and signal processing. An overview of techniques for the detection of nonlinearities is presented in Vanhoenacker et al. (2002). Moreover, excitation signal design is for example addressed in Godfrey (1993); Schoukens and Dobrowiecki (1998); Guillaume et al. (1991) and signal processing techniques are discussed in for example Pintelon and Schoukens (2012); Schoukens et al. (2006); Pintelon et al. (2010a,b).

The concept behind the detection of nonlinear effects in the frequency domain is often based on two approaches. First, the presence of nonlinearities will cause a change in linear approximation of the dynamics when the input signal changes. Hence, a variance analysis on an ensemble of appropriately selected input signals allows to quantify the effects of nonlinearities (D'haene et al., 2005; Vanhoenacker et al., 2001). Moreover, nonlinearities can be detected by analyzing the power appearing in the output spectrum at spectral lines that are not excited by the input signal (Pintelon et al., 2004b,a). This approach both allows quantification of nonlinear effects and characterization of the nature of the nonlinearities. A detailed discussion of these methods is

³See also Pintelon and Schoukens (2012); Schoukens et al. (1998); Pintelon and Schoukens (2002).

outside the scope of this work but an example is presented at the end of this section that illustrates both methods.

Both the identification of the BLA and means to detect nonlinearities are often discussed for single input, single output systems that are identified in open loop. However, extensions for multi input, multi output systems are presented in Dobrowiecki and Schoukens (2007); Schoukens et al. (2010). Moreover, identification of the BLA and estimation of nonlinear effects in closed loop is addressed in for example Pintelon et al. (2011a,b). Finally, the following example concludes this section and illustrates the identification of the BLA in practice.

Example 2.5 (experimental identification of a high precision motion stage).

Consider again the high precision motion stage from a transmission electron micro-

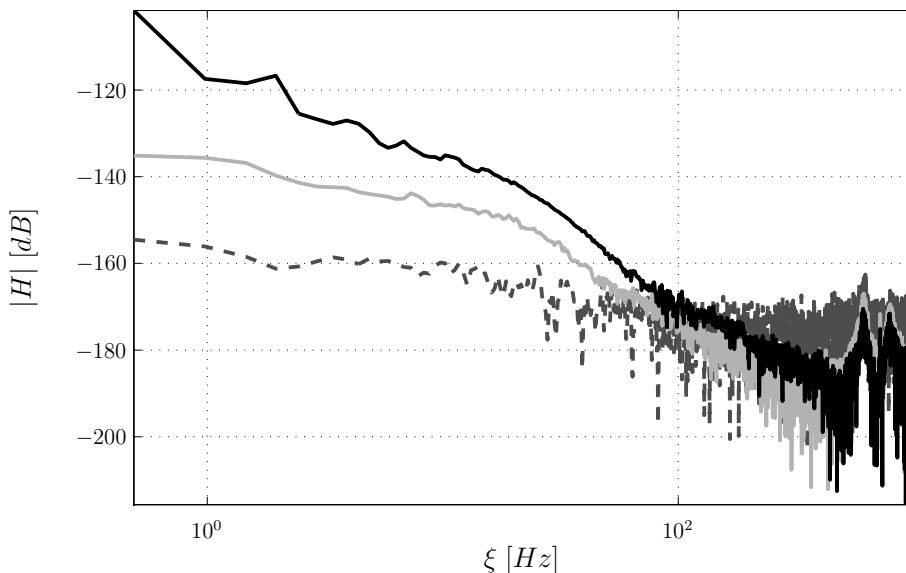


Figure 2.7: Linear approximation identified with different powers of the input signal. (–) $u_{rms} = 0.10$ [V], (– grey) $u_{rms} = 0.50$ [V] and (– black) $u_{rms} = 1.0$ [V].

scope as in Example 2.4. In the following both the BLA of this system is identified and the effects of nonlinearities on the dynamics are quantified. However, first consider a conventional identification experiment using band limited white noise with three different root mean square (rms) values. The estimates depicted in Figure 2.7 clearly indicate nonlinear behavior as the FRF changes with the rms value of the input signal. This indicates that further analysis of the validity of a linear model is required. Therefore, the BLA is identified in a setting that allows to quantify nonlinear effects and assess the validity of this linear approximation.

In this example the BLA is identified under the assumptions in Lemma 2.1. Hence, the system is assumed to be in the class of $\overline{\text{WS}}$ systems and using Gaussian Riemann equivalent input signals yields an invariant estimate of the BLA for a given power spectrum of the input signal. In the following, random odd multisine excitation signals are used (Definition B.1, p. 95), which are Gaussian Riemann equivalent.

Table 2.2: Estimated variables (see Appendix B.1)

| variable | description |
|---------------------------|---|
| \mathfrak{B}_u | best linear approximation |
| \mathfrak{Y}_F | output spectrum |
| $\sigma_{\mathcal{N}}^2$ | variance on \mathfrak{Y}_F due to noise |
| $\sigma_{\mathcal{Z}}^2$ | variance on \mathfrak{Y}_F due to nonlinearities |
| $\mathcal{P}(\ell_{o/e})$ | power at non-excited odd (<i>o</i>) and even (<i>e</i>) lines |

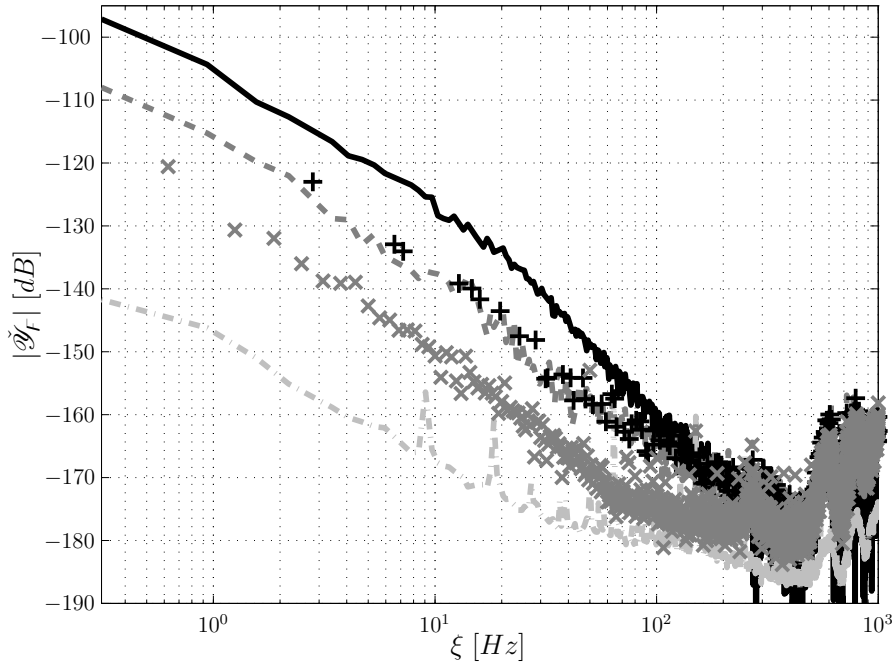
When using random odd multisines, there are two ways to detect nonlinearities in the spectral representation of the measured response. First of all, energy may appear on non-excited lines in the output spectrum, yielding both the level and odd / even nature of the nonlinearity. Secondly, a variance, larger than to be expected based on stochastic distortions, is observed on the measured output spectrum, using different realizations of the multisine. In this example these detection methods are combined to both quantify the extend of nonlinear effects and classify them.

The identification procedure consists of exciting the system with several periods of different realizations of a random multisine. Computation of the averages and variances then yields the BLA and an estimate of nonlinear influences based on both variance information and energy appearing at non excited lines. The signal processing involved is discussed in Appendix B.1 and yields the estimated variables in Table 2.2.

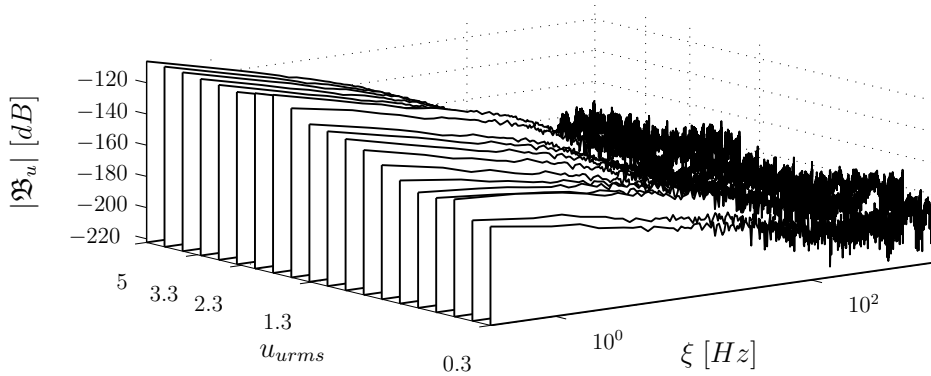
Ten realizations of the odd random phase multisine have been generated and the response has been measured for ten consecutive periods. Furthermore, this experiment is repeated for twenty different rms values of the multisines which are logarithmically scaled between 0.3 [V] and 5.0 [V]. Measurements are performed using a SigLab measurement system with a measurement frequency of 2560 [Hz] and a block length of 8192 measurement points. The multisine signal is defined according to Definition B.1, with $\xi_0 = 0.3125$ [Hz]. Finally, signal processing as in Appendix B.1 is applied to each measurement set, yielding a typical output spectrum as depicted in Figure 2.8a.

Figure 2.8a shows that nonlinear effects have an average level that is 10 [dB] lower than the power generated in the output spectrum by the BLA of the system. Analysis of the non-excited lines shows that the nonlinearities have both an odd and even nature, but the odd components dominate by almost 20 [dB]. Furthermore, it becomes clear that the variation due to nonlinearities is of the same order of magnitude as the odd nonlinearities that are detected. Finally the variation due to process and / or measurement noise is almost 30 [dB] lower than the variation due to nonlinear effects.

Figure 2.8b depicts the BLA of the system as a function of both the rms value and frequency of the input. This figure indicates that for high input power, the system behaves more linear. This becomes clear from the fact that both the gradient $\partial|\mathfrak{B}_u|/\partial u_{rms}$ and the value of the variation due to nonlinear influences decreases relative to the BLA of the gain of the system for increasing input power.



(a) Output spectrum of a typical multisine experiment. (—) output spectrum $\check{\Psi}_F$, (--- dark grey) variance due to nonlinearities σ_{Ψ} , (--- light grey) variance due to noise ($\sigma_{\mathcal{N}}$). Power detected at non-excited lines $\mathcal{P}(\ell_{o/e})$: (+) odd lines, (x) even lines.



(b) BLA for different excitation levels.

Figure 2.8: Estimated output spectrum and BLA for different excitation levels.

2.5 Comparison

In this section a comparison between the different frequency domain models and the corresponding signal and system classes is provided. First, the different system and signal classes for which the models are defined and compared. Next, a qualitative comparison between the frequency domain models is provided yielding an overview of the applicability of the different models and the nonlinear effects that can be detected using each of the model types. Finally, Table 2.6 on p. 35 presents an overview of the relevant literature related each of the models considered in this chapter.

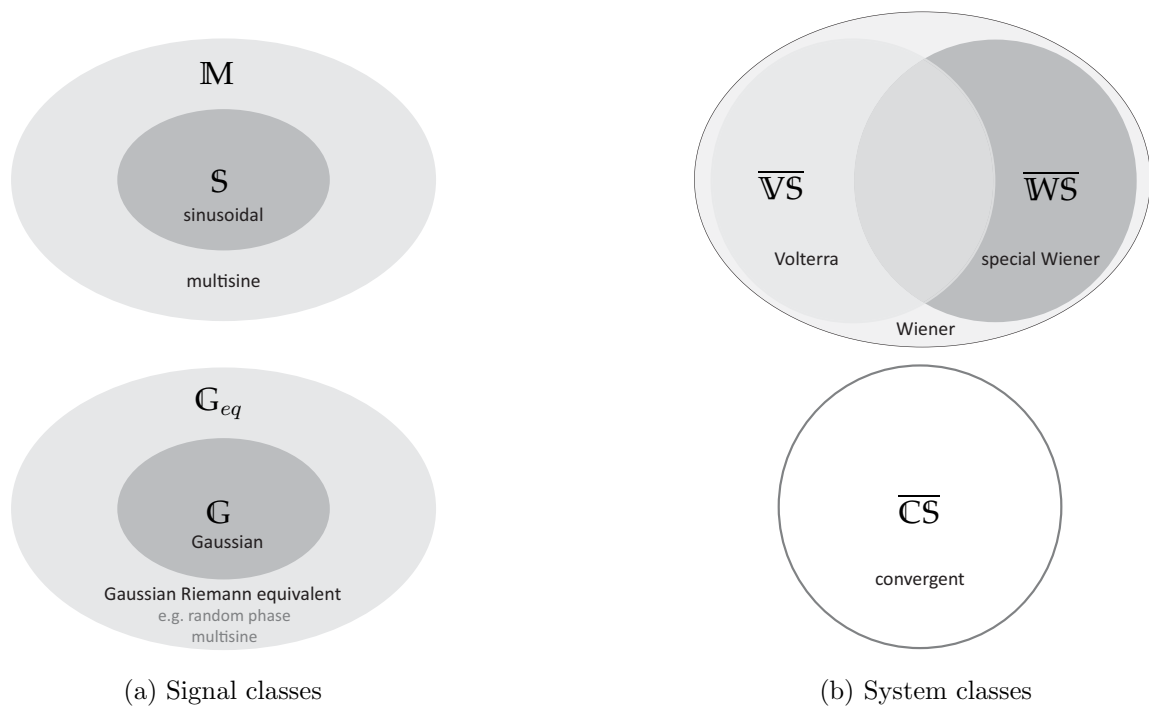


Figure 2.9: Comparison of the system and signal classes.

System and Signal Classes

In Figure 2.9 an overview of the signal and system classes discussed in this chapter is provided. Both random and deterministic signals are considered. The relation between different signal classes is straightforward. By definition, the class of sinusoidal signals (Definition 1.5) is a subset of the class of multisine signals (Definition 1.4). Similarly, the class of Gaussian signals (Definition 1.3) is a subset of the class of Gaussian Riemann equivalent signals (Definition 2.10).

Next, consider the comparison of the different system classes depicted in Figure 2.9b. The classes of Volterra and special Wiener systems can directly be compared as both prescribe the same type of mathematical model. The classes of Volterra and special Wiener systems partially overlap, but neither is a subset of the other, e.g. Volterra systems with discontinuous Fourier transforms are in the class of special Wiener systems. The class of Wiener systems includes the classes of Volterra and special Wiener systems as the continuity condition on the Fourier transform is relaxed in this case.

The class of convergent systems can not be easily related to the classes of Volterra and special Wiener systems. Convergence is a property of a state space realization of a system and concerns the existence and stability of a unique limit solution of the nonlinear system. This requires the definition of initial conditions and a well defined notion of a limit solution solution. As the Volterra series does not include the definition of an initial condition it can not straightforwardly be related to the notion of convergence.

| system | signal | deterministic | | random |
|--|--------|------------------------|---------------|--|
| | | S (sinusoidal) | M (multisine) | \mathbf{G}_{eq} (Gaussian Riemann eq.) |
| $\overline{\mathbf{V}}\mathbf{S}$ (Volterra) | | GFRF GDF SIDF | GFRF GDF | GFRF |
| $\overline{\mathbf{W}}\mathbf{S}$ (special Wiener) | | SIDF | | BLA |
| $\overline{\mathbf{C}}\mathbf{S}$ (convergent) | | HOSIDF NFRF SIDF | | |

Table 2.3: Model types ordered by signal and system class (according to definitions used in references).

In Boyd and Chua (1985) a concept similar to convergence, called Fading Memory (FM), is introduced. On the one hand, convergence relates to the existence, stability and uniqueness of a steady state solution, which is independent of initial conditions and therefore convergence is concerned with the input to state properties of a state space realization. FM, on the other hand, relates to the dependence of the steady state solution on the input signals themselves and is concerned with the input to output properties of an operator. For an operator that has a realization of some sort, the notion of FM may allow to prove the existence of a unique steady state solution for a subset of input signals and initial conditions (Boyd and Chua, 1985). However, the following two arguments illustrate why FM and convergence are not equivalent. First of all, an operator may not have a state space realization (1.3). Hence, even if an operator has FM, a state space realization may not exist, such that convergence cannot be claimed. Secondly, a operator which has a realization (1.3) that includes unstable non-observable dynamics may still have FM. However, the corresponding realization cannot be convergent.

Frequency Domain Models

This section concludes the chapter by providing a comparison of the frequency domain methods for nonlinear systems considered. First, consider the overview presented in Table 2.3. This table depicts the applicability of each model type for each combination of input signal and class of nonlinear systems. For all model types, apart from the SIDF^2 (see p. 21), the definitions used in literature are used to generate Table 2.3. The GFRF is applicable for all signal types considered, but is limited to modeling Volterra systems. The corresponding GDF is applicable to Volterra systems as well, but valid for multisine inputs only. For convergent systems the HOSIDF and NFRF allow to model the systems dynamics, but these are restricted to sinusoidal inputs. The SIDF can be computed for all system classes considered in this chapter, but is restricted to sinusoidal inputs as well. Finally, the BLA when considered under the conditions in Lemma 2.1, is defined for special Wiener systems subject to Gaussian Riemann equivalent signals.

| model | information | excited frequencies | | non-excited frequencies | |
|-------------|--------------|---------------------|-------|-------------------------|-------|
| | | gain | phase | gain | phase |
| GFRF | | + | + | + | + |
| NFRF | NS/OFRF | + | + | + | + |
| | NL Bode plot | + | – | – | – |
| DF | SIDF | + | + | – | – |
| | GDF | + | + | – | – |
| | HOSIDF | + | + | + | + |
| BLA | | + | + | ± | – |

Table 2.4: Overview of the information available from different models. (+ available, ±: can be partially recovered, but additional analysis required, – information not available.)

Moreover, Table 2.4 provides an overview of the information present in each model type. To fully reconstruct the response of a nonlinear system to a given input signal the corresponding model needs to model both the response at excited and non excited frequencies and both phase and gain information needs to be recoverable from the model. This is the case for the GFRF and this model therefore allows to fully reconstruct the response of a given Volterra system to a class of input signals. The HOSIDF and NFRF also allow to fully reconstruct the steady state response of a uniformly convergent system to any given sinusoidal input signal although the representation of the nonlinear dynamics in both model types is different. However, the nonlinear Bode plot corresponding to the NFRF does not allow to reconstruct the full response as all phase information is lost in this representation. Finally, the SIDF, GDF and BLA do not allow to fully reconstruct the output of a nonlinear system as information about spectral components at non-excited frequencies is not available in these models.

Finally, Table 2.5 presents an overview of the ability of the different models to detect the effects of nonlinearities introduced in Table 2.1. As becomes clear, all methods considered here are able to detect gain compression and expansion. Detection of desensitization however, requires multi-tone inputs and detection at excited spectral lines. Hence, only the GFRF, GDF and BLA are able to detect desensitization. To detect intermodulation, multi-tone inputs are also required, but detection must appear at non-excited spectral lines as well. Hence, the GFRF is able to capture intermodulation and the signal processing related to the BLA can be adapted to detect intermodulation. For the detection of higher harmonics a sinusoidal excitation suffices, but detection must appear at non-excited harmonic spectral lines as captured in the HOSIDF. Moreover, the GFRF models the generation of harmonics and these can be detected by adapting the signal processing related to the BLA as well. Finally, the appearance of harmonics in the systems output are captured by the NFRF, but the effects of gain compression / expansion and the generation of harmonics are hard to distinguish in the corresponding nonlinear Bode plot.

In the preceding sections an overview and comparison of four main approaches

| | GFRF | NFRF | DF | | | BLA |
|------------------------------|------|------|------|-----|--------|-----|
| | | | SIDF | GDF | HOSIDF | |
| gain compression & expansion | + | + | + | + | + | + |
| desensitization | + | - | - | + | - | + |
| intermodulation | + | - | - | - | - | ± |
| harmonics | + | + | - | - | + | ± |

Table 2.5: Effects of nonlinearities visualized by different models. (+ visible, ±: detectable, but additional analysis required, - not visible.)

to the frequency domain analysis of nonlinear systems was presented. To conclude this chapter, a discussion concerning the application of the different methods is presented. The following reflects the personal opinion of the author and may serve as a guideline for those seeking to use any of the frequency domain methods discussed in this chapter.

First of all, the GFRF provides a useful tool for the analysis of Volterra systems and allows model the response to an extensive class of input signals. However, the practical application of the GFRF is limited as identification of high order kernels / GFRFs is difficult. Moreover, even if a model is known, the GFRF may be used for prediction, but the model structure is complex, which limits application to practical analysis or control design. Secondly, the nonlinear Bode plot provides means to assess the gain of a nonlinear system and may be used for sensitivity analysis as well (van de Wouw et al., 2008). However, this model is only valid for sinusoidal inputs and the corresponding NFRF can be hard to identify in practice.

Thirdly, the HOSIDF are easily identifiable and provide a fast method to assess nonlinear effects in practice. However, although the HOSIDF provide some means to assess performance degrading nonlinear effects (see Chapter 5), this model is valid for sinusoidal inputs only. This limits their (real-time) application when non sinusoidal inputs are required. Finally, the BLA provides means to attain a well defined linear approximation of the nonlinear dynamics as well as a measure of the quality of this linear approximation. This yields a useful method to identify LTI approximations of weakly nonlinear systems. However, if severe nonlinearities are present or small nonlinearities negatively influence the performance of the system, the BLA provides insufficient information to address or model these effects.

Summarizing, if an LTI approximation of the systems dynamics is required, identification of the BLA is recommended as it is easy to identify, yields a widely valid linear approximation and provides a corresponding quality measure. If more information about the nonlinear behavior is required, the nonlinear Bode plot allows for a gain and sensitivity analysis of the nonlinear system. Finally, if even more information about the nonlinearity is required, the HOSIDFs provide gain and phase information about the nonlinear behavior, allowing analysis and control of the nonlinear effects.

Table 2.6: Suggested references for each research area.

| | Background | Introduction | Analysis | Applications |
|------|---|--|--|--|
| GFRF | Volterra (1887, 1959) Wiener (1942) George (1959) Eykhoff (1974) Schetzen (1980) Rugh (1981) | Yue et al. (2005a) | Yue et al. (2005a) Jing et al. (2006) Lang et al. (2007) | Billings and Tsang (1989a) Billings and Tsang (1989b) Billings et al. (1990) |
| NFRF | Pavlov et al. (2006) | Pavlov et al. (2007b) | Pavlov et al. (2007c) Pavlov and van de Wouw (2008) | van de Wouw et al. (2008) Heertjes et al. (2010) |
| DF | Gelb and Vander Velde (1968) | Gelb and Vander Velde (1968) Peyton Jones and Billings (1990) Nuij et al. (2006) | Peyton Jones and Billings (1991) Nuij et al. (2008b) Rijlaarsdam et al. (2011) | Nuij et al. (2008a) Nuij et al. (2008c) |
| BLA | Pintelon and Schoukens (2012) | Pintelon and Schoukens (2012) | Schoukens et al. (1998) Pintelon and Schoukens (2002) Schoukens et al. (2005) Dobrowiecki and Schoukens (2007) Schoukens et al. (2009) | Pintelon et al. (2004b) D'haene et al. (2005) Rijlaarsdam et al. (2010) |

Chapter 3

Frequency Domain Analysis of Block Structured Nonlinear Systems[†]

When analyzing and modeling nonlinear dynamical systems in the frequency domain, the effects of nonlinearities need to be taken into account. To further investigate the application of frequency domain methods to nonlinear systems an analysis of block structured systems with polynomial nonlinearities is provided in this Section. Specifically, an analysis of static polynomial mappings subject to a sinusoidal input is presented, which provides insight in the effects of such nonlinearities in the frequency domain. These results are then utilized to derive a connection between the GFRF (Definition 2.2) and HOSIDF (Definition 2.8).

First, in Section 3.1, new analytical results are presented that allow for spectral analysis of the dynamics of nonlinear systems consisting of separable LTI and nonlinear components. A mapping from the parameters defining the LTI dynamics and polynomial nonlinearities to the output spectrum and HOSIDFs is derived. Second, in Section 3.2, these results are used to connect two different frequency domain models for nonlinear systems: the GFRF and the HOSIDF. Necessary and sufficient conditions for this novel relation to exist are provided as well as a numerically efficient procedure to compute the HOSIDF from the GFRF and *vice versa*. All theoretical results are accompanied by illustrative analytical and numerical examples.

[†]The results presented in this chapter are published in:

D. Rijlaarsdam, P. Nuij, J. Schoukens and M. Steinbuch, Spectral analysis of block structured nonlinear systems and higher order sinusoidal input describing functions, *Automatica*, 47(12):2684-2688, 2011

D. Rijlaarsdam, T. Oomen, P. Nuij, J. Schoukens and M. Steinbuch, Uniquely connecting frequency domain representations of given order polynomial Wiener-Hammerstein systems, *prov. accepted*

3.1 Frequency Domain Analysis of Polynomial Nonlinearities

The analysis presented in the following deals with the frequency domain analysis of systems with polynomial nonlinearities. These results contribute to the analysis of the effects of nonlinearities by supplying new analytic results that provide an analytic relation between the parameters of the nonlinear system and the input-output dynamics in the frequency domain. The analysis focuses on sinusoidal excitation signals and yields an intuitive insight into the effect of polynomial nonlinearities in the frequency domain. First, in Section 3.1, the application of trigonometric analysis to static polynomial nonlinearities is shown to yield a mapping from the parameters defining the nonlinearity and input signal to the output spectrum. This constitutes the main result of this section and is summarized in Theorem 3.1. Next, these results are extended to dynamical systems which yields an analytic expression for the corresponding HOSIDFs.

Spectral Analysis of Polynomial Nonlinearities

Consider a static polynomial nonlinearity of degree P :

$$y(t) = \sum_{p=1}^P \alpha_p u^p(t) \quad (3.1)$$

with $u(t)$, $y(t) \in \mathbb{R}$ the input and output of the system and $\alpha_p \in \mathbb{R}$ the polynomial coefficients. Next, an analysis of the output spectrum of (3.1) is presented when the system is subject to the following sinusoidal input:

$$u(t) = \gamma \cos(2\pi\xi_0 t + \varphi_0) \quad (3.2)$$

with γ , $\varphi_0 \in \mathbb{R}$ the amplitude and phase and $\xi_0 \in \mathbb{R}_{>0}$ the frequency of the input signal in [Hz]. If (3.1) is subject to (3.2), the output spectrum consists solely of higher harmonics $k\xi_0$, $k = 0, 1, 2, \dots$ of the input frequency, i.e.

$$y(t) = \sum_{p=1}^P \alpha_p \gamma^p \cos^p(2\pi\xi_0 t + \varphi_0) = \sum_{k=0}^P A_k(\gamma) \cos(2\pi k\xi_0 t + \phi_k(\varphi_0)) \quad (3.3)$$

with $A_k(\gamma)$, $\phi_k(\varphi_0) \in \mathbb{R}$ the amplitude and phase of the k^{th} harmonic component. Next, the power series in (3.3) is rewritten to the sum of sinusoids using the following relationship (Gradshteyn and Ryzhik, 2000):

$$\cos^{2n-\sigma}(x) = \frac{1}{2^{2n-1-\sigma}} \left\{ (1-\sigma) \binom{2n}{n} + \sum_{m=0}^{n-1} \binom{2n-\sigma}{m} \cos((2(n-m)-\sigma)x) \right\} \quad (3.4)$$

with $n \in \mathbb{N}_{\geq 1}$, $\sigma \in \{0, 1\}$ and the binomial coefficient such that $\binom{a}{b} = \frac{a!}{b!(a-b)!} \forall a, b \in \mathbb{N}$, $0 \leq b \leq a$ and 0 otherwise. Applying (3.4) to each of the terms on the left hand

side of (3.3) and taking the Fourier transform (1.4) yields::

$$\begin{aligned} \text{FT}\{\alpha_p \gamma^p \cos^p(\cdot)\} &= \alpha_p \gamma^p (1 - \sigma_p) \frac{n}{2^{2n}} \binom{2n}{n} \delta(0) \\ &+ \frac{\alpha_p \gamma^p}{2^{2n-\sigma_p}} \sum_{m=0}^{n-1} \binom{2n-\sigma_p}{m} (c\delta(\xi - d\xi_0) + c^* \delta(\xi + d\xi_0)) \end{aligned} \quad (3.5)$$

with $\delta(\cdot)$ the Dirac delta function, $\sigma_p = p \bmod 2$, $n = \frac{1}{2}(p + \sigma_p)$, $d = 2(n - m) - \sigma_p \in \mathbb{N}_{\geq 1}$, $c = e^{id\varphi_0} \in \mathbb{C}$ and $*$ the complex conjugate. Next, consider the contribution of all polynomial terms to a spectral component $\mathcal{Y}(k\xi_0)$ by considering terms in (3.5) such that $d = 2(n - m) - \sigma_p = k$, for each power p in (3.1). Summing these contributions over all p yields the spectral components of the single sided spectrum $\mathcal{Y}(\xi) \in \mathbb{C}$ at harmonics $k\xi_0$ of the input frequency:

$$\mathcal{Y}(0) = \sum_{p=1}^P (1 - \sigma_p) \left[\alpha_p \left(\frac{\gamma}{2}\right)^p \binom{p}{\frac{p}{2}} \frac{p}{2} \right] \quad (3.6)$$

$$\mathcal{Y}(k\xi_0) = \sum_{p=1}^P \sigma_{pk} \left[2\alpha_p \left(\frac{\gamma}{2}\right)^p \binom{p}{\frac{p-k}{2}} e^{ik\varphi_0} \right] \quad (3.7)$$

with $k \in \mathbb{N}_{\geq 1}$ and $\sigma_{p(k)}$ defined in Theorem 3.1. This yields the main result of this section: a generalized mapping from the system parameters and the properties of the input signal to the output spectrum.

Theorem 3.1 (polynomial coefficients and output spectra).

Consider a static polynomial mapping (3.1), subject to a sinusoidal input (3.2). Then, the single sided spectrum of the output $y(t)$ is given by the following mapping $\mathbb{R}^P \mapsto \mathbb{C}^{P+1}$, from the polynomial coefficients $\boldsymbol{\alpha}$ to the single sided output spectrum $\mathcal{Y}(\xi)$:

$$Y = \Phi(\varphi_0) \Omega \Gamma(\gamma) \boldsymbol{\alpha} \quad (3.8)$$

where the different components are defined below.

- **output spectrum (vector)** $Y \in \mathbb{C}^{P+1}$: the output spectrum vector $Y = [\mathcal{Y}(0) \ \mathcal{Y}(\xi_0) \ \mathcal{Y}(2\xi_0) \ \dots \ \mathcal{Y}(P\xi_0)]^T$ contains the nonzero spectral lines in the output spectrum, at harmonics of the input frequency.
- **input phase matrix** $\Phi(\varphi_0) \in \mathbb{C}^{(P+1) \times (P+1)}$: the input phase matrix relates the phase of the input signal to the output spectrum and is defined as $\Phi_{k+1, k+1}(\varphi_0) = e^{ik\varphi_0}$, $k = 0, 1, 2, \dots, P$ and 0 otherwise.
- **input gain matrix** $\Gamma(\gamma) \in \mathbb{R}^{P \times P}$: the input gain matrix relates the amplitude of the input signal to the output spectrum and is defined as $\Gamma_{p,p}(\gamma) = \left(\frac{\gamma}{2}\right)^p$, $p = 1, 2, \dots, P$ and 0 otherwise.

- **inter-harmonic gain matrix** $\Omega \in \mathbb{R}^{(P+1) \times P}$: the inter-harmonics gain matrix relates the spectral content of the input and output spectrum and is defined as:

$$\begin{aligned}\Omega_{1,p} &= (1 - \sigma_p) \binom{p}{\frac{p}{2}} \frac{p}{2} \\ \Omega_{k+1,p} &= 2 \binom{p}{\frac{p-k}{2}} \sigma_{pk} \quad \forall k \leq p \text{ and } k = 1, 2, \dots, P\end{aligned}$$

and 0 otherwise. With $\sigma_p = p \bmod 2$, $\sigma_k = k \bmod 2$ and $\sigma_{pk} = \sigma_p \sigma_k + (1 - \sigma_p)(1 - \sigma_k)$.

- **polynomial coefficients** $\alpha \in \mathbb{R}^P$: the coefficient vector $\alpha = [\alpha_1 \ \alpha_2 \ \dots \ \alpha_P]^T$ contains the coefficients of the polynomial nonlinearity.

Proof. (3.8) follows from (3.6) - (3.7) by rewriting the sums to a matrix product. \square

Remark. Equation (3.8) can be interpreted as a generalized output frequency response function (Lang et al., 2007) for static polynomial systems.

Theorem 3.1 allows numerically efficient computation of output spectra of a class of nonlinear systems and provides insight into the mechanisms that generate these spectra. The following example illustrates the application of the theorem.

Example 3.1 (output spectrum).

Consider a polynomial mapping (3.1), with $P = 3$ subject to (3.2). Then, Theorem 3.1 yields the corresponding output spectrum in terms of the system parameters and the parameters of the input signal:

$$Y = \Phi(\varphi_0) \Omega \Gamma(\gamma) \alpha = \begin{bmatrix} 1 & 0 & 0 & 0 \\ 0 & e^{1i\varphi_0} & 0 & 0 \\ 0 & 0 & e^{2i\varphi_0} & 0 \\ 0 & 0 & 0 & e^{3i\varphi_0} \end{bmatrix} \begin{bmatrix} 0 & 2 & 0 \\ 2 & 0 & 6 \\ 0 & 2 & 0 \\ 0 & 0 & 2 \end{bmatrix} \begin{bmatrix} \left(\frac{\gamma}{2}\right)^1 & 0 & 0 \\ 0 & \left(\frac{\gamma}{2}\right)^2 & 0 \\ 0 & 0 & \left(\frac{\gamma}{2}\right)^3 \end{bmatrix}$$

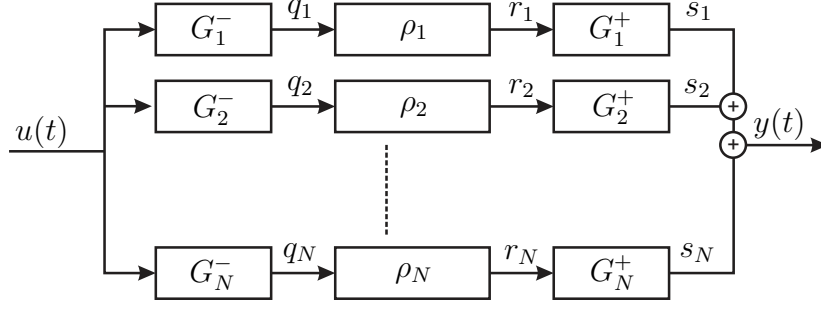
which in turn yields the output spectrum:

$$Y = \begin{bmatrix} \mathcal{Y}(0) \\ \mathcal{Y}(\xi_0) \\ \mathcal{Y}(2\xi_0) \\ \mathcal{Y}(3\xi_0) \end{bmatrix} = \begin{bmatrix} A_0(\gamma) e^{i\phi_0}(\varphi_0) \\ A_1(\gamma) e^{i\phi_1}(\varphi_0) \\ A_2(\gamma) e^{i\phi_2}(\varphi_0) \\ A_3(\gamma) e^{i\phi_3}(\varphi_0) \end{bmatrix} = \begin{bmatrix} \frac{1}{2}\alpha_2\gamma^2 \\ \left(\frac{3}{4}\alpha_3\gamma^3 + \alpha_1\gamma\right) e^{1i\varphi_0} \\ \frac{1}{2}\alpha_2\gamma^2 e^{2i\varphi_0} \\ \frac{1}{4}\alpha_3\gamma^3 e^{3i\varphi_0} \end{bmatrix}$$

Next, the results in Theorem 3.1 are extended to a class of block structured nonlinear dynamical systems.

Analysis of Block Structured Nonlinear Systems

This section presents the analysis of a class of nonlinear systems called parallel Wiener - Hammerstein systems with polynomial nonlinearities as, for example, discussed in Giri and Bai (2010); Schoukens et al. (2011), which are defined as follows.

Figure 3.1: $\overline{\text{LPIL}}$ block structured system.

Definition 3.1 ($\overline{\text{LPIL}}$: block structures).

Consider an N -branch, block structured configuration as depicted in Figure 3.1. Each branch consists of a series connection of an LTI block $G_n^-(\xi)$, a static nonlinear mapping ρ_n and another LTI block $G_n^+(\xi)$. The system has one input $u(t) \in \mathbb{R}$, one output $y(t) \in \mathbb{R}$ and intermediate signals $q_n(t)$, $r_n(t)$ and $s_n(t)$. The nonlinearity $\rho_n : \mathbb{R} \mapsto \mathbb{R}$ is a static, polynomial mapping of degree P_n :

$$\rho_n : r_n(t) = \sum_{p=1}^{P_n} \alpha_p^{[n]} q_n^p(t) \quad (3.9)$$

with $\alpha_p^{[n]} \in \mathbb{R}$. If $G_n^-(\xi) = 1$ or $G_n^+(\xi) = 1 \forall n \in \mathbb{N}_{\geq 1}$, the remaining $\overline{\text{PIL}}$ or $\overline{\text{LP}}$ system equals a parallel Hammerstein or Wiener system with polynomial nonlinearities.

The output spectrum of an $\overline{\text{LPIL}}$ systems, subject to (3.2), follows from Theorem 3.1. Consider the input $u(t)$ as it passes through the first linear block $G_n^-(\xi)$. The filtered signal $q_n(t)$ then serves as an input for the nonlinear block ρ_n , which yields the corresponding output spectrum R_n .

$$R_n(\xi_0, \varphi_0) = \Phi(\varphi_0 + \angle G_n^-(\xi_0)) \Omega \Gamma(\gamma |G_n^-(\xi_0)|) \boldsymbol{\alpha}^{[n]}$$

Next, each signal $r_n(t)$ is modified by the corresponding (second) linear block $G_n^+(\xi)$, which yields the output spectrum of the n^{th} branch:

$$\mathcal{S}_n(\xi_0, \varphi_0) = \Delta(\xi_0) G_n^+(\xi) \Phi(\varphi_0 + \angle G_n^-(\xi_0)) \Omega \Gamma(\gamma |G_n^-(\xi_0)|) \boldsymbol{\alpha}^{[n]} \quad (3.10)$$

where $\Delta(\xi_0)$ is defined in Lemma 3.1, which yields an analytic description of the output spectrum of an $\overline{\text{LPIL}}$ system.

Lemma 3.1 (spectrum of $\overline{\text{LPIL}}$ systems).

Consider an $\overline{\text{LPIL}}$ system subject to a sinusoidal input (3.2). Then, the output spectrum of this system equals:

$$Y(\xi_0, \gamma, \varphi_0) = \sum_{n=1}^N \Delta(\xi_0) G_n^+(\xi) \Phi(\angle G_n^-(\xi_0)) \Omega \Gamma(\gamma |G_n^-(\xi_0)|) \boldsymbol{\alpha}^{[n]} \quad (3.11)$$

with $\Delta(\xi_0) = \text{diag}([\delta(\xi - 0) \delta(\xi - \xi_0) \delta(\xi - 2\xi_0) \dots \delta(\xi - P_n \xi_0)]) \in \mathbb{R}^{(P_n+1) \times (P_n+1)}$ a diagonal matrix of δ -functions, i.e. $\Delta(\xi_0) G_n(\xi) = \text{diag}([G(0) G(\xi_0) G(2\xi_0) \dots G(P_n \xi_0)])$.

Proof. (3.11) follows from summation of (3.10) over all N branches. \square

Lemma 3.1 extends the results in Theorem 3.1 to $\overline{\mathbb{LPI}}$ systems. Next, these results are used to derive an analytical expression for the corresponding HOSIDFs.

Higher Order Sinusoidal Input Describing Functions

In Nuij et al. (2006) the output of a class of nonlinear systems, subject to a sinusoidal input (3.2) is considered. This output is composed of K harmonics of the input frequency and is given by:

$$y(t) = \sum_{k=0}^K |\mathfrak{H}_k(\xi_0, \gamma)| \gamma^k \cos(k(2\pi\xi_0 t + \varphi_0) + \angle \mathfrak{H}_k(\xi_0, \gamma))$$

where $\mathfrak{H}_k(\xi_0, \gamma) \in \mathbb{C}$ is the k^{th} order HOSIDF (Definition 2.8) which describes the response (gain and phase) at harmonics of the excitation frequency ξ_0 . Using Definition 2.8 and Lemma 3.1 the HOSIDFs of $\overline{\mathbb{LPI}}$ systems are analytically related to the system and input signal parameters, i.e.

Lemma 3.2 (HOSIDFs of $\overline{\mathbb{LPI}}$ systems).

Consider an $\overline{\mathbb{LPI}}$ system subject to a sinusoidal input (3.2). Then, the HOSIDFs of the system are given by:

$$H(\xi_0, \gamma) = \Upsilon^{-1} \sum_{n=1}^N \Delta(\xi_0) G_n^+(\xi) [\Phi(\angle G_n^-(\xi_0)) \Omega \Gamma(|G_n^-(\xi_0)| \gamma) \alpha^{[n]}] \quad (3.12)$$

with $H(\xi_0, \gamma) = [\mathfrak{H}_0(\xi_0, \gamma) \ \mathfrak{H}_1(\xi_0, \gamma) \ \mathfrak{H}_2(\xi_0, \gamma) \ \dots \ \mathfrak{H}_{\max_n P_n}(\xi_0, \gamma)]^T$ and the gain compensation matrix such that $\Upsilon_{k+1, k+1}(\gamma) = \gamma^k, k = 0, 1, 2, \dots, \max_n P_n$ and 0 otherwise.

Proof. see Appendix A.1.1 \square

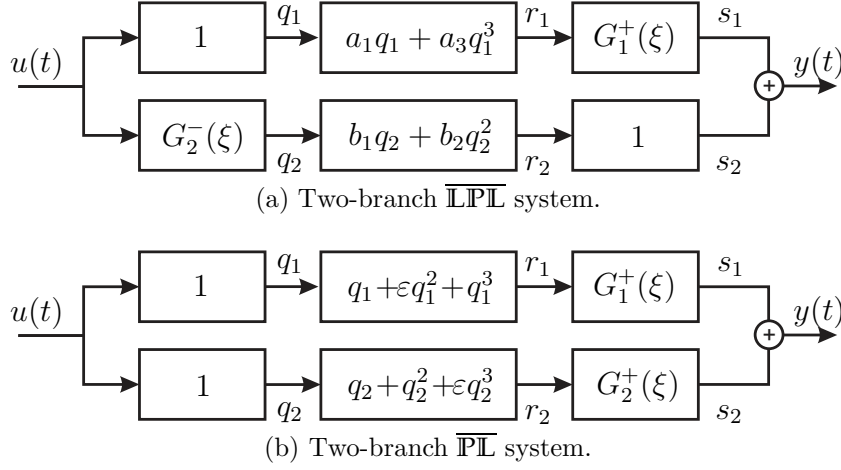
Remark. The results in Lemma 3.2 show that the HOSIDFs of $\overline{\mathbb{LPI}}$ systems are independent of the phase of the input signal.

Hence, using Theorem 3.1 the system parameters of $\overline{\mathbb{LPI}}$ systems can be analytically related to the input-output dynamics in the frequency domain as shown in Lemma 3.1 and Lemma 3.2. Moreover, for $\overline{\mathbb{PI}}$ systems, a subclass of $\overline{\mathbb{LPI}}$ systems, a set of amplitude independent basis functions that fully describe the corresponding HOSIDFs exists. These are referred to as the fundamental HOSIDF and allow to separate amplitude and frequency effects in this describing function, i.e.

Definition 3.2 ($\mathfrak{F}_p(\xi)$): fHOSIDFs of $\overline{\mathbb{PI}}$ systems).

Consider a $\overline{\mathbb{PI}}$ system subject to a sinusoidal input (3.2). Then, the Fundamental Higher Order Sinusoidal Input Describing functions (fHOSIDF) $\mathfrak{F}_p(\xi) \in \mathbb{C}$ of a $\overline{\mathbb{PI}}$ are defined as:

$$\mathfrak{F}_p(\xi_0) = \sum_{n=1}^N G_n^+(\xi_0) \alpha_p^{[n]} \quad (3.13)$$

Figure 3.2: Two examples of $\overline{\text{LPL}}$ systems.

The *fHOSIDFs* as defined in (3.13) constitute a set of amplitude independent basis functions for the *HOSIDFs* and provide decoupling of amplitude and frequency effects as well, i.e.

$$H(\xi_0, \gamma) = [\Upsilon^{-1}(\gamma)\Delta(\xi_0)\Omega\Gamma(\gamma)]F(\xi_0)$$

where the *fHOSIDFs* are collected in $F(\xi) = [\mathfrak{F}_1(\xi_0)\mathfrak{F}_2(\xi_0)\dots\mathfrak{F}_{\max P_n}(\xi_0)]^T$.

To conclude this section, two examples are provided illustrating the application of the preceding results. First, an analytic expression for the output spectrum and the *HOSIDF* for an $\overline{\text{LPL}}$ system is presented in Example 3.2. Secondly, Example 3.3 concludes this section by providing an analysis and visualization of the dynamics of a $\overline{\text{PL}}$ system.

Example 3.2 (spectrum and *HOSIDFs* of $\overline{\text{LPL}}$ systems).

Consider the two branch $\overline{\text{LPL}}$ system depicted in Figure 3.2a, subject to (3.2). Application of Lemma 3.1 yields the analytic expression for the output spectrum:

$$\begin{aligned} Y(\xi_0, \gamma, \varphi_0) &= \Delta(\xi_0)G_1^+(\xi)\Phi(\varphi_0)\Omega\Gamma(\gamma)\boldsymbol{\alpha}^{[1]} + \Delta(\xi_0)\Phi(\varphi_0 + \angle G_2^-)\Omega\Gamma(\gamma|G_2^-|)\boldsymbol{\alpha}^{[2]} \\ &= \begin{bmatrix} \frac{b_2\gamma^2}{2}|G_2^-(\xi_0)|^2 \\ \gamma \left[(a_1 + \frac{3}{4}a_3\gamma^2)G_1^+(\xi_0) + b_1G_2^-(\xi_0) \right] e^{i\varphi_0} \\ \frac{b_2\gamma^2}{2}[G_2^-(\xi_0)]^2 e^{2i\varphi_0} \\ \frac{a_3\gamma^3}{4}G_1^+(3\xi_0) e^{3i\varphi_0} \end{bmatrix} \end{aligned}$$

The corresponding *HOSIDFs* are computed using Lemma 3.2 and require neither computation of the output spectrum, nor knowledge of the phase of the input signal, i.e.

$$H(\xi_0, \gamma) = \begin{bmatrix} \mathfrak{H}_0(\xi_0, \gamma) \\ \mathfrak{H}_1(\xi_0, \gamma) \\ \mathfrak{H}_2(\xi_0, \gamma) \\ \mathfrak{H}_3(\xi_0, \gamma) \end{bmatrix} = \begin{bmatrix} \frac{b_2\gamma^2}{2}|G_2^-(\xi_0)|^2 \\ \left[(a_1 + \frac{3}{4}a_3\gamma^2)G_1^+(\xi_0) + b_1G_2^-(\xi_0) \right] \\ \frac{b_2}{2}(G_2^-(\xi_0))^2 \\ \frac{a_3}{4}G_1^+(3\xi_0) \end{bmatrix}$$

Example 3.3 (spectral analysis of $\overline{\mathbb{P}\mathbb{L}}$ systems).

Consider the $\overline{\mathbb{P}\mathbb{L}}$ system depicted in Figure 3.2b, which is an $\overline{\mathbb{L}\mathbb{P}\mathbb{L}}$ system with $N = 2$, $\boldsymbol{\alpha}^{[1]} = [1 \ \varepsilon \ 1]^T$, $\boldsymbol{\alpha}^{[2]} = [1 \ 1 \ \varepsilon]^T$ and $G_n^-(\xi) = 1, n = 1, 2$. First, Definition 3.2 is applied, which yields analytic expressions for the fHOSIDFs of this system as given below:

$$F(\xi) = \begin{bmatrix} \mathfrak{F}_1(\xi) \\ \mathfrak{F}_2(\xi) \\ \mathfrak{F}_3(\xi) \end{bmatrix} = \begin{bmatrix} G_1^+(\xi) + G_2^+(\xi) \\ \varepsilon G_1^+(\xi) + G_2^+(\xi) \\ G_1^+(\xi) + \varepsilon G_2^+(\xi) \end{bmatrix} \quad (3.14)$$

The HOSIDFs of this system follow from Lemma 3.2 and Definition 3.2 and equal.

$$H(\xi, \gamma) = \begin{bmatrix} \frac{\gamma^2}{2} \mathfrak{F}_2(0) \\ \mathfrak{F}_1(\xi) + \frac{3\gamma^2}{4} \mathfrak{F}_3(\xi) \\ \frac{1}{2} \mathfrak{F}_2(2\xi) \\ \frac{1}{4} \mathfrak{F}_3(3\xi) \end{bmatrix} = \begin{bmatrix} \frac{\gamma^2}{2} (\varepsilon G_1^+(0) + G_2^+(0)) \\ G_1^+(\xi) + G_2^+(\xi) + \frac{3\gamma^2}{4} (G_1^+(\xi) + \varepsilon G_2^+(\xi)) \\ \frac{1}{2} (\varepsilon G_1^+(2\xi) + G_2^+(2\xi)) \\ \frac{1}{4} (G_1^+(3\xi) + \varepsilon G_2^+(3\xi)) \end{bmatrix} \quad (3.15)$$

Now, consider again the system depicted in Figure 3.2b, with $\xi = 0$ and define $G_1^+(\xi)$ as a bandpass filter, such that $|G_1^+(\xi)| = 1 \ \forall \ \xi \in f_1$ and 0 otherwise. Furthermore, define $G_2^+(\xi)$ as a bandstop filter, such that $|G_2^+(\xi)| = 0 \ \forall \ \xi \in f_2$ and 1 otherwise. Finally, define the sets $f_1 = [\xi_1^- \ \xi_1^+]$, $f_2 = [\xi_2^- \ \xi_2^+]$ and assume that the bandstop and bandpass filters overlap.

First, consider the relation between the second and third (f)HOSIDFs, the LTI dynamics and the polynomial nonlinearities in (3.14) - (3.15). Substituting $\varepsilon = 0$ yields that $\mathfrak{F}_2(\xi) = G_2^+(\xi)$ and $\mathfrak{F}_3(\xi) = G_1^+(\xi)$. The corresponding HOSIDFs $\mathfrak{H}_2(\xi)$, $\mathfrak{H}_3(\xi)$ equal the same LTI dynamics, scaled in magnitude by appropriate constants and contracted in ξ (Figure 3.3a). Second, consider the effect of the nonlinearities on the first (f)HOSIDF. As all fHOSIDFs, $\mathfrak{F}_1(\xi)$ is an amplitude independent, linear combination of the LTI dynamics as depicted in Figure 3.3b. Moreover, in this example the second and third HOSIDF $\mathfrak{H}_2(\xi)$, $\mathfrak{H}_3(\xi)$ are independent of the excitation level as well. However, (3.15) yields that $\mathfrak{H}_1(\xi)$ is amplitude dependent if $G_1^+(\xi) \neq 0$. This is illustrated in Figure 3.3c where the amplitude dependency is present only for $\xi \in f_1$. Furthermore, note that the amplitude dependency $|\mathfrak{H}_1(\xi)| \propto \gamma^2$, $\gamma \gg 1$ which is predicted by (3.15) can be observed from Figure 3.3c as well.

Hence, the third order term in ρ_1 has two distinct effects on the systems dynamics, when analyzed in the frequency domain. First of all, harmonics are generated according to a scaled bandpass filter that analytically relates to the corresponding LTI dynamics. Second, an amplitude dependent response is observed at the base frequency within the frequency range on which the original bandpass filter acts. Finally, similar effects can be observed for the bandstop filter $G_2^+(\xi)$ and the related HOSIDFs $\mathfrak{H}_0(\xi)$ and $\mathfrak{H}_2(\xi)$.

The results presented in Theorem 3.1, Lemma 3.1 and Lemma 3.2 yield new, efficient analytical tools that allow spectral analysis of the output of a class of nonlinear systems. This provides insight in the dynamics of block structured dynamical systems

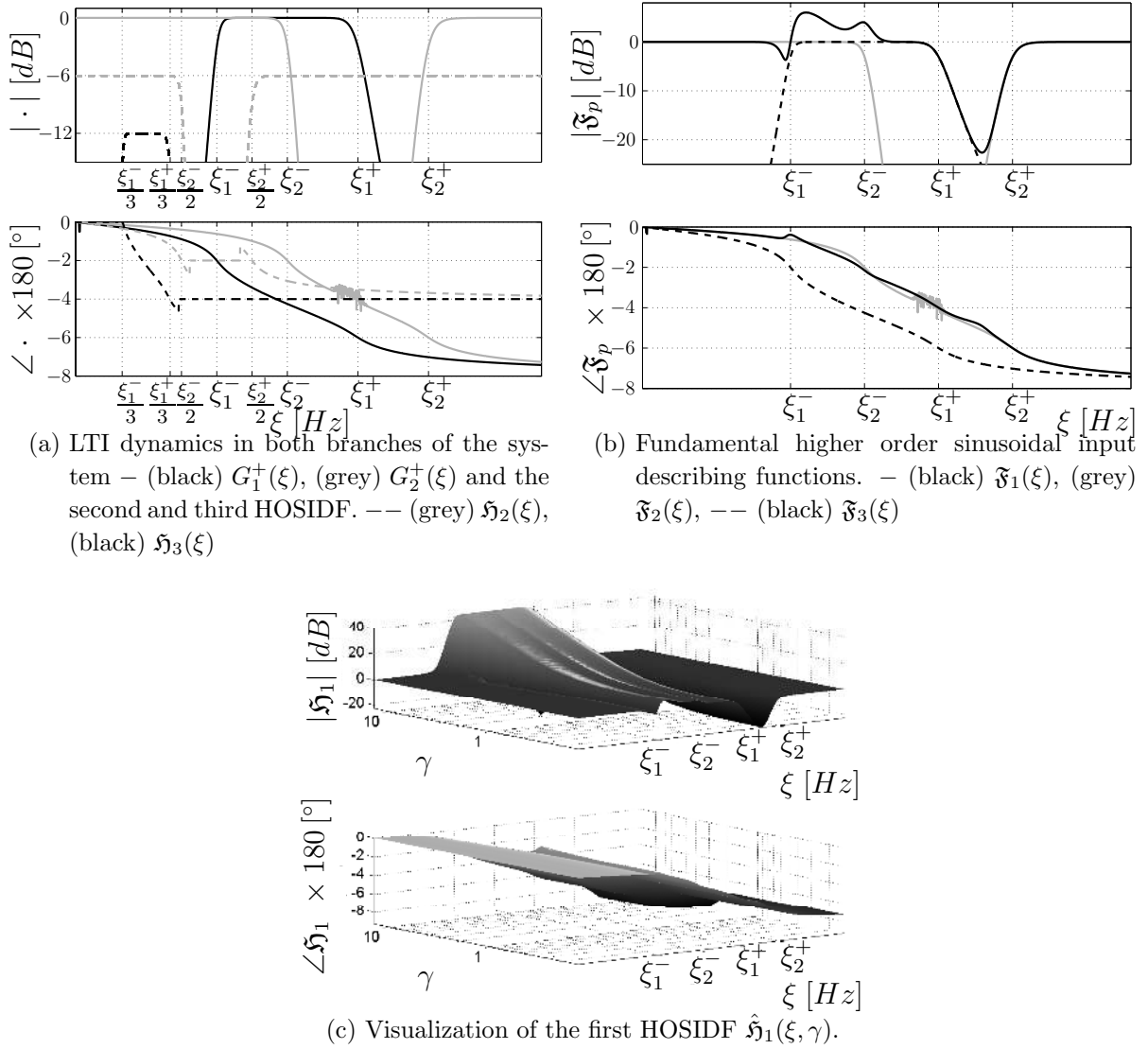
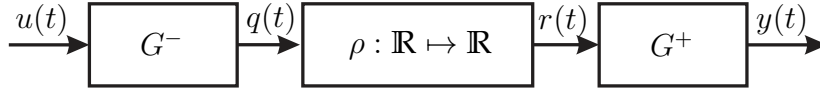


Figure 3.3: LTI dynamics and (f)HOSIDFs of the system in Figure 3.2b.

and allows analytic description and analysis of the corresponding HOSIDFs. Given the systems linear dynamics, the output spectra and HOSIDFs can be described as a simple polynomial function, which is linear in the parameters defining the nonlinearity. Moreover, these results allow to derive an analytical mapping between the HOSIDFs and GFRFs (see Chapter 2) for a subclass of $\overline{\text{LPL}}$ systems. This analysis is presented in the next section.

3.2 Uniquely Connecting Frequency Domain Representations of Block Structured Nonlinear Systems

Although seemingly different approaches have been independently developed to analyze and model nonlinear systems in the frequency domain, the differences and equivalences

Figure 3.4: $\overline{\text{PWH}}$ system.

between alternative methods have not yet been established. In this section an explicit, analytical relation between the GFRF and HOSIDF is established using the results derived in Section 3.1. Apart from providing valuable insight in the mechanisms that generate the HOSIDFs and GFRFs, these results allow to formalize statements on uniqueness and equivalence of both model types. Finally, they yield a numerically efficient analytical relation to compute the GFRF from the HOSIDFs and *vice versa*. First, consider the following subclass of $\overline{\text{LPL}}$ systems, called polynomial Wiener-Hammerstein systems, which is used throughout this section.

Definition 3.3 ($\overline{\text{PWH}}$ Systems).

Consider the system depicted in Figure 3.4, which consists of a series connection of an LTI block $G^-(\xi)$, a static nonlinear mapping $\rho : \mathbb{R} \mapsto \mathbb{R}$ and another LTI block $G^+(\xi)$. The system has one input $u(t) \in \mathbb{R}$, one output $y(t)$ and intermediate signals $q(t)$ and $r(t)$. The nonlinearity ρ is a static, polynomial mapping of degree P , polynomial coefficients $\alpha_p \in \mathbb{R}$ and $p = 1, 2, \dots, P$ and is defined as:

$$\rho : r(t) = \sum_{p=1}^P \alpha_p q^p(t) \quad (3.16)$$

Frequency Response Functions for Nonlinear Systems

In the following, two notions of frequency response functions for nonlinear systems are considered: the GFRF (Definition 2.2) and the HOSIDF (Definition 2.8). The connection between these frequency domain representations for $\overline{\text{PWH}}$ systems is established through their dependence on the model parameters. However, first consider the following intermediate results that yield an analytic relation between the system parameters and the GFRFs and HOSIDFs respectively. For $\overline{\text{PWH}}$ systems the relation between the GFRF and the model parameters is presented in Shanmugam and Jong (1975), i.e.

Lemma 3.3 (GFRF of $\overline{\text{PWH}}$ systems).

Consider a $\overline{\text{PWH}}$ system as in Definition 3.3. Then the p^{th} order GFRF $\mathfrak{F}_p(\varpi_p)$, as in Definition 2.2, is given by:

$$\mathfrak{F}_p(\varpi_p) = \alpha_p \lambda_p(\varpi_p) \quad (3.17)$$

$$\lambda_p(\varpi_p) = G^+ \left(\sum_{\ell=1}^p \varpi_p[\ell] \right) \prod_{\ell=1}^p G^-(\varpi_p[\ell]) \quad (3.18)$$

where $\varpi_p[\ell] = \xi_\ell$ denotes the ℓ^{th} element of $\varpi_p = (\xi_1, \xi_2, \dots, \xi_p)$.

Proof. see (Shanmugam and Jong, 1975) □

Next, consider a similar relation between the system parameters and the HOSIDFs as follows from Theorem 3.1.

Corollary 3.1 (HOSIDFs of $\overline{\mathbb{P}\text{WH}}$ systems).

Consider a $\overline{\mathbb{P}\text{WH}}$ system as in Definition 3.3. Then, the corresponding HOSIDFs of order one and above are given by:

$$\check{H}(\xi_0, \gamma) = \check{\Upsilon}^{-1}(\gamma) \check{\Delta}(\xi_0) G^+(\xi) \left[\check{\Phi}(\angle G^-(\xi_0)) \check{\Omega} \Gamma(|G^-(\xi_0)|\gamma) \boldsymbol{\alpha} \right] \quad (3.19)$$

with $\check{H}(\xi_0, \gamma) = [\check{\mathfrak{H}}_1(\xi_0, \gamma) \ \check{\mathfrak{H}}_2(\xi_0, \gamma) \ \dots \ \check{\mathfrak{H}}_P(\xi_0, \gamma)]^T$ and $\check{\Omega} = T^T \Omega$, $\check{\Phi}(\angle G^-(\xi_0)) = T^T \Phi(\angle G^-(\xi_0)) T$, $\check{\Delta}(\xi_0) = T^T \Delta(\xi_0) T$ and $\check{\Upsilon}(\gamma) = T^T \Upsilon(\gamma) T$. Where, the variables Ω , $\Phi(\cdot)$, $\Delta(\cdot)$ and $\Upsilon(\cdot)$ are defined in Theorem 3.1, Lemma 3.1 and Lemma 3.2. The matrix $T \in \mathbb{R}^{(P+1) \times P}$ is defined such that $T_{m, m-1} = 1$ for $m = 2, 3, \dots, P+1$ and 0 otherwise. Finally, $\Gamma(\gamma)$ and $\boldsymbol{\alpha}$ are defined as in Theorem 3.1.

Proof. Corollary 3.1 follows directly from Theorem 3.1. \square

Connecting the GFRF and HOSIDF

In the following, the GFRFs and HOSIDFs for $\overline{\mathbb{P}\text{WH}}$ systems are explicitly related, which constitutes the main result of this section. Hereto, consider a $\overline{\mathbb{P}\text{WH}}$ system with a polynomial nonlinearity (3.16) of degree P and known linear blocks $G^\pm(\xi)$. Then, using Definition 2.2 and Lemma 3.3, define:

$$\begin{aligned} T &= [\mathfrak{T}_1(\varpi_1) \ \mathfrak{T}_2(\varpi_2) \ \dots \ \mathfrak{T}_P(\varpi_P)]^T \\ \Lambda &= \text{diag}([\lambda_1(\varpi_1) \ \lambda_2(\varpi_2) \ \dots \ \lambda_P(\varpi_P)]) \end{aligned}$$

where $T(\varpi_1, \varpi_2, \dots, \varpi_P) : \mathbb{R} \times \mathbb{R}^2 \times \dots \times \mathbb{R}^P \mapsto \mathbb{C}^P$ contains the GFRFs up to order P and $\Lambda(\varpi_1, \varpi_2, \dots, \varpi_P) : \mathbb{R} \times \mathbb{R}^2 \times \dots \times \mathbb{R}^P \mapsto \mathbb{C}^{P \times P}$ is a diagonal expansion matrix containing the expansion terms $\lambda_p(\varpi_p)$, as in (4.6), that map the LTI dynamics $G^\pm(\xi)$ and polynomial coefficients α_p to the GFRFs $\mathfrak{T}_p(\varpi_p)$. Next, consider the sets $\mathbb{W}_p \subseteq \mathbb{R}^p$, such that:

$$\mathbb{W}_p = \left\{ (\xi_1, \dots, \xi_p) \in \mathbb{R}^p \left| G^+ \left(\sum_{\ell=1}^p \xi_\ell \right) \neq 0 \text{ and } G^-(\xi_\ell) \neq 0 \right. \right\}$$

and define $\mathbb{W} = \mathbb{W}_1 \times \mathbb{W}_2 \times \dots \times \mathbb{W}_P$ and $\boldsymbol{\varpi}_P = \{\varpi_1, \varpi_2, \dots, \varpi_P\}$. The first step in connecting the GFRF and HOSIDF is to relate the polynomial coefficients to the GFRF, see also Lemma 3.3.

Lemma 3.4 (polynomial coefficients & GFRF).

Consider a $\overline{\mathbb{P}\text{WH}}$ system. If and only if $\boldsymbol{\varpi}_P \in \mathbb{W}$, then the following bijective mapping $\mathbb{R}^P \mapsto \mathbb{C}^P$ from the polynomial coefficients to the GFRF exists:

$$T(\boldsymbol{\varpi}_P) = \Lambda(\boldsymbol{\varpi}_P) \boldsymbol{\alpha} \quad (3.20)$$

Proof. see Appendix A.1.2 □

Next, considering Corollary 3.1 and Lemma 3.4 and substitution of the inverse of (3.20) in (3.19) yields a mapping from the GFRFs to the corresponding HOSIDFs and *vice versa*.

Theorem 3.2 (connecting the GFRF and HOSIDF).

Consider a $\overline{\text{PWH}}$ system as in Definition 3.3. If and only if,

1. $\varpi_P \in \mathbf{W}$;
2. $\xi_0 \in \mathbb{R}_{>0}$;
3. $\gamma \neq 0$,

then, the GFRFs and HOSIDFs of a $\overline{\text{PWH}}$ system are uniquely related by the following bijective mapping $\mathbf{C}^P \mapsto \mathbf{C}^P$:

$$\check{H}(\xi_0, \gamma) = \check{\mathfrak{R}}(\varpi_P, \xi_0, \gamma) T(\varpi_P, \xi_0, \gamma) \quad (3.21)$$

with

$$\check{\mathfrak{R}}(\varpi_P, \xi_0, \gamma) = \check{\Upsilon}^{-1}(\gamma) \check{\Delta}(\xi_0) G^+(\xi) \check{\Phi}(\angle G^-(\xi_0)) \check{\Omega} \Gamma(|G^-(\xi_0)| \gamma) \Lambda^{-1}(\varpi_P) \quad (3.22)$$

and where the parameters in (3.21) are defined in Corollary 3.1.

Proof. see Appendix A.1.3 □

Remark. Although violation of conditions 1-3 implies that (3.21) is not unique, this does not imply that the GFRFs cannot be otherwise identified.

Although (3.21) can be viewed in an identification setting, the fact that the LTI dynamics are assumed to be known, limits the applicability of these results for system identification. However, the results from Theorem 3.2 yield results on the properties of the HOSIDF and GFRF for linear systems.

Lemma 3.5 (GFRF and HOSIDF for Linear Systems).

Consider a $\overline{\text{PWH}}$ system and assume conditions 1-3 in Theorem 3.2 are satisfied. Then the following statements are equivalent:

1. The system is linear.
2. Only the first HOSIDF is nonzero, i.e. $\mathfrak{H}_k = 0 \forall k \neq 1$.
3. Only the first GFRF is nonzero, i.e. $\mathfrak{Z}_p = 0 \forall p \neq 1$.

Proof. see Appendix A.1.4. □

Theorem 3.2 yields the first connection between the GFRF and HOSIDF. Moreover, it yields clear insight in the mechanism that generates the GFRFs from the HOSIDFs and *vice versa*. Next, a numerical example is provided that illustrates the application of these results.

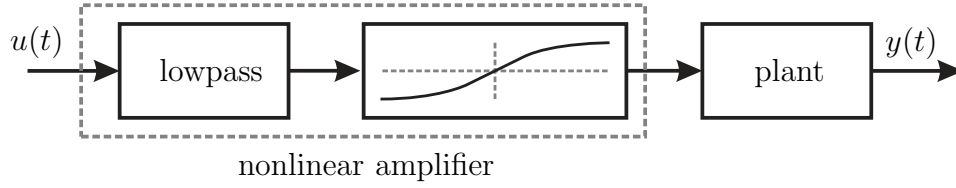


Figure 3.5: Example of $\overline{\text{PWH}}$ system representing a nonlinear amplifier driving an LTI plant.

Example 3.4 (analysis of a nonlinear amplifier).

When supplying an excitation signal to an electromechanical system, the signal is often amplified to reach a sufficient level of excitation. Ideally, the amplifier used to drive the system is linear. However, in practice many amplifiers suffer from nonlinear effects such as saturation.

Consider a simplified model of a saturating amplifier driving a fourth order linear, time invariant mechanical plant. Such system fits the structure of a $\overline{\text{PWH}}$ system as depicted in Figure 3.5. The dynamics of the amplifier are modeled by a low-pass characteristic and a static polynomial nonlinearity is used to model the nonlinear saturation effect. Next, suppose the static polynomial nonlinearity is unknown, but the linear dynamics $G^\pm(s) \triangleq G^\pm(2\pi i\xi)$ are known and given by:

$$G^-(s) = \frac{10000}{s^2 + 2513s + 1.579 \cdot 10^6} \quad G^+(s) = \frac{750000s^2 + 1.875 \cdot 10^6s + 3.75 \cdot 10^8}{s^4 + 7.8s^3 + 1601s^2 + 400s + 50000}$$

Next, Theorem 3.2 is applied to compute the GFRFs from the HOSIDFs. The required HOSIDFs $H(\xi_0, \gamma)$ are identified at a single frequency amplitude combination by exciting the system in Figure 3.5 with a sinusoidal input with amplitude $\gamma = 1$ and frequency $\xi_0 = 10$ [Hz]. Both the excitation signal and the response are depicted in Figure 3.6a. These results reveal that the response contains second and third harmonics of the input signal and a DC term. Hence, as an approximation, the first three GFRFs are selected to model the systems dynamics.

To compute the GFRFs, the results from Theorem 3.2 are applied which requires the identification of the first three HOSIDFs at a single frequency, amplitude combination. From the simulation depicted in Figure 3.6a, these are readily computed using Definition 2.8 and equal:

$$\check{H}(\xi_0 = 10, \gamma = 1) = \begin{bmatrix} \check{\mathfrak{H}}_1(10, 1) \\ \check{\mathfrak{H}}_2(10, 1) \\ \check{\mathfrak{H}}_3(10, 1) \end{bmatrix} = \begin{bmatrix} -1.7 - 0.1i \\ -1.0 \cdot 10^{-4} + 1.5 \cdot 10^{-5}i \\ -6.6 \cdot 10^{-7} + 1.8 \cdot 10^{-7}i \end{bmatrix}$$

Next, by application of (3.21) the corresponding GFRFs are computed for a range of frequencies as depicted in Figures 3.6b - 3.6d. By application of the results in Shanmugam and Jong (1975), these results are compared to the exact GFRFs, which yields that the results are very close to the true value. The corresponding first and third HOSIDFs are depicted in Figure 3.6e - 3.6f for comparison.

Conclusions

New, efficient analytical tools and results are presented that allow spectral analysis of the output of a class of nonlinear systems. This provides insight in the dynamics of block structured dynamical systems and allows analytic description and analysis of the corresponding HOSIDFs. Given the systems linear dynamics, the output spectra and HOSIDFs can be described as a simple polynomial function of the parameters defining the nonlinearity.

Moreover, using the preceding results, a novel connection is presented between the GFRF and HOSIDF, which both model the dynamics of nonlinear systems in the frequency domain. An explicit analytical relation between these models is derived for polynomial Wiener-Hammerstein systems and necessary and sufficient conditions are derived for this bijective mapping to exist. Moreover, properties of the GFRFs and HOSIDFs for linear and time invariant systems are presented. This analysis yields clear insight into the mechanisms that generate the GFRFs and HOSIDFs and provides a numerically efficient method to compute the GFRFs from the HOSIDFs and *vice versa*.

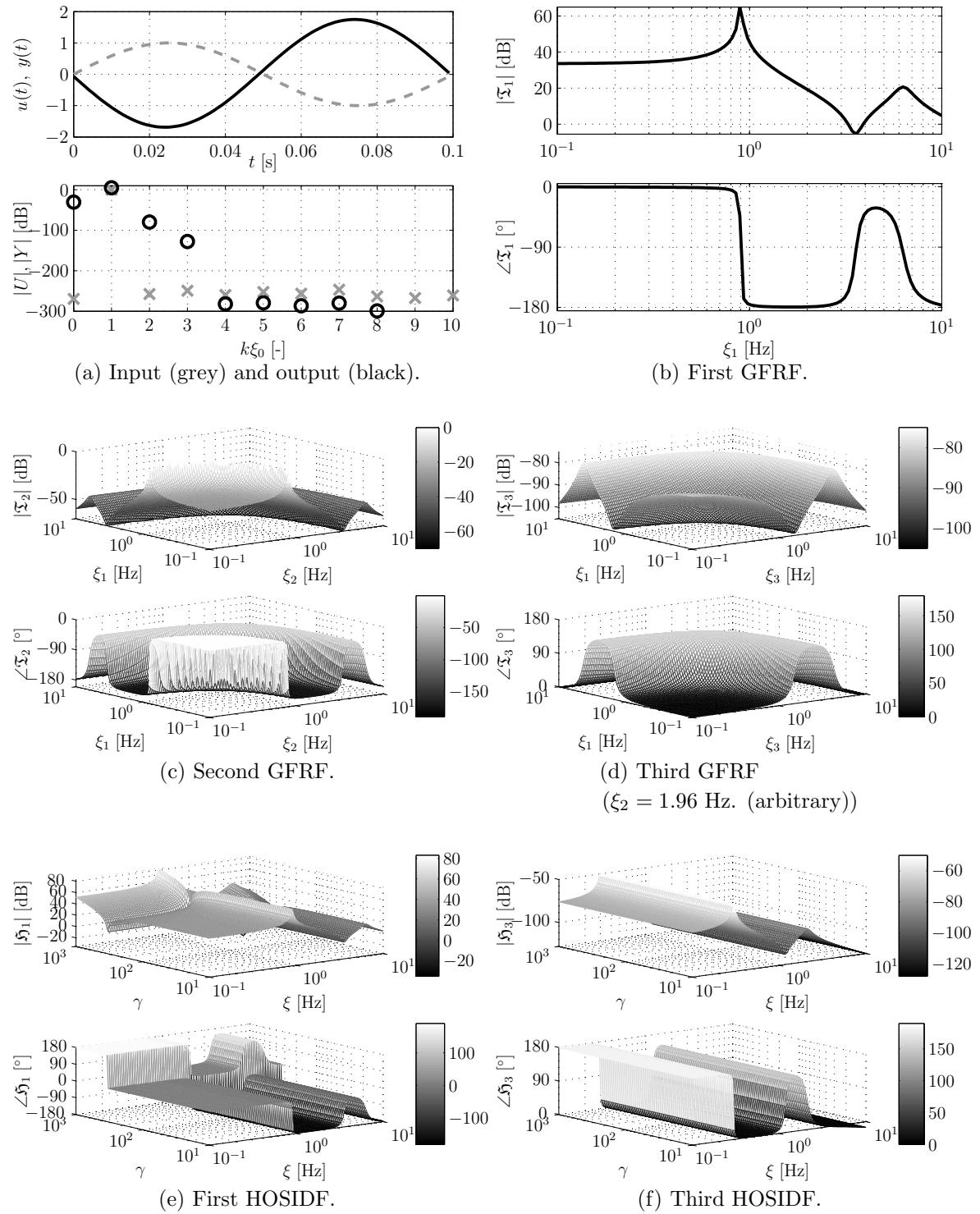


Figure 3.6: The systems response, the GFRF and the HOSIDF.

Chapter 4

Frequency Domain Based Nonlinearity Detection and Compensation in Lur'e Systems[†]

Nonlinearities can lead to performance degradation in controlled dynamical systems. This chapter provides a new, frequency domain based method, for detection and optimal compensation of performance degrading nonlinear effects in Lur'e-type systems. It is shown that for Lur'e-type, systems a sinusoidal response to a sinusoidal input is necessary and sufficient to show the existence of an equivalent linear time invariant dynamical model that fully captures the systems dynamics for a well defined set of input signals and initial conditions. This allows to quantify nonlinear effects using a frequency domain performance measure and yields a novel method to design optimized static compensator structures that minimize performance degrading nonlinear effects. The theoretical results are accompanied by examples illustrating their application.

For Linear and Time Invariant (LTI) controlled dynamical systems, performance is often assessed and optimized using a frequency domain representation of the dynamics. The application of frequency domain methods has led to significant progress in linear control design (Bode, 1945). However, most frequency domain methods fail to capture nonlinear phenomena and the notion of performance is generally nontrivial to define for nonlinear systems. The results presented in this chapter, however, yield that, for a class of nonlinear systems, frequency domain analysis provides a clear and well defined notion of performance as well as means to optimize this performance.

When assessing and optimizing the performance of controlled nonlinear systems, frequency domain methods have been shown to be applicable in for example Jing et al. (2008c, 2010), where the Volterra series based GFRF is applied to optimally

[†]The results presented in this chapter are published in: D. Rijlaarsdam, A. Setiadi, P. Nuij, J. Schoukens and M. Steinbuch, Frequency domain based nonlinearity detection and compensation in Lur'e systems, *submitted, under review*

utilize nonlinear effects to attain a user defined output spectrum. This is done as well in Nuij et al. (2008c) by application of a describing function approach. Finally, in van de Wouw et al. (2008); van de Wouw and Pavlov (2008); Heertjes et al. (2010) convergence based control design is applied to optimize performance of motion systems with nonlinearities in the feedback loop.

Whether or not a frequency domain model of a system is available or even exists, a frequency domain based analysis of the input-output (i/o) behavior can still yield valuable information about nonlinear effects. This is discussed both in this chapter and in Chapter 5 where an industrial case study is considered. In the sequel, frequency domain analysis of Lur'e-type systems is shown to yield a well defined performance measure. These results are applied to design static compensator structures that optimally compensate the performance degrading effects of nonlinearities.

First, in Section 4.1 so called Lur'e type systems are analyzed which yields a frequency domain performance measure that is applied to optimize the performance of these nonlinear systems. These results are then illustrated by practical examples in Section 4.2. Finally, Section 4.3 presents conclusions.

4.1 Frequency Domain Based Performance

The following presents a frequency domain analysis of Lur'e-type systems. Lur'e-type systems include a variety of practically relevant phenomena such as friction, saturation in feedback loops, gravitational effects in rotating dynamics and the nonlinear effect of magnetic and electric fields. First of all, the analysis presented in this chapter yields a well defined notion of performance of such systems. Secondly, further analysis reveals that this yields means to optimize this performance by designing optimal nonlinear compensators as well.

In the following, the class of Lur'e-type systems is defined and sufficient conditions for convergence of this type of systems are provided. Next, it is shown that, under mild assumptions, a sinusoidal response to a sinusoidal input is necessary and sufficient to show there exists a linear and time invariant model that fully captures the dynamics of nonlinear Lur'e-type systems for a well-defined set of inputs and initial conditions. Finally, these results are applied to develop a methodology to detect, quantify and ultimately compensate performance degrading nonlinear effects by the design of optimized nonlinear compensators.

Analysis of Lur'e-type Systems

Lur'e systems comprise a large set of nonlinear systems consisting of interconnected linear and nonlinear components Khalil (2002). In the following nonlinear systems consisting of a multi input, multi output LTI component and a single input, single output static nonlinear component in feedback are considered. These are defined as follows:

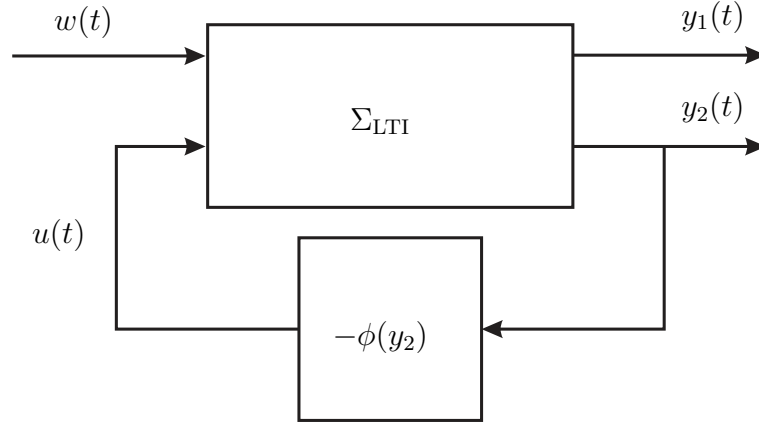


Figure 4.1: Lur'e-type system.

Definition 4.1 (Lur'e-type systems).

Consider the Lur'e-type system depicted in Figure 4.1 such that:

$$\begin{aligned}
 \dot{x}(t) &= Ax(t) + B_u u(t) + B_w w(t) & x(t_0) &= x_0 \\
 \begin{bmatrix} y_1(t) \\ y_2(t) \end{bmatrix} &= \begin{bmatrix} C_1 \\ C_2 \end{bmatrix} x(t) + \begin{bmatrix} D_{1,w} & D_{1,u} \\ D_{2,w} & D_{2,u} \end{bmatrix} \begin{bmatrix} w(t) \\ u(t) \end{bmatrix} \\
 u(t) &= -\phi(y_2(t))
 \end{aligned} \tag{4.1}$$

with $w \in \mathbb{B}_p$ an external input, $y_1(t), y_2(t) \in \mathbb{R}$ the outputs and $x(t) \in \mathbb{R}^n$ the states of the system. Furthermore, $A \in \mathbb{R}^{n \times n}$, $B_u \in \mathbb{R}^{n \times 1}$, $B_w \in \mathbb{R}^{n \times 1}$, $C_\ell \in \mathbb{R}^{1 \times n}$ and $D_{\ell, u/w} \in \mathbb{R}$, $\ell = 1, 2$ constitute a state space representation (4.1) of the dynamics and $u(t) \in \mathbb{R}$ is a nonlinear feedback generated by a static nonlinear mapping $\phi : \mathbb{R} \mapsto \mathbb{R}$.

To assure existence, uniqueness and stability of the solutions of (4.1), the class of uniformly convergent (Definition 2.3) Lur'e-type systems is considered. To this end, consider the following sufficient condition for uniform convergence of Lur'e-type systems which follows from Yakubovich (1964); Khalil (2002); Pavlov et al. (2006); van de Wouw et al. (2008).

Lemma 4.1 (convergence of Lur'e-type systems).

Consider a Lur'e-type system according to Definition 4.1 with input $w \in \mathbb{B}_p$. Then, the system is uniformly convergent (Definition 2.3) with respect to the class of piecewise continuous signals \mathbb{B}_p if there exists a $\vartheta \in \mathbb{R}_{>0}$ such that:

1. A is Hurwitz;
2. $\Re\{C_2(2\pi i \xi I - A)^{-1} B_u + D_{2,u}\} > -\frac{1}{\vartheta} \forall \xi \in \mathbb{R}$;
3. $0 \leq \frac{\phi(y_2) - \phi(y_1)}{y_2 - y_1} \leq \vartheta \forall y_1, y_2 \in \mathbb{R}$;
4. $u = -\phi(C_2 x + D_{2,u} u + D_{2,w} w)$ has a unique solution for every x and w in the domain of interest.

For uniformly convergent Lur'e-type systems it is possible to detect nonlinear effects and design an optimal compensator to minimize performance degrading nonlinear effects based on frequency domain analysis of the output spectrum. This method is discussed in the following and aims to linearize the systems dynamics by attaining a sinusoidal response to a sinusoidal input. To prove that such analysis indeed yields optimal compensation of the nonlinearity consider the following theorem. This theorem shows that the existence of a sinusoidal response to a sinusoidal input is necessary and sufficient to show the existence of an LTI model that captures the full dynamics of the Lur'e-type system, for a well defined class of inputs and initial conditions, i.e.

Theorem 4.1 (linearity of Lur'e-type systems).

Consider a Lur'e-type system according to Definition 4.1 with input $w(t)$, outputs $y_1(t), y_2(t)$ and states $x(t)$. Next, let $w \in \mathbf{S}_{\xi_0}$ be a sinusoidal input with frequency ξ_0 , let $v \in \mathbb{R}_{>0}$ and assume that the following holds:

- A_1 : the system is uniformly convergent with respect to the class of sinusoidal input signals \mathbf{S} ;
- A_2 : the steady state outputs $\bar{y}_{1,w}(t)$ and $\bar{y}_{2,w}(t)$ are nonzero for some sinusoidal input $w \in \mathbf{S}_{\xi_0}$;
- A_3 : $|C_\ell(2\pi i\xi - A)^{-1}B_u + D_{\ell,u}| \neq 0 \forall \xi \in \mathbb{R}, \ell = 1, 2$.

Then, the following statements are equivalent:

- S_1 : $\bar{y}_{1,w} \in \mathbf{S}_{\xi_0}$.
- S_2 : $\bar{y}_{2,w} \in \mathbf{S}_{\xi_0}$ with amplitude v .
- S_3 : there exist $\tilde{A} \in \mathbb{R}^{n \times n}$, $\tilde{B} \in \mathbb{R}^{n \times 1}$, $\tilde{C} \in \mathbb{R}^{2 \times n}$ and $\tilde{D} \in \mathbb{R}^{2 \times 1}$ that constitute an LTI state space realization:

$$\begin{aligned} \dot{\tilde{x}}(t) &= \tilde{A}\tilde{x}(t) + \tilde{B}w(t) & \tilde{x}(t_0) &= x_0 \\ \tilde{y}(t) &= \tilde{C}\tilde{x}(t) + \tilde{D}w(t) \end{aligned} \quad (4.2)$$

such that (4.2) is equivalent to (4.1), in the sense that for all

$$(x_0, w) \in \{(x_0, w) \in \mathbb{R}^n \times \mathbb{B}_p \mid \|y_2(t)\|_\infty \leq v\}$$

the solution and output of (4.1) and (4.2) satisfy $x(t) = \tilde{x}(t)$ and $y(t) = \tilde{y}(t)$ for all $t \in \mathbb{R}_{\geq t_0}$.

(proof: Appendix A.2.1)

Remark. The results in Theorem 4.1 indicate that using a sinusoidal input allows to conclusively assess the 'local linearity' of the systems dynamics from output measurements only. This allows to detect nonlinear effects without requiring a priori knowledge about the systems dynamics and provides a stepping stone towards compensation of performance degrading nonlinear effects by linearization based on output measurements.

Remark. The results in Theorem 4.1 are not dependent on the dimensions of the LTI dynamics, which allows for the analysis of complex linear models subject to a static nonlinearity.

Remark. Note that S_3 relates the input and initial conditions to the norm of the output. Such condition is both feasible and useful in many applications, such as controlled systems with a nonlinearity in the feedback loop or systems where the nonlinearity relates to property that is physically constrained (examples of both are provided in Section 4.2).

Loosely speaking, Theorem 4.1 states that only if a sinusoidal input yields a sinusoidal output at either output of a Lur'e-type system, the system behaves linearly in a given subset of state space. First of all, this allows to detect nonlinearities based on the output spectrum of either $y_1(t)$ or $y_2(t)$. Hence, even if $y_2(t)$ is not available, this yields a tool to detect nonlinear effects, but compensation of these effects is generally difficult as the level v , at which the nonlinearity is excited, is unknown. Although compensator design is possible in this case if nonlinear effects only occur at $y_2(t) = 0$, the (level of the) signal $y_2(t)$ is generally required to design meaningful compensators. In the next section a methodology is developed to design optimal static compensators that minimize nonlinear effects in Lur'e-type systems based on Theorem 4.1.

Performance Optimization by Linearization

Although existing nonlinearities may be utilized (Jing et al., 2010) or even added to the control loop (van de Wouw et al., 2008; Heertjes et al., 2010) to optimize the performance of nonlinear systems, such effects often yield performance degrading effects. In motion systems, for example, nonlinear friction is a common performance degrading factor and nonlinearities in amplifiers and linear motors lead to performance reduction in high-end applications. To counteract such effects, optimal (nonlinear) compensation is required.

In this section the results from Theorem 4.1 are used to design optimized static nonlinear compensators for Lur'e type systems. By subjecting the system to a sinusoidal input and optimizing the compensator structure to attain a sinusoidal output, the nonlinearity is optimally compensated (see Definition 4.2). As all systems for which Theorem 4.1 is valid are uniformly convergent, the output of such system is periodic with the same period as the input (Pavlov et al., 2006). When such systems are subject to a sinusoidal input, nonlinear effects will therefore only appear in the output spectrum at harmonics of the input frequency. Hence, by application of Theorem 4.1 optimal linearization can be achieved by minimizing these harmonic components and as such attaining a sinusoidal response to a sinusoidal input. Therefore, a performance cost is proposed that measures the spectral content at harmonic lines relative to that at the excitation frequency. This leads to the following, frequency domain based, notion of performance.

Definition 4.2 (optimal performance).

Consider a Lur'e-type system such that assumptions A_1 - A_3 in Theorem 4.1 are satisfied and assume the dynamics depend on a set of (controller) parameters $\kappa \in \mathbb{R}^{n_\kappa}$. Now, let $w \in \mathcal{S}_{\xi_0}$ be a sinusoidal input with frequency ξ_0 and consider the corresponding single sided spectrum of the steady state outputs $\bar{y}_{\ell,w}(t)$, $\ell = 1, 2$, denoted by $\bar{\mathcal{Y}}_{\ell,w}(\xi) \in \mathbb{C}$. Then, the performance of the system is defined by the following frequency domain based cost function:

$$\aleph(\kappa) = \frac{1}{K} \sqrt{\sum_{\substack{k=0 \\ k \neq 1}}^K \frac{|\bar{\mathcal{Y}}_{\ell,w}(k\xi_0, \kappa)|^2}{|\bar{\mathcal{Y}}_{\ell,w}(\xi_0, \kappa)|^2}} \quad (4.3)$$

where K is the number of harmonic lines included in the cost function. The performance defined in (4.3) is said to be optimal for a parameter set κ^* if:

$$\kappa^* = \arg \min_{\kappa} \aleph(\kappa) \quad (4.4)$$

Remark. Theorem 4.1 and Definition 4.2 show that a sinusoidal input of arbitrary frequency allows to optimally compensate nonlinear effects while the resulting compensation is valid for arbitrary input signals.

Remark. Although Theorem 4.1 implies that if $\aleph(\kappa^*) = 0$ the system is fully linearized over a given subset of state space, the optimization in (4.4) may result in an optimal parameter set such that $\aleph(\kappa^*) \neq 0$. As the cost function value depends on the characteristics of the LTI dynamics as well as the nonlinearity, a lower value of the cost function does not necessarily correspond to an improved linearization of the static nonlinearity. For example, in systems with strong filtering properties, harmonic content may be attenuated resulting in a decrease in the performance cost function although the static nonlinearity is not further linearized. However, in the case studies considered in this thesis, the influence of the LTI dynamics was not found to significantly influence the result of the optimization. In cases where the LTI characteristics are expected to influence the optimization, this may be taken into account when selecting the frequency of the excitation signal. However, in general the analysis of nonzero cost function values is recommended for future research.

Remark. The definition of optimal performance as in Definition 4.2 can be based on either output of the system. In most cases, the output driving the nonlinearity $y_2(t)$ is required to design meaningful compensators as the level at which the nonlinearity is excited is required to assess the range of validity of the compensator. In special cases, however, other outputs may be used to compute the performance measure as well. Examples of such cases include friction and cases where the excitation level of the nonlinearity is known but alternative outputs are better suited for optimization (see the examples in the following and in Chapter 5).

Remark. Note that when applying Definition 4.2 in practice, only statistically relevant harmonic lines should be included in (4.3). A statistical test is therefore required to distinguish between relevant harmonics and measurement noise (see Section 5.1).

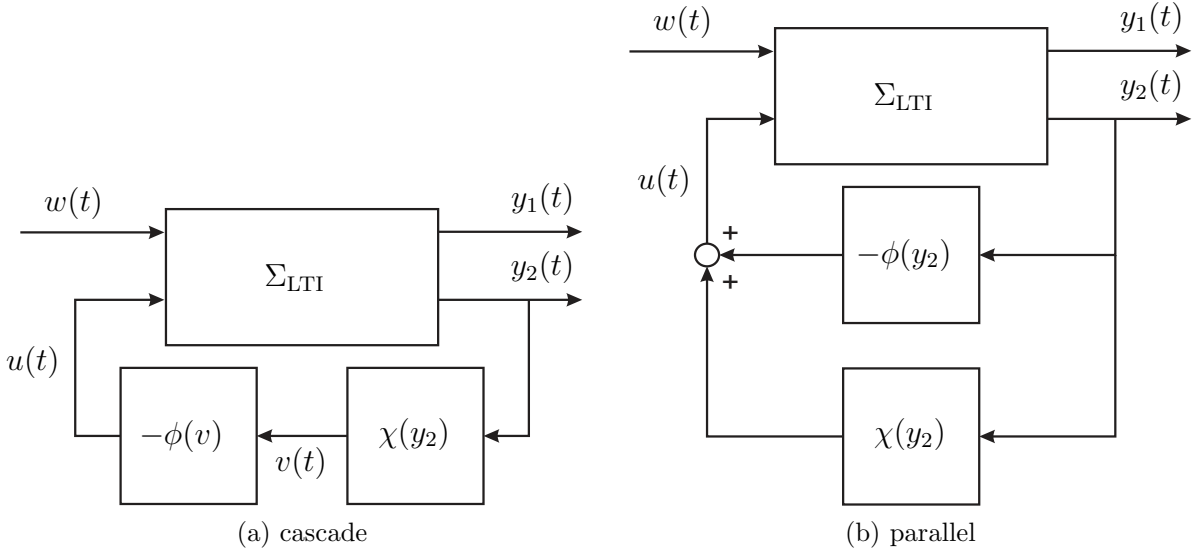


Figure 4.2: Compensator configurations for Lur'e-type systems.

In addition to the notion of optimal performance in Definition 4.2, both the compensator structure and configuration need to be selected. In this chapter, static cascade and parallel compensator configurations are considered as depicted in Figure 4.2. These configurations imply that the output driving the nonlinearity is known and the control input either acts directly on the input of the nonlinearity (cascade) or on the same input of the system as the nonlinearity (parallel). Although, additional requirements on, or knowledge about the LTI dynamics may be used to design compensators based on alternative outputs acting on different inputs of the system, this is not considered in this work.

In general the static compensators can be constructed from an arbitrary set of basis functions. For numerical conditioning it is however recommended to use orthogonal basis functions and polynomial functions may be preferred from an implementation point of view. The static compensators used in the following are based on Chebyshev polynomials. It is expected that the orthogonality of these polynomials will improve numerical conditioning of the optimization problem. However, the orthogonality conditions for these basis functions were not checked in detail and they should therefore be used with care. The compensators are defined as follows.

Definition 4.3 (Chebyshev based compensator structure).

Consider a Lur'e-type system as in Definition 4.1 and a static compensator $\chi : \mathbb{R} \mapsto \mathbb{R}$ in a cascade or parallel configuration as depicted in Figure 4.2. Next, the compensator χ is selected to be of polynomial form such that it can be constructed from Chebyshev polynomials, i.e.

$$\chi(\nu) = \sum_{n=0}^N \beta_n T_n(\nu) = \lambda \nu + \sum_{\substack{n=0 \\ n \geq 2}}^N b_n \nu^n \quad \nu \in \mathbb{R} \quad (4.5)$$

where $\kappa = \{\beta_1, \beta_2, \dots, \beta_N\} \in \mathbb{R}$ as in Definition 4.2 and $T_n(\nu)$ is the n^{th} Chebyshev polynomial of the first kind, which is defined as follows:

$$T_0(\nu) = 1 \quad T_1(\nu) = \nu \quad T_{n+1}(\nu) = 2\nu T_n(\nu) - T_{n-1}(\nu)$$

Finally, $b_n \in \mathbb{R}$ follows from β_n and the coefficients of the Chebyshev polynomials and λ equals the gain of the linear feedthrough of χ .

Although Definition 4.3 yields a well defined compensator structure, (4.5) is over-parameterized in the sense of Definition 4.2 as any compensator χ yielding a linear feedback in Figure 4.2 minimizes (4.3). Hence, a constraint is required to arrive at a unique solution. This constraint can be selected by the user, depending on the requirement on the compensated system, i.e. the required linear feedback gain after compensation.

To arrive at a set of applicable constraints, consider the cascade and parallel compensator configurations depicted in Figure 4.2 and the Chebyshev based compensator structure as in (4.5). Then, it follows that λ in (4.5) equals:

$$\lambda = \sum_{m=1}^{\text{floor}(N/2)} (-1)^{m+1} (2m-1) \beta_{2m-1} \quad (4.6)$$

Furthermore, for any Lur'e-type system, the nonlinearity can be written as $\phi(\nu) = \rho\nu + f_\phi(\nu)$ with $\rho \in \mathbb{R}$ and $\partial f_\phi / \partial \nu|_{\nu=0} = 0$. This yields the following constraints on the parametrization of χ and the resulting linear feedback gain, after optimization of the compensator.

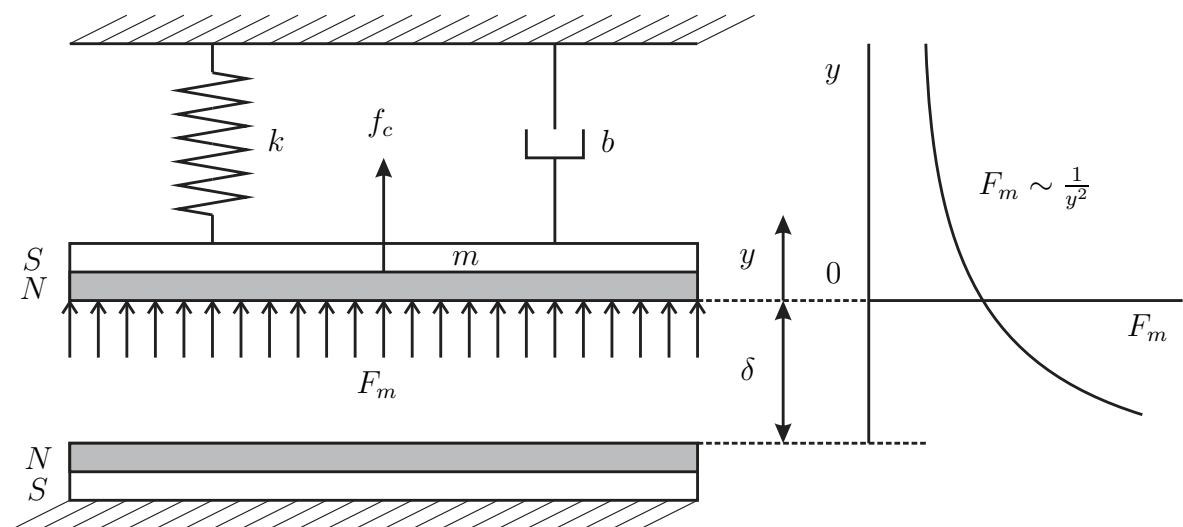
Table 4.1: Constraint on parametrization of the compensator χ and the resulting linear feedback gain after compensation, (with $\alpha \in \mathbb{R}$ and derivations presented in Appendix A.2.2).

| | CONSTRAINT | FEEDBACK GAIN |
|------------------------------|--------------------|-----------------|
| <i>cascade compensation</i> | $\lambda = \alpha$ | $-\alpha\rho$ |
| <i>parallel compensation</i> | $\lambda = \alpha$ | $\alpha - \rho$ |

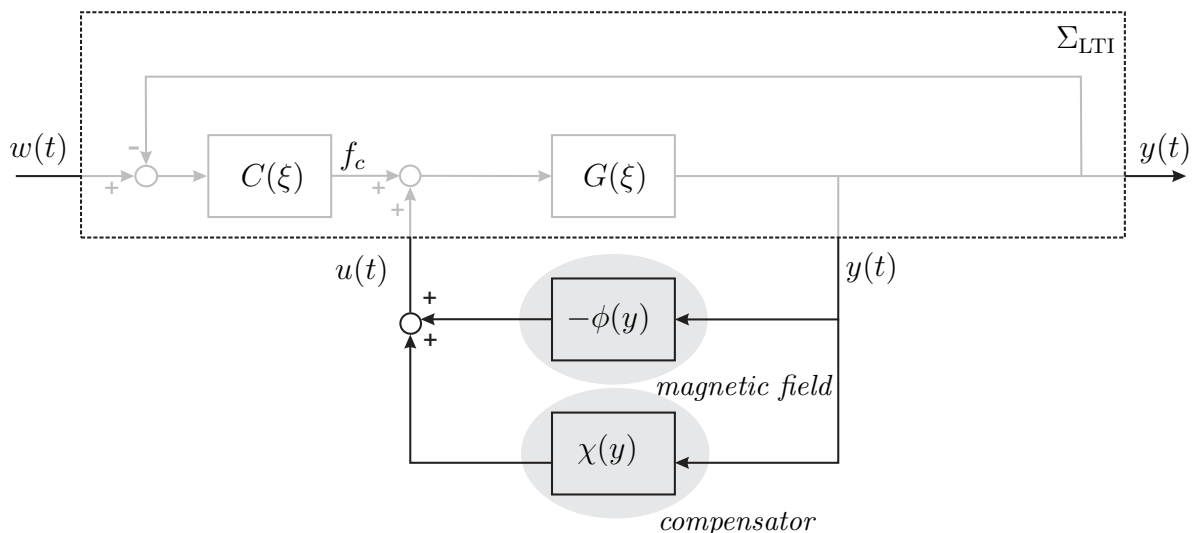
The constraints in Table 4.1 allow to select the appropriate compensator behavior without prior knowledge of the nonlinearity. The application of these results is illustrated by two examples in the next section.

4.2 Numerical Examples

To illustrate the preceding results, two examples are presented in this section. The examples focus on the practical application of the performance optimization discussed in Section 4.1. First, optimal compensation of a nonlinear magnetic field is discussed to illustrate the application of the methodology in, for example, linear drives. Second, a case study of a saturating amplifier is considered and it is shown that the linear operating range of such amplifier can be extended by application of the method introduced in Section 4.1.



(a) Schematic depiction of a mass, subject to a nonlinear magnetic field.



(b) Lur'e form.

Figure 4.3: Schematic depiction of a mass subject to a nonlinear magnetic field and the corresponding representation in Lur'e form.

Linearization of a Magnetic Field

In many high tech applications, such as waferscanners and maglev applications, magnetic drives are used as actuators. The magnetic field in such systems depends nonlinearly on the distance between the magnet and the object to be actuated. To this end, consider the simplified case of a mass interacting with a nonlinear magnetic field as depicted in Figure 4.3. In this case study the aim is to minimize the nonlinear influence of the magnetic field.

The system depicted in Figure 4.3a consists of a mass m with corresponding limited displacement $y(t) \in (-\eta\delta, \eta\delta)$, $\eta \in (0, 1)$. The mass is connected to a linear spring with stiffness k and a damper b and the system is subject to a linear feedback control force f_c , that aims to track a reference signal $w(t)$. Moreover, the nonlinear

magnetic field exerts a force F_m on the mass that varies nonlinearly with the position of the mass such that:

$$F_m(y) = \frac{1}{\alpha_0 + \alpha_1 y + \alpha_2 y^2}$$

where the parameters $\alpha_k \in \mathbb{R}$ are selected such that $F_m(y)$ is monotonically decreasing. Next, consider the alternative representation in Lur'e form as depicted in Figure 4.3b, where $-\phi(y) = F_m(y)$ and define

$$G(\xi) = \frac{K}{-4(\pi\xi)^2 + 4i\pi\zeta\omega_n\xi + \omega_n^2} \quad (4.7)$$

$$C(\xi) = K_p + 2i\pi K_d\xi \quad (4.8)$$

with $\omega_n = \sqrt{\frac{k}{m}}$, $\zeta = \frac{b}{2km}$ the natural frequency and dimensionless damping of the mass-spring-damper system and $K_p, K_d \in \mathbb{R}$ the parameters of the Proportional-Differential (PD) controller. The parameters of the PD controller are selected arbitrarily, while the static nonlinear block χ is defined as in Definition 4.3 and remains to be designed in the remainder of this example. Finally, the parameters used in the simulations are summarized in Table 4.2.

Table 4.2: Parameters of the system depicted in Figure 4.3

| PARAMETER | VALUE | PARAMETER | VALUE | PARAMETER | VALUE |
|------------|-------|-----------|-------|------------|-------|
| ω_n | 100 | K_p | 300 | α_0 | 0.151 |
| ζ | 5 | K_d | 0.1 | α_1 | 0.102 |
| K | 100 | δ | 1 | α_2 | 0.001 |
| | | η | 0.75 | | |

Analysis

Prior to applying the method discussed in Section 4.1, the assumptions in Theorem 4.1 need to be verified. First of all, application of Lemma 4.1 yields that for $\|y(t)\|_\infty < \delta$ the system in Figure 4.3 is uniformly convergent for $\chi(y) = 0$ and for the parameters presented in Table 4.2. Hence, A_1 is satisfied. Moreover, as $\left| \frac{G(\xi)}{1+C(\xi)G(\xi)} \right| \neq 0 \forall \xi \in \mathbb{R}$, assumption A_3 in Theorem 4.1 is satisfied. Finally, simulations yield a nonzero response to sinusoidal inputs, which implies A_2 is satisfied. Hence, Theorem 4.1 applies and the method discussed in Section 4.1 can be applied to optimally design the compensator.

Optimization and Results

To minimize the nonlinear effect of the magnetic field, the performance of the system is optimized in the sense of Definition 4.2 by exciting the system with a sinusoidal signal $w \in \mathcal{S}$ with frequency 2 [Hz], such that $\|y(t)\|_\infty = \eta\delta$. The selection of the excitation frequency is arbitrary as long as the nonlinearity is excited at a sufficiently high level, i.e. $\|y(t)\|_\infty = \eta\delta$. Next, an optimal compensator is designed as in Definition 4.3. As the input to the nonlinearity cannot be directly controlled, compensation in a parallel

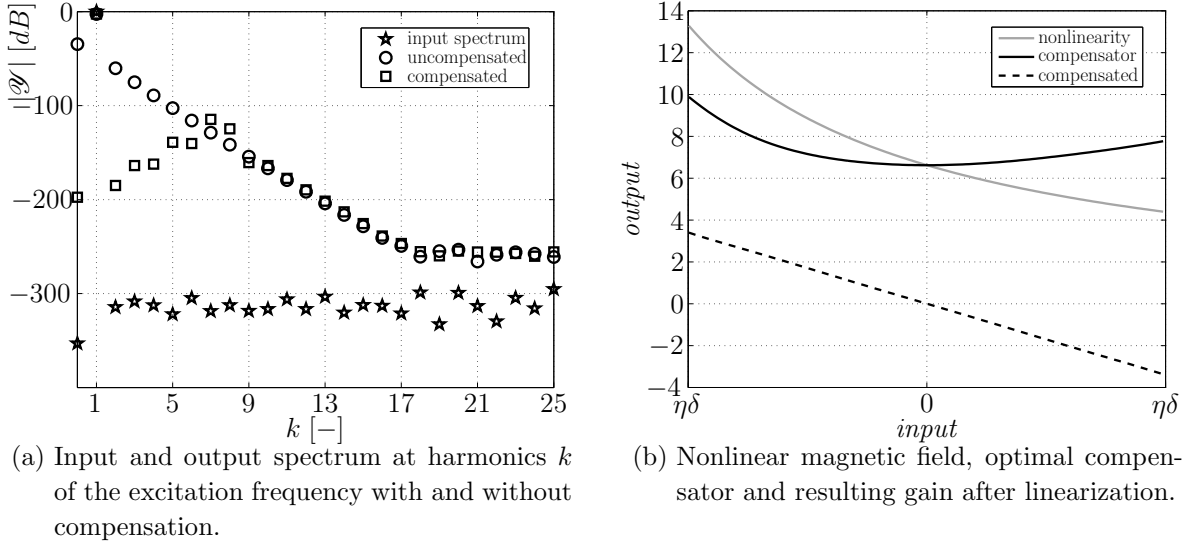


Figure 4.4: Comparison between uncompensated and optimally compensated nonlinear magnetic field.

configuration is applied as in (Figure 4.2b). Moreover, as the system has only one output, the performance cost as in Definition 4.2 is necessarily based on this output as well. Finally, since the influence of the magnetic field is to be linearized, but not otherwise changed, the constraint on the parametrization of χ is selected to $\lambda = 0$ (Table 4.1).

The optimization (4.4) is performed in Matlab. The compensator is constructed using Chebyshev polynomials up to order 10 and the input to the compensator is scaled by $\frac{1}{2\delta}$ to improve numerical conditioning of the optimization problem. Moreover, initial conditions were selected to equal $\beta_k = 0 \forall k = 0, 1, 2, \dots, 10$ which corresponds to the physical case of the uncompensated situation. In repeated simulations random initial conditions in the interval $[-1, 1]$ yielded the same optimum as the zero initial conditions, but larger initial conditions are found to converge to local minima. This non-convex behavior of the cost function is recommended for future research and the initial conditions are based on the physical case of the uncompensated system in the sequel.

The results of the optimization are depicted in Figure 4.4. Figure 4.4a shows that the harmonic components present in the output due to the nonlinearity in the magnetic field are reduced significantly by the application of the optimized compensator. Moreover, the original nonlinearity and the optimal compensator are depicted in Figure 4.4b. As $\lambda = 0$ the linear feedback gain resulting from the application of χ equals $\rho = -\partial\phi/\partial y|_{y=0}$. Hence, by application of the algorithm in Section 4.1, the nonlinear effect of the magnetic field has been significantly reduced, yielding an optimized performance by linearization of the systems dynamics.

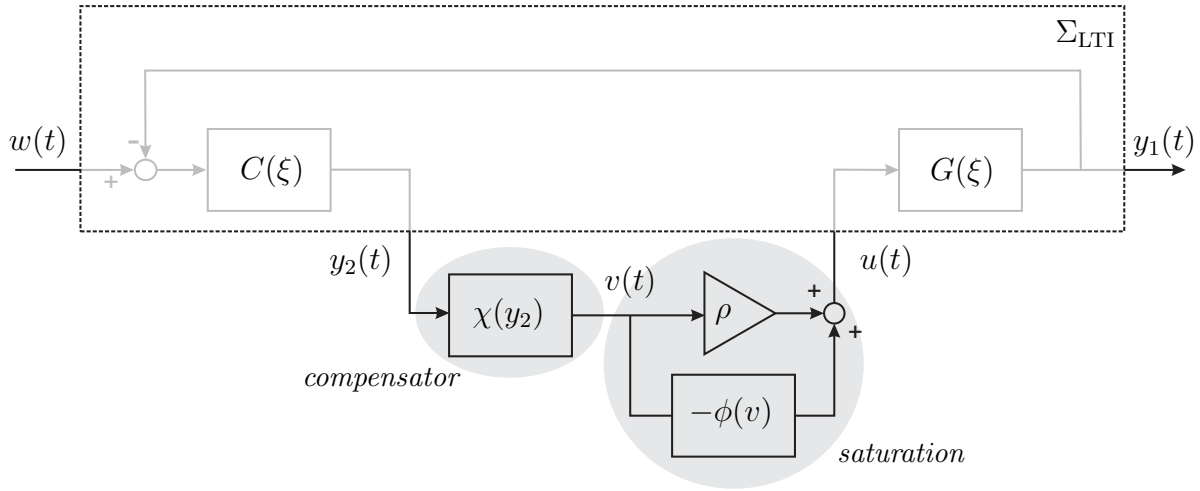


Figure 4.5: Hammerstein system with linear output feedback (in Lur'e form).

Detection and Compensation of Saturation Nonlinearities

In many practical applications, amplifiers are used to convert low power control signals to the high power signals that drive the plant. Although most amplifiers are designed to provide linear amplification in their operating range, nonlinear effects appear at the boundaries of the operating range when the amplifier starts to saturate. In this example the aim is to extend the linear operating range by optimally compensating these nonlinear effects.

Consider the Hammerstein structure with linear feedback as depicted in Figure 4.5. The system consists of a mass-spring-damper system modeled by the transfer function $G(\xi)$ and a PD controller with arbitrarily selected parameters, denoted by $C(\xi)$ as in (4.7)-(4.8). Moreover, χ is a static nonlinear compensator that is to be designed to optimize the performance of the system. The saturation nonlinearity is a smooth nonlinearity as depicted in Figure 4.6a (solid grey line). The amplifier has a linear gain of ρ for $|y_2| < \delta$ and saturates smoothly towards a maximum output of ϱ at $y_2 \geq \Delta$. Finally, the parameters used in the simulations are summarized in table 4.3.

Table 4.3: Parameters of the system depicted in Figure 4.5

| PARAMETER | VALUE | PARAMETER | VALUE | PARAMETER | VALUE |
|------------|-------|-----------|-------|-----------|-------|
| ω_n | 125.7 | K_p | 1 | δ | 1.8 |
| ζ | 0.9 | K_d | 0.01 | Δ | 2.4 |
| K | 100 | ρ | 100 | ϱ | 216 |

Analysis

In order to verify if Theorem 4.1 is applicable, Lemma 4.1 is applied. This yields that the system in Figure 4.5 is uniformly convergent for $\chi(y_2) = 1$, such that assumption A_1 in Theorem 4.1 is satisfied. Moreover, as $|G(\xi)| \neq 0$ and $|C(\xi)G(\xi)| \neq 0 \quad \forall \xi \in \mathbb{R}$

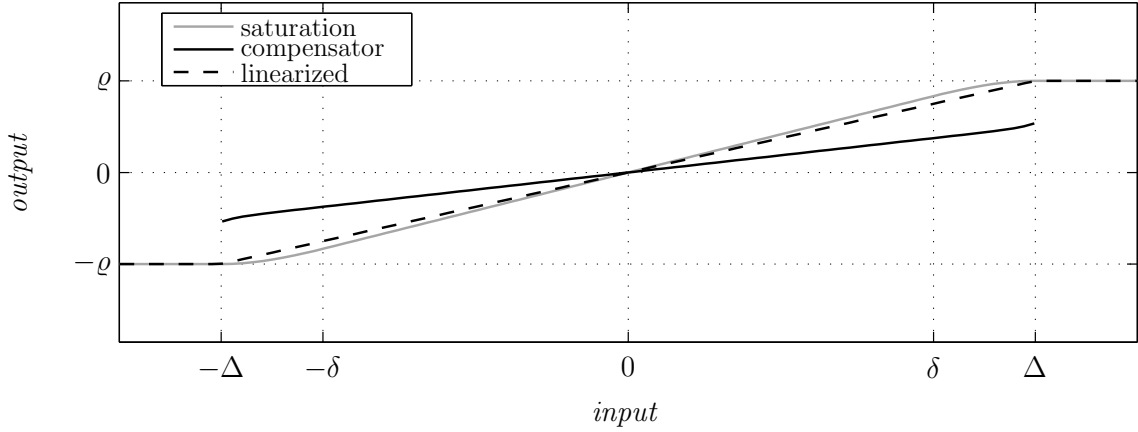
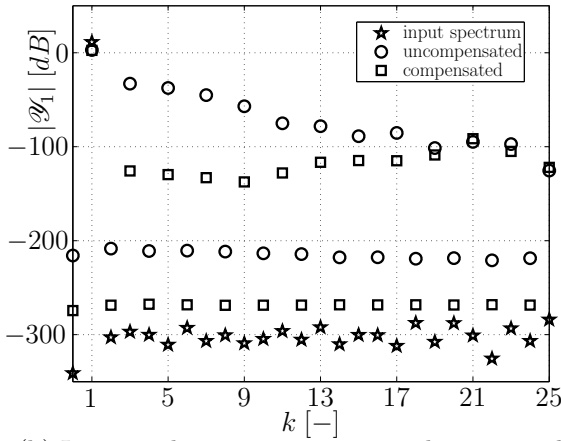
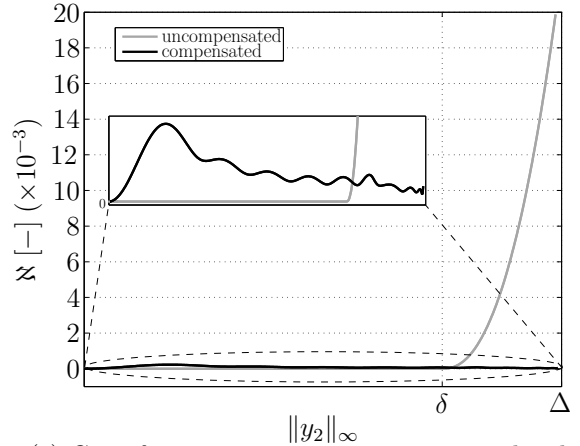
(a) Saturation nonlinearity, optimal compensator ($\times 50$) and linearized amplifier.(b) Input and output spectrum at harmonics k of the excitation frequency with and without compensation.(c) Cost function versus excitation amplitude and zoom at $25\times$ vertical magnification.

Figure 4.6: Comparison between uncompensated and optimally compensated saturation nonlinearity.

assumption A_3 is satisfied as well. Moreover, simulations yield nonzero response to sinusoidal inputs, which implies A_2 is satisfied. Hence, Theorem 4.1 applies and the method discussed in Section 4.1 can be applied to optimally design the compensator.

Optimization and Results

To optimally compensate the nonlinear 'tails' of the saturation nonlinearity, the performance of the system is optimized in the sense of Definition 4.2 by exciting the system with a sinusoidal signal $w \in \mathbf{S}$ with a frequency of 2 [Hz] and an amplitude of 3.71 such that $\|y_2(t)\|_\infty = \Delta$. The optimization of the performance cost function (4.3) is performed using the output spectrum of $y_1(t)$. Hence, as the level of excitation of the nonlinearity is known (Δ), alternative (easier available) outputs can be used for performance optimization. The system configuration in this case calls for a cascade compensation configuration as the user is most likely to have access to the controller

output for modification. Finally, the remaining gain after compensation is required to be nonzero to retain a meaningful closed loop structure. In order to extend the linear operating range of the amplifier to Δ within the saturation limits, the remaining linear gain should be less than ρ . This is selected to be 90% and the constraint on the parametrization of χ is therefore set to $\lambda = 0.9$ (see in Table 4.1).

The optimization of (4.4) is again performed in Matlab. The compensator is constructed using the first 10 odd Chebyshev functions as the saturation nonlinearity is symmetric. Moreover, the input of the compensator is scaled by $\frac{1}{\Delta}$ to improve the numerical conditioning of the optimization problem. Initial conditions were selected to equal $\beta_k = 0 \forall k = 3, 5, \dots, 19$ and $\beta_1 = 1$, which corresponds to the physical case of the uncompensated situation. In repeated simulations random initial conditions in the interval $[-1 \ 1]$ yielded the same optimum as the initial conditions corresponding to the uncompensated system, but larger initial conditions may converge to local minima. This non-convex behavior of the cost function is recommended for future research and the initial conditions are based on the physical case of the uncompensated system in the sequel.

Figure 4.6 shows the results of the optimization. As depicted in figure 4.6b, detection of nonlinear effects is based on y_1 , which yields a significant decrease in spectral content at harmonics of the excitation frequency. Figure 4.6a shows the original saturation nonlinearity, the corresponding compensator and the linearized dynamics. Moreover, Figure 4.6c shows how the value of the cost function depends on the maximum value of the controller output y_2 . In the uncompensated situation the cost function clearly indicates the increased effects of the nonlinearity for $\|y_2(t)\| > \delta$. On the other hand, after optimization hardly any nonlinear effect is observed. However, the zoomed window indicates that the compensator causes some nonlinear influences to appear in the region where the amplifier was originally linear. Summarizing, optimal compensator design yields an increased linear operating range of the amplifier, but also yields a decrease in gain as well as small nonlinear effects in the region where the amplifier is originally linear.

4.3 Conclusions

A novel, frequency domain based method to quantify and optimize the performance of Lur'e-type systems is presented. It is shown that, under mild conditions, a sinusoidal response to a sinusoidal input is necessary and sufficient to show the existence of an equivalent linear time invariant dynamical model that fully captures the systems dynamics for a well defined set of input signals and initial conditions. The preceding results yield a novel method to detect and compensate performance degrading effects of nonlinearities. Although the analysis focuses on convergent Lur'e-type systems, the assessment of nonlinearities based on spectral information is expected to be applicable to a wider class of convergent systems. Moreover, similar methods have been shown to yield significant performance improvement for non-convergent systems as well as

discussed in Chapter 5. The methods discussed in this chapter allow to quantify performance of nonlinear systems, based on output measurements only while requiring little knowledge about the nonlinearity and other system dynamics. This yields a useful tool to optimize performance in practice without requiring advanced nonlinear modeling or identification techniques. Finally, due to the well defined and easily measurable performance measure, this methodology is applicable in a real time, automated setting as well.

Chapter 5

Frequency Domain Based Feed Forward Design for Friction Compensation[†]

In Chapter 4, the application of frequency domain techniques for performance assessment and optimization of nonlinear system is introduced. Specifically, the application of static compensators in Lur'e-types systems is addressed. In this chapter the concept of frequency domain based performance is applied to detect and optimally compensate the performance degrading effects of friction in an industrial Transmission Electron Microscope (TEM) system, using feed forward compensation. It is shown that the frequency domain approach yields a tool to fast and easily design friction control in practice with high detection sensitivity and orthogonal tuning of the controller parameters, while providing a well defined notion of optimal performance.

Friction is a performance limiting factor in many industrial high precision motion systems. Both model and non-model based friction compensation techniques exist, which are applied in feedback as well as in feed forward control strategies (Armstrong-H'elouvry, 1991; Armstrong-H'elouvry et al., 1994). Non-model based techniques range from the application of integral control to reduce the steady state tracking error, to more advanced friction compensators based on friction estimators such as discussed in Ramasubramanian and Ray (2001). Model based friction compensation in feedback and feed forward is demonstrated in for example Johnson and Lorenz (1992). Moreover, in Tsai et al. (2004) a feed forward compensator is described that compensates both the performance degrading effects of friction and the error induced by the command path. Furthermore, in de Bruin et al. (2009) a globally asymptotically stable controller for systems with non-collocated friction is presented. Model based feed forward techniques based on the Dahl, LuGre, Leuven and generalized Maxwell

[†]The results presented in this chapter are published in: D. Rijlaarsdam, P. Nuij, J. Schoukens and M. Steinbuch, Frequency domain based nonlinear feed forward control design for friction compensation, *Mechanical Systems and Signal Processing*, 27(2):551-562, 2012

slip model¹ are discussed in Lampaert et al. (2004) and compared to non-model based friction compensation using a disturbance observer. Friction compensation at extreme low velocities is investigated using two model based friction compensation techniques in Zhang et al. (2002) and model based feed forward design for motion systems is discussed in Torfs et al. (1998); Tjahjowidodo et al. (2007).

Apart from the above mentioned results, a well known and regularly applied way to compensate for the effects of friction in practice is the application of Coulomb (Coulomb, 1785) friction feed forward. In practice, the parameters for this feed forward controller are often identified using time domain data, which has three distinct disadvantages:

1. the effects of nonlinear Coulomb friction and linear viscous damping are not independent in the time domain;
2. optimal approximation of the complex, true nonlinear dynamics by the simplified Coulomb friction model is nontrivial in the time domain;
3. the detection sensitivity of time domain analysis to the effects of friction is limited.

The application of the frequency domain based methodology introduced in this chapter aims to address these issues. As discussed in Chapter 4, this methodology is expected to be more widely applicable. However, in this case study, the discussion is limited to optimization of Coulomb friction feed forward to illustrate the applicability of this method to the compensation of strong nonlinearities in a setting with industrial relevance.

The chapter is structured as follows. First, in Section 5.1 the experimental application is linked to the analysis presented in Chapter 4. Next, the notion of frequency domain based performance is further discussed in relation to the application at hand. The application of these techniques to optimally control friction in a high precision, industrial motion stage of a TEM is then presented in Section 5.2. Moreover, in Section 5.3 the experimental results are discussed and the frequency domain tracking performance measure is related to the time domain performance of the system. Finally, conclusions are provided in Section 5.4.

5.1 From Analysis to Application

In this section the theory presented in Chapter 4 is linked to feed forward design for friction compensation. First of all, differences and similarities between the theoretical results and the application in practice are highlighted. Next, frequency domain based analysis for performance optimization is discussed in relation to the practical case study at hand. Finally, the influence of measurement noise is discussed and the performance measure is extended to include a measure of statistical significance.

¹For more information on these friction models see: Dahl (1968); Canudas de Wit et al. (1995); Swevers et al. (2000); Lampaert et al. (2002); Al-Bender et al. (2005).

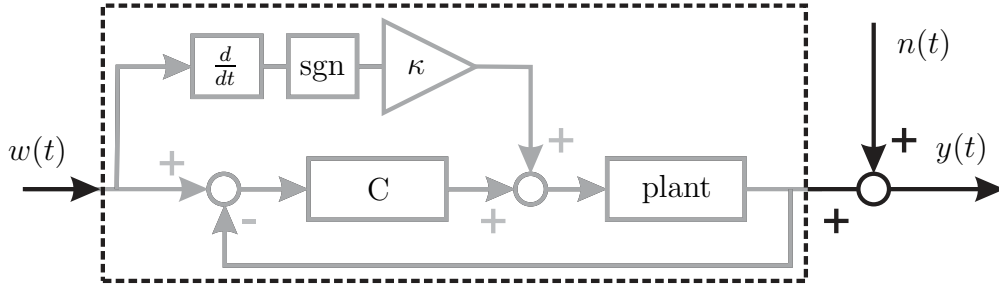


Figure 5.1: Closed loop system subject to Coulomb friction feed forward.

Comparison with the Results in Chapter 4

Consider a closed loop single input, single output system as depicted in Figure 5.1 and assume the system is stable, causal, time invariant and has a harmonic response to a sinusoidal input. The plant is a mass-spring-damper system subject to Coulomb friction in closed loop with a stabilizing controller C . The input and output of the system are $w(t)$ and $y(t)$ and the output is subject to stationary (colored) measurement noise $n(t)$. Finally, the system is subject to a feed forward with gain κ [V] that aims to compensate for Coulomb friction in the plant. The system depicted in Figure 5.1 has strong similarities to the class of nonlinear systems considered in Chapter 4. For example, Coulomb friction can be modeled by a Lur'e-type structure as in Figure 4.1. However, two main differences stand out as well:

1. The system as depicted in Figure 5.1 ($\kappa = 0$) is not uniformly convergent, e.g. for $w(t) = 0$ there exist multiple limit solutions for initial conditions that start the system in stick mode.
2. Feed forward compensation is used to address the performance degrading nonlinear effects, rather than the output feedback considered in Chapter 4.

Firstly, the fact that the system under consideration is not uniformly convergent implies that assumption A_1 in Theorem 4.1 is not satisfied. Secondly, the feed forward compensator can be viewed in light of the Lur'e compensator structures discussed in Section 4.1. However, the reference velocity is used to drive the feed forward compensator, while the friction depends on the true velocity. Hence, the structures in Figure 4.2 do not apply. The first problem is inherent to the practical application as it can generally not be shown that a real life system is uniformly convergent. However, the results presented in the following indicate that the theory introduced in Chapter 4 can be extended to the non-convergent case of friction compensation. Secondly, a feed forward structure is selected as this is a common way to compensate friction in practice and because no stability issues are involved when designing such compensator. Therefore, the following results are presented under the premise that if sufficient tracking is achieved, the feed forward acts similar to a velocity feedback. Experimental results indicate that application of the concepts introduced in Chapter 4 can indeed yield significant performance improvement when applied to the design of a feed forward structure as well.

Frequency Domain Based Optimal Feed Forward Design

The aim in this case study is to optimally compensate the performance degrading effects of friction in the plant in Figure 5.1 by the design of a feed forward controller. As motivated in Chapter 4, the design of the feed forward compensator aims at attaining a sinusoidal output for sinusoidal inputs. Moreover, as Coulomb friction is a static nonlinearity that is constant except around zero velocity, it suffices to test the input-output behavior for an arbitrary sinusoidal input (see Section 4.1). This also allows to optimize the performance in the sense of Definition 4.2, based on position rather than velocity measurements. However, as the true friction present in a system is generally more complex and other types of nonlinearities may be present as well, this assumption on frequency and amplitude invariance does not generally hold. This is outside the scope of this work and the following results show that optimization of the feed forward compensator using a single sinusoidal input signal already yields a significant performance improvement (see Section 5.3).

To quantify the performance of the nonlinear feed forward compensator in terms of the methodology introduced in Chapter 4, the system in Figure 5.1 is excited with a sinusoidal input $w \in \mathbf{S}$. The performance of the system is then quantified by the ratio between higher harmonic components $|\bar{\mathcal{Y}}_w(k\xi_0)|$ in the systems steady state output and the spectral component at the excitation frequency $|\bar{\mathcal{Y}}_w(\xi_0)|$ in a way that is similar to Definition 4.2. The following formalizes this definition of optimal tuning of the feed forward compensator².

Definition 5.1 (optimal feed forward compensation: $n(t) = 0$).

Consider the system depicted in Figure 5.1 and assume that $n(t) = 0$. Then, the feed forward compensator is said to be optimal if the system is subject to a sinusoidal input $w \in \mathbf{S}_{\xi_0}$, all transient effects have vanished and $\kappa = \kappa_{opt}^*$ such that:

$$\kappa_{opt}^* = \arg \min_{\kappa \in \mathbf{R}} \frac{1}{K-1} \frac{\sum_{k=2}^K |\bar{\mathcal{Y}}_w(k\xi_0, \kappa)|}{|\bar{\mathcal{Y}}_w(\xi_0, \kappa)|} \quad (5.1)$$

where $\bar{\mathcal{Y}}_w(\xi)$ is the spectrum of the steady state response of the system.

In practice, the optimal value κ_{opt}^* depends on the tracking performance of the system and on the feedback controller. Hence, the feed forward compensator is designed for a fixed feedback structure and the excitation frequency ξ_0 is selected to be significantly smaller than the bandwidth of the closed loop system to assure sufficient tracking. Next, the root-mean-square (rms) tracking error is selected as the time domain performance criterion for comparison with the frequency domain optimality

²The definition of optimal feed forward compensation in Definition 5.1 differs from the definition of optimal performance in Definition 4.2. This is due to the fact that the results based on Definition 5.1 were developed first and the definition as presented Definition 4.2 was later selected to emphasize larger spectral components in the cost function. In general, the selection of the cost is an open subject for investigation.

condition. In general, the selection of tracking criterium (rms error, maximal error, etc.) is application depend. However, in the following, the rms tracking error is selected because it is used in practice to provide a measure of the power of the tracking error, which is often used as a performance measure for motion systems.

Definition 5.2 (optimal tracking performance).

Consider the system depicted in Figure 5.1. Then, the tracking performance of the system is called optimal when subject to a sinusoidal input $w \in \mathfrak{S}$ if all transient effects have vanished and $\kappa = \kappa_{track}^*$ such that:

$$\kappa_{track}^* = \arg \min_{\kappa \in \mathbb{R}} \max_{n \in \mathbb{N}_{\geq 1}} \sqrt{\frac{1}{T_0} \int_{(n-1)T_0}^{nT_0} (w(t) - y(t))^2 dt} \quad (5.2)$$

with $T_0 = 1/\xi_0$. In the following the performance measure is denoted by $\epsilon(\kappa)$.

The preceding discussion yields a frequency domain perspective on the performance of dynamical systems with friction, but disregards the influence of measurement noise. The next section presents an extension of the frequency domain performance criterion that incorporates the effects of measurement noise in the performance criterion.

Influence of Measurement Noise

This section discusses the application of the time and frequency domain performance criteria in Definition 5.1 and 5.2 in practice. The influence of noise on both criteria is analyzed which leads to an extension of the frequency domain performance criterion taking into account the quality of the measured spectral components, prior to including them in the performance criterion.

Consider the system in Figure 5.1 subject to a sinusoidal input $w \in \mathfrak{S}_{\xi_0}$. Next, assume that the measurements performed during this experiment have a sufficiently high signal to noise ratio (SNR). The rms error is a measure of the power of the tracking error which predominantly consists of low frequent components of frequencies similar to the excitation frequency. These components have a high SNR corresponding the the SNR of the measurements. The influence of noise on the performance measure in Definition 5.2 is therefore small and is neglected in the remainder of this chapter.

However, the frequency domain criterion in Definition 5.1 is based specifically on the high frequent components, i.e. multiples of the excitation frequency, that describe the input-output behavior of the system. The SNR of these high frequent components is generally lower than those dominating the tracking error and decreases with increasing frequency. This motivates a quality condition on the measured spectral lines allowed to be included in the cost function. Hence, to reduce the sensitivity to noise and the variability on the cost function, Definition 5.1 is adapted for application to noisy experimental data.

To achieve this, consider the output of the system as in Figure 5.1 subject to N periods of the sinusoidal input signal $w \in \mathbf{S}$ after transient effects have vanished. This yields N output spectra³ $\mathcal{Y}_n(\xi)$, $n = 1, 2, \dots, N$, with frequency resolution ξ_0 . Next, consider the sample mean $\hat{\mathcal{Y}}(k\xi_0)$ as in (B.6) and the variance on the sample mean $\sigma_{\hat{\mathcal{Y}}}^2(k\xi_0)$ as in (B.7). To decide whether a measured harmonic line is sufficiently accurately measured to be included in the performance measure (5.1) a statistical test is required (see for example Rabijns et al. (2004)). In Appendix B.2 a statistical analysis is presented, which yields the following quality condition on a measured harmonic line.

Definition 5.3 (η -significance).

Consider the sample mean $\hat{\mathcal{Y}}(k\xi_0)$ as in (B.6) and the variance on the sample mean $\sigma_{\hat{\mathcal{Y}}}^2(k\xi_0)$ as in (B.7). Then, the sample mean is called η -significant, if its expected value $\mathbf{E}\{\hat{\mathcal{Y}}(k\xi_0)\} \neq 0$ with at least an η confidence level, i.e. if:

$$\frac{|\hat{\mathcal{Y}}(k\xi_0)|^2}{\sigma_{\hat{\mathcal{Y}}}^2(k\xi_0)} > F_{2,2(N-1)}^\eta \quad (5.3)$$

where $F_{2,2(N-1)}^\eta$, such that the cumulative $F_{2,2(N-1)}$ distribution $\text{cdf}(F_{2,2(N-1)}^\eta) = \eta$.

Using these results, Definition 5.1 is extended to include a condition on the measurement quality of the harmonic lines that are included in the performance criterion.

Definition 5.4 (optimal feed forward compensation: $n(t) \neq 0$).

Consider the system depicted in Figure 5.1 and assume $n(t)$ is stationary (colored) noise. Then, the feed forward compensator is said to be optimal if the system is subject to a sinusoidal input signal $w \in \mathbf{S}_{\xi_0}$, all transient effects have vanished and $\kappa = \kappa_{opt,n}^*$ such that:

$$\begin{aligned} \kappa_{opt,n}^* &= \arg \min_{\kappa \in \mathbf{R}} \frac{1}{N_{\mathbf{K}}} \frac{\sum_{k \in \mathbf{K}} |\mathbf{E}\{\mathcal{Y}(k\xi_0, \kappa)\}|}{|\mathbf{E}\{\mathcal{Y}(\xi_0, \kappa)\}|} \\ \mathbf{K} &= \{k \in \mathbf{N}_{\geq 2} \mid \mathbf{E}\{\mathcal{Y}(k\xi_0, \kappa)\} \neq 0 \text{ with } \eta\text{-confidence level}\} \end{aligned} \quad (5.4)$$

where $\mathbf{E}\{\cdot\}$ denotes the expected value, $\mathcal{Y}(\xi)$ is the spectrum of the steady state response of the system and the performance measure is normalized with respect to the number of significant harmonic lines $N_{\mathbf{K}}$. In the following, the performance measure is denoted by $\zeta(\kappa)$.

In the following the confidence level is selected to be 99.99% as is further discussed in Section 5.2. This confidence level assures elimination of harmonic components that are likely to be generated by stochastic disturbances (see Figure 5.3).

³Measured spectra do generally not exactly equal the theoretical spectra of the steady state output denoted by $\tilde{\mathcal{Y}}_w$ and are therefore denoted by $\mathcal{Y}(\xi)$ in the remainder of this chapter.

| | Time Domain | Frequency Domain |
|----------------------------|--|---|
| Optimal Compensator | $A \cos(2\pi\xi_0 t + \varphi_0)$ $\Rightarrow B \cos(2\pi\xi_0 t + \psi)$ | minimize $\frac{1}{K-1} \sum_{k=2}^K \frac{ \bar{\mathcal{Y}}_w(k\xi_0) }{ \bar{\mathcal{Y}}_w(\xi_0) }$ harmonic disturbance |
| Optimal Tracking | $A \cos(2\pi\xi_0 t + \varphi_0)$ $\Rightarrow A \cos(2\pi\xi_0 t + \varphi_0)$ | minimize $\sqrt{\underbrace{ \bar{\mathcal{Y}}_w(\xi_0) - \mathcal{W}(\xi_0) ^2}_{\text{tracking phase and amplitude}} + \sum_{k=2}^K \underbrace{ \bar{\mathcal{Y}}_w(k\xi_0) ^2}_{\text{harmonic disturbance}}}$ |

Table 5.1: Time domain and frequency domain performance measures for optimal tracking and optimal nonlinear compensation (sinusoidal reference signal $w \in \mathbb{S}$).

Discussion: Time and Frequency Domain Based Performance

In the following the terms frequency and time domain performance are often used. This terminology refers to the representation of the data used to compute a given performance measure. It should be noted that the information contained in the time or frequency domain representation of a signal is fully equivalent. Hence, any information present in either representation is also present in the other. However, as certain information is easier accessible in the time domain than in the frequency domain, a particular representation may be preferable for a given application. This difference is utilized in the performance analysis discussed in this thesis.

In general, the time and frequency domain performance measures introduced in the preceding analysis provide different notions of optimality. Hence, the best tracking performance observed in the time domain does not necessarily correspond to an optimal setting of the nonlinear feed forward controller and vice versa. Table 5.1 compares the goal of optimizing tracking performance to that of optimal design of the feed forward compensator. When aiming at an optimal design of the feed forward compensator as in Definition 5.4, the goal is to have a sinusoidal response to a sinusoidal input signal. However, a difference between the amplitude and phase of the input and output signal at the excitation frequency is not penalized. When optimizing the tracking of a sinusoidal reference signal in the time domain (Definition 5.2), one aims not only to have a sinusoidal response to a sinusoidal input, but to have the same sinusoidal response as the sinusoidal input that is applied to the system. This implies equal amplitude and phase of the input and output signal at the excitation frequency and therefore requires the extension of the corresponding frequency domain performance criterion with a measure of tracking performance. Note that it is the appearance of this tracking term that clouds the time domain perspective on the nonlinear effects of friction.

Although the frequency domain optimality conditions do not necessarily imply optimal tracking in the time domain, the results clearly indicate the optimal setting

for a given nonlinear controller. Further improvement in tracking should then be obtained by adding appropriate and additional (non)linear control action. Apart from yielding an optimal approximation of the true, more complex nonlinear dynamics by the simplified Coulomb friction feed forward model, the frequency domain method possesses high detection sensitivity. Moreover, as linear and nonlinear effects appear 'separated' in the frequency domain, this method allows to independently tune linear and nonlinear controller parameters related to, for example, nonlinear friction and linear viscous damping.

5.2 Friction Compensation in a TEM

The results presented in this section demonstrate the application of the preceding theory to optimal design of a feed forward friction compensator for an industrial high precision motion stage of a Transmission Electron Microscope (TEM). The TEM motion stage is introduced in more detail in the first part of this section. Next, the frequency domain based tuning method introduced in the preceding section is applied to optimally compensate the performance degrading effects of friction.

Set-Up and Problem Statement

The methodology presented in this chapter is used to optimize the performance of a motion stage of a TEM (Figure 5.2). Performance requirements on such motion stages are high as the sample positioning determines how accurate and fast the area of interest can be moved into view. Moreover, apart from speed and accuracy, many applications require smooth motion as well. Combining these requirements with a system that operates in high vacuum and is required to be at complete standstill during long term image acquisition, yields a control loop requiring optimal friction compensation to achieve the required performance.

Figure 5.2 shows a schematic depiction of the motion stage in a TEM and the main components in the drive train. The motion stage is used as a one degree of freedom manipulator and is mounted on the outside of the microscope. As the motion stage manipulates the position of the sample in the electron beam it determines which part of the sample is magnified and projected on the projection plane or CCD camera.

A Bosch Rexroth NYCe4000 controller is used for data acquisition and allows full Matlab/Simulink functionality in the controller and experiment design. The controlled large stroke drive consists of a Maxon DC motor and a precision reduction unit which facilitates the high gear ratio required. The resulting small motion at the output of the gearbox is further reduced by a lever on which a quadrature encoder is mounted to measure the displacement of the rod that drives the sample. This rod then enters the vacuum chamber through a sealed ball bearing.

In the TEM motion stage, friction becomes a dominant performance limiting factor during high accuracy point to point motion and slow movement of the stage.

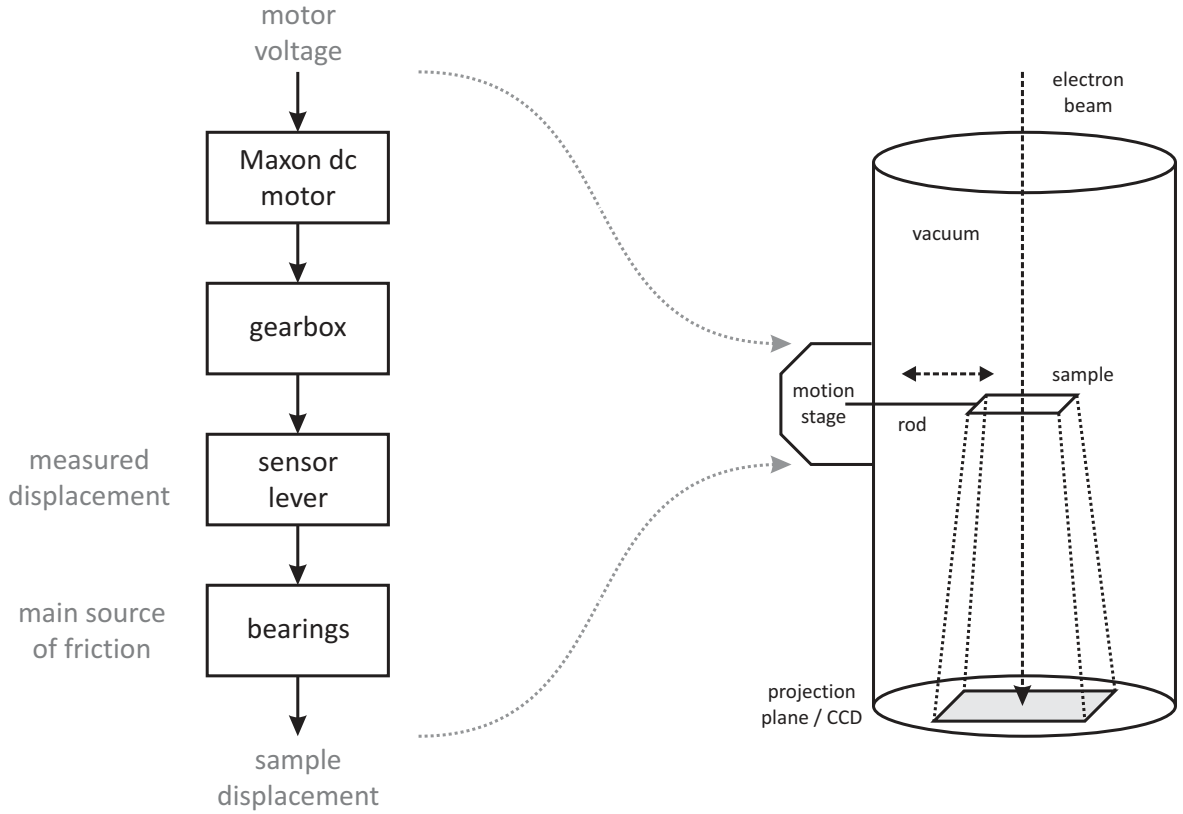


Figure 5.2: Schematic depiction of the motion stage in a transmission electron microscope.

While many industrial applications use a high gain proportional feedback to cope with friction, the accuracy required in the TEM stage requires a loop gain that cannot result in a stable loop, using proportional (and derivative) control only. Although the application of more advanced (nonlinear) feedback controllers is possible, the application of feed forward is to be preferred for two reasons. First, as opposed to feedback, feed forward does not compromise the stability of the closed loop system. Second, many industrial controllers have Coulomb friction feed forward available, whereas advanced nonlinear feedback control is often not available. Next, the theory presented in Section 5.1 is applied to optimally design a feed forward friction compensator for the TEM motion stage.

Experiment Design

Consider the TEM motion stage in a closed loop with a stabilizing proportional feedback controller $C = P_c$ and subject to a feed forward as depicted in Figure 5.1. Next, the performance measure introduced in Definition 5.4 is used to investigate the influence of the feed forward parameter κ by applying the following experimental scheme:

1. $m = 1$: the experiment series starts with no feed forward, i.e. $\kappa^{[1]} = 0$,
2. the system is excited for N periods of the sinusoidal signal $w \in \mathbb{S}$ after transient effects have vanished, yielding N output spectra $\mathcal{Y}_n^{[m]}(\xi)$,

3. $m = m + 1$: if the maximum feed forward parameter κ^{max} is not reached, the feed forward gain: $\kappa^{[m+1]} = \kappa^{[m]} + \Delta_\kappa$ is increased with $\Delta_\kappa = \frac{\kappa^{max}}{M}$ (return to step 2).

This procedure yields $M \cdot N$ output spectra $\mathcal{Y}_n^{[m]}(\xi)$, which are analyzed according to Definition 5.4 to obtain the optimal parameter setting $\kappa_{opt,n}^*$.

The experiment is performed by evaluating κ in the interval $[0 \ 0.3]$ [V] at $M = 80$ equally spaced values, i.e. $\Delta_\kappa = 0.00375$ [V] and the maximum feed forward gain $\kappa^{max} = 0.3$ [V] is determined experimentally by slightly overcompensating the system and the value of M is selected to obtain an accurate estimation of the cost function over the given interval. Furthermore, the influence of the feedback controller is investigated by performing two series of experiments: one with a low feedback gain ($P_c = 5 \cdot 10^6$) and one with a high feedback gain ($P_c = 2 \cdot 10^7$) which is the maximum stabilizing proportional feedback. The confidence level in Definition 5.4 is selected to be 99.99% to reduce the number of non-significant measurement points included in the cost function.

In all experiments the reference signal is a sinusoidal input signal $w \in \mathbf{S}$ with amplitude $\gamma = 6$ [μm] and frequency $\xi_0 = 0.5$ [Hz]. While the selection of γ is arbitrary (as long as the system starts to move), the selection of the excitation frequency depends on the bandwidth of the controller and on the available time for experiments. On the one hand, a higher frequency allows for faster experiments, but on the other hand good tracking is required to assure effective feed forward control. This trade-off is specific to the application and $\xi_0 = 0.5$ [Hz] was shown to yield good results in this case study. Finally, although the optimal feed forward gain depends marginally on the excitation amplitude, the corresponding change in compensator gain and the effect on the systems performance are small and are not considered in this chapter.

Results

The computation of the performance measure in Definition 5.4 starts with indicating the relevant harmonic lines based on the quality of the measurement. An example of the selection of the relevant harmonic lines as prescribed by Definition 5.3 and 5.4 is provided in Figure 5.3. Figure 5.3a shows the measured output amplitude spectrum with no feed forward, while Figure 5.3b depicts the output spectrum with optimal feed forward compensation. In Figure 5.3 the bottom plots indicate the decision variables that indicate whether a measured point is η -significant according to Definition 5.3 with $\eta = 0.9999$. A diamond indicates a positive result and corresponds to a black circle in the top plot which indicates a measurement that is included in the performance measure.

Figure 5.4 - 5.6 show the experimental results for both the high and low feedback gain experiment. In Figure 5.4a the performance measure $\zeta(\kappa)$ from Definition 5.4 is depicted as well as the energy at harmonics, relative to the energy at the excitation frequency. Since the observed friction is predominantly an odd nonlinearity, the dominant behavior of the odd harmonics is to be expected. As the feed forward gain

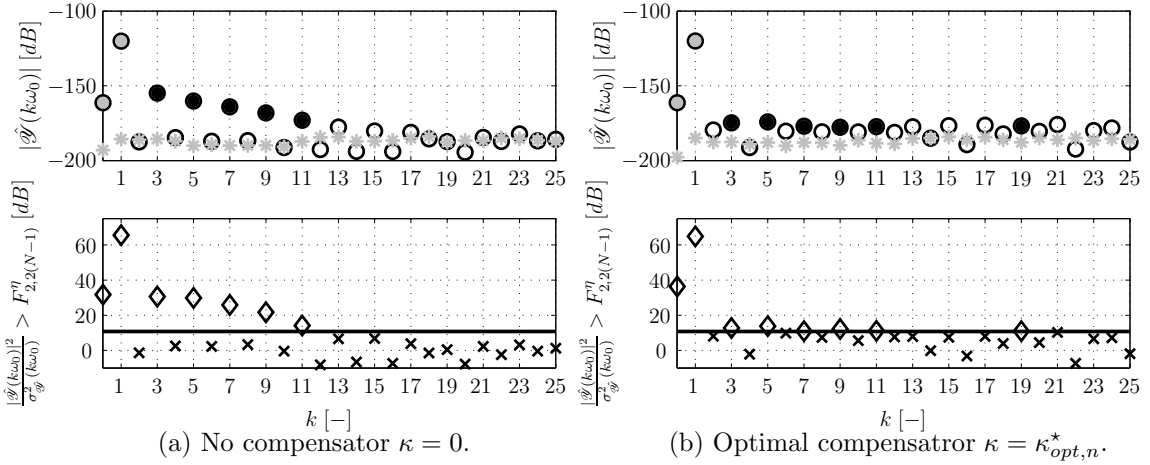


Figure 5.3: Selection of relevant harmonic lines, based on the η -significance bound in Definition 5.4, 5.3 ($\eta = 0.9999$) (low gain feedback).

Bottom: η -significance test: (—): η -significance bound $F_{2,2(N-1)}^\eta$ and measured test quantities (\diamond): η -significant and (\times): not η -significant.

Top: Amplitude spectrum: (\circ): $|\hat{\Psi}(k\xi_0)|$ modulus of the sample average, ($*$): $\sigma_{\hat{\Psi}}^2(k\xi_0)$ variance on the sample average and (\bullet): η -significant harmonics.

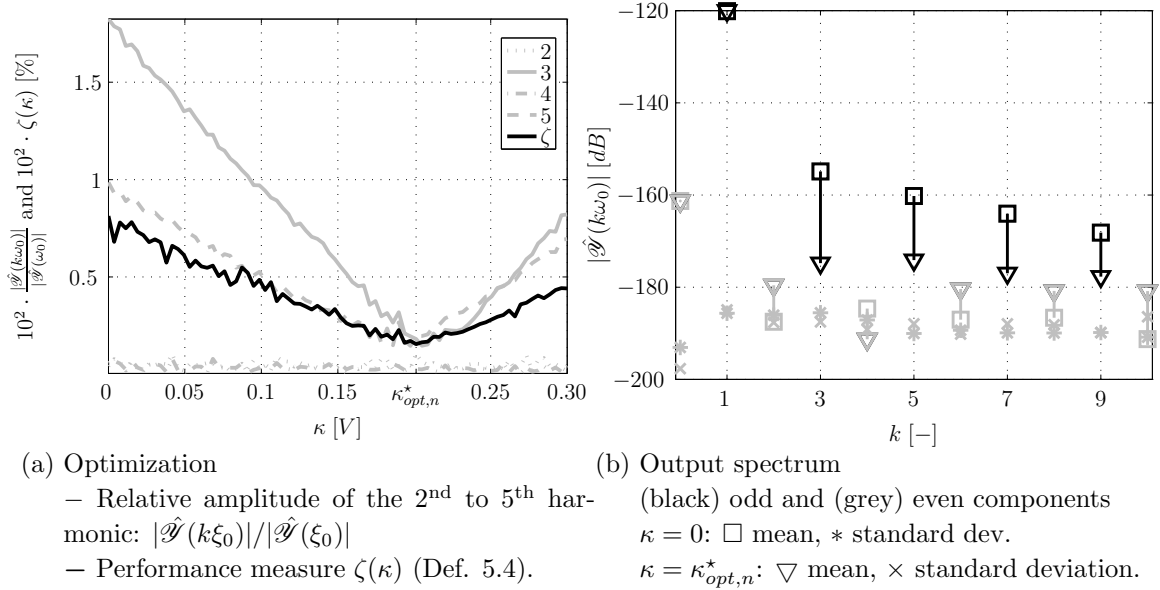


Figure 5.4: Optimization of feed forward control, based on frequency domain data (low gain feedback).

5.4a: Performance measure (Definition 5.4) and average output amplitude spectrum at harmonics, relative to the amplitude spectrum at the excitation frequency.

5.4b: Average output amplitude spectra with / without optimal feed forward.

is increased, a decrease in the energy observed at the relevant harmonics, relative to the energy at the excitation frequency, appears until a minimum is reached. As the minimum of the performance measure combines the behavior of all harmonic lines, this

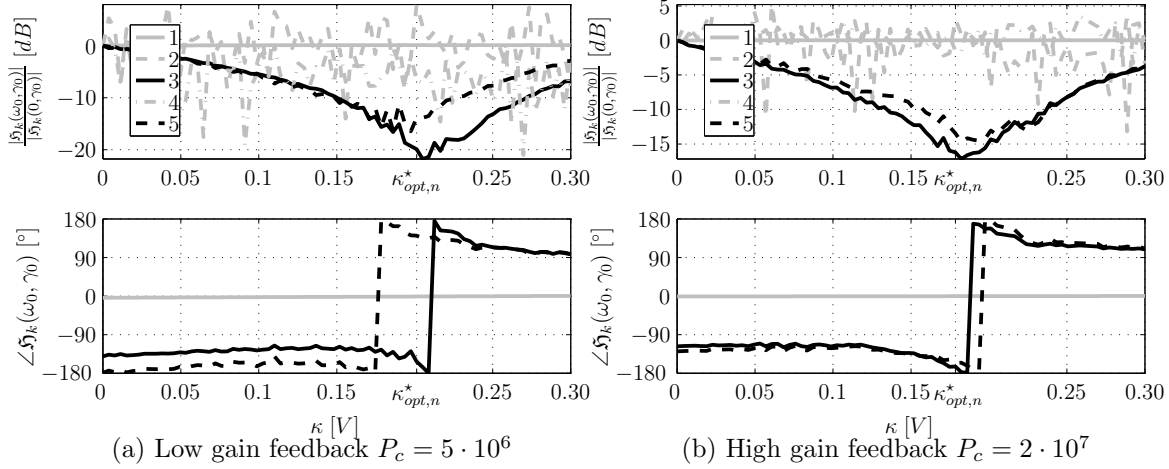


Figure 5.5: First five higher order sinusoidal input describing functions at $\xi_0 = 0.5$ [Hz], $\gamma_0 = 1$ [μm] for varying values of κ .

indicates that $\kappa_{opt,n}^* = 0.2013$ [V], which yields the optimal feed forward compensator according to Definition 5.4 in case of low gain feedback. This optimal feed forward gain is not a physical system parameter as it depends on both the physical friction parameters and on properties of the systems such as the motor constants.

Figure 5.4b shows the average energy at harmonics of the input frequency both with and without optimal feed forward. This indicates that optimal feed forward reduces, for example, the energy level at the third harmonic in the output spectrum by a factor 10. Moreover, the performance measure in Figure 5.4a drops by a factor 5.3, showing less than 19% of the average amplitude at harmonics when optimal feed forward is applied.

Next, consider the corresponding HOSIDFs (Definition 2.8), which provide both amplitude and phase information about the nonlinear behavior of the closed loop system as a function of the feed forward parameter κ . Figure 5.5 shows the normalized HOSIDFs for varying feed forward gain. Corresponding to the decreasing energy at harmonic lines, the HOSIDFs show a minimum close to $\kappa_{opt,n}^*$. Moreover, the HOSIDFs show a phase shift around the optimum that may be used to efficiently detect the optimum. Generally, the minima of the different HOSIDF (and the corresponding harmonics in Figure 5.4a) differ. This phenomena has not been studied in detail. However, the cost function $\zeta(\kappa)$ combines the effects of all harmonics and yields an optimum where the total amplitude of the harmonics is minimized.

5.3 Frequency Domain Based Performance in Practice

In this section three observations are discussed with respect to frequency domain based optimal tuning of a feed forward friction compensator. First, the difference between time and frequency domain performance, as observed in experiments, is analyzed. Se-

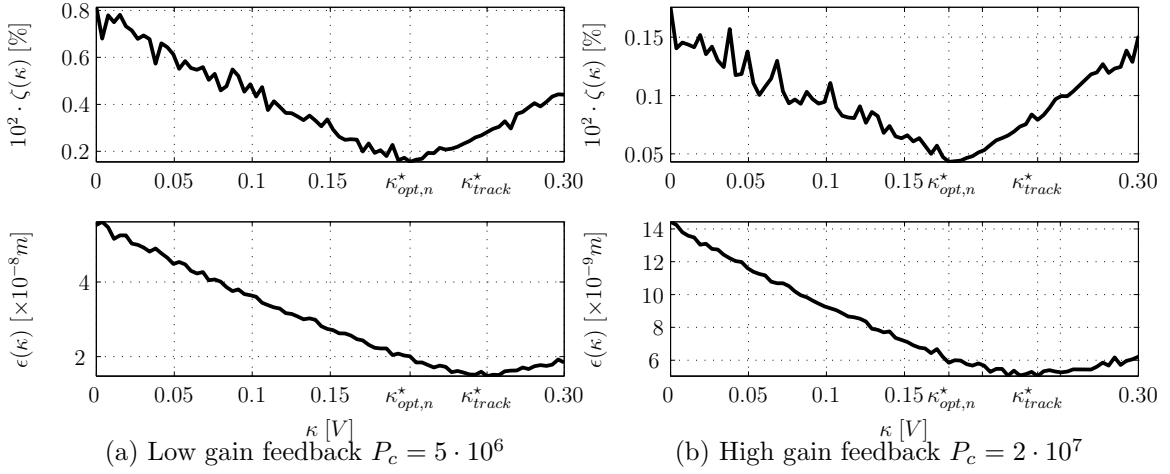


Figure 5.6: Comparison of time and frequency domain performance measures (Top) optimal feed forward compensation using a frequency domain performance measure $\zeta(\kappa)$ (Definition 5.4). (Bottom) corresponding time domain tracking performance $\epsilon(\kappa)$ (Definition 5.2).

cond, the effect of the feedback controller on the optimal feed forward setting is discussed. Finally, optimal feed forward compensator design is shown to significantly improve the performance of the TEM motion stage by facilitating low speed jogging motion which is often required by microscopists.

Time Domain Versus Frequency Domain Performance

In Section 5.1 it is indicated that the time and frequency domain optimality conditions in Definition 5.2 and 5.4 generally yield different controller settings. In Figure 5.6 the frequency domain performance measure $\zeta(\kappa)$ (Definition 5.4) and the corresponding tracking performance $\epsilon(\kappa)$ (Definition 5.2) are compared. The top figures show the frequency domain performance measure indicating the optimal value of the feed forward parameter $\kappa_{opt,n}^*$. The bottom plot depicts the corresponding tracking performance and indicate a different optimal value of the feed forward parameter κ_{track}^* . The discrepancy between both performance measures is expected to be caused by the presence of viscous damping which is not otherwise compensated for during the experiment. As the Coulomb friction feed forward gain is the only tunable parameter, the minimal tracking error occurs at a value of $\kappa_{track}^* > \kappa_{opt,n}^*$, where the Coulomb feed forward compensates for part of the viscous damping as well. At first glance, this appears to yield a better tracking performance. However, the harmonics in the output spectrum are not minimized for $\kappa > \kappa_{opt,n}^*$ and the effects of linear viscous damping are compensated using a nonlinear friction compensator. The apparent optimum in performance is therefore local as it depends on the excitation signal and the true optimal value of the feed forward gain is located at $\kappa_{opt,n}^*$. To further improve tracking performance, additional control action is required.

| | $P_c = 5 \cdot 10^6$ | $P_c = 2 \cdot 10^7$ | $\kappa_{high}^*/\kappa_{low}^*$ |
|-------------------------------------|----------------------|----------------------|----------------------------------|
| $\kappa_{opt,n}^*$ | 0.2013 | 0.1785 | 0.8867 |
| κ_{track}^* | 0.2506 | 0.2354 | 0.9393 |
| $\kappa_{track}^*/\kappa_{opt,n}^*$ | 1.2449 | 1.3188 | |

Table 5.2: Experimental results for different values of the feedback gain P_c

Influence of the Feedback Gain

Figure 5.6 depicts the performance measures as in Definition 5.2 and 5.4 for the experiments with high and low gain feedback. The initial amount of energy at harmonics when using high gain feedback is less than in the low gain experiment as increasing the feedback gain linearizes the closed loop behavior. However, the optimal values $\kappa_{opt,n}^*$ observed in the high and low feedback gain experiments differ as well.

Table 5.2 summarizes the numerical results from both experiments. It shows that the optimal feed forward gains $\kappa_{opt,n}^*$ for the low and high gain experiment differ by approximately 11%. Figure 5.6a shows that the decrease in energy at harmonic lines in the low gain feedback is approximately 80%. When using high gain feedback this is reduced only slightly to a decrease of approximately 75% as shown in figure 5.6b. The relative difference between the optimal value $\kappa_{opt,n}^*$ based on the frequency domain performance measure and the apparent optimum indicated by the time domain tracking performance κ_{track}^* differs from 24% to almost 32% between both experiments.

Application to Low Speed Jogging

In electron microscopy, extreme slow jogging motion ($< 100 \text{ nm/s}$) is often required while retaining good visualization of the sample under investigation. For example, when the microscope is user operated, good visual inspection of the sample is required to detect interesting features. Figure 5.7a depicts the measured displacement when a constant velocity of 20 nm/s is required, the system is subject to a proportional, integral, differential feedback controller and no feed forward compensation is present. The stick-slip induced jumps in position make accurate positioning hard to achieve and severely deteriorate the visualization of the sample. When the feed forward compensation is optimized according to Definition 5.4, the response is depicted in Figure 5.7b. Clearly, the application of an optimally designed feed forward compensator yields a significant improvement in performance in terms of smoothness of motion and allows for more accurate positioning and better visualization.

5.4 Conclusions

The methodology introduced in Chapter 4 allows to incorporate frequency domain information in the performance measure of controlled nonlinear systems. In this chapter, this methodology is applied in a modified setting for optimal feed forward friction com-

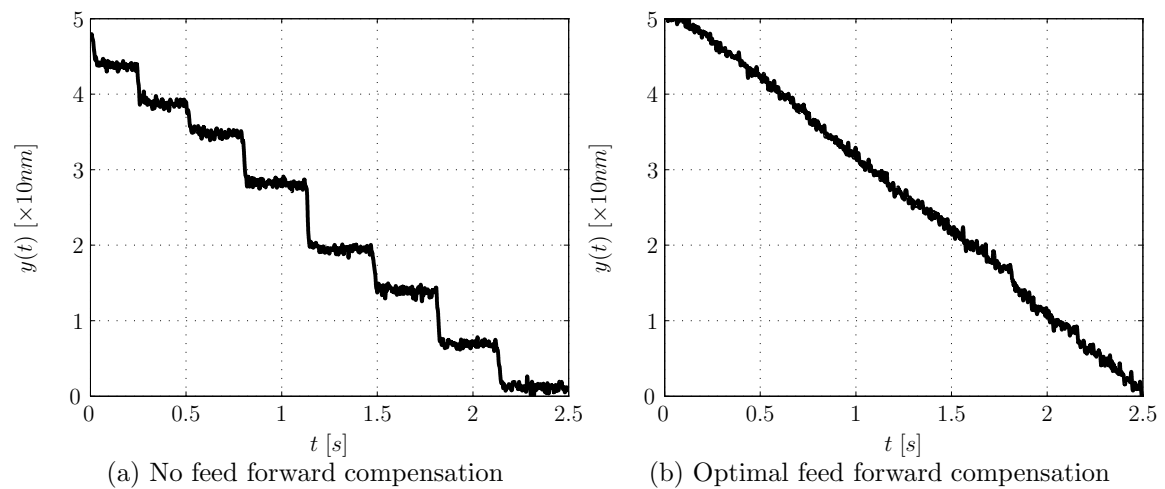


Figure 5.7: Low speed jogging performance improvement by application of optimal feed forward compensation.

pensation in motion systems. The application of the frequency domain methodology allows to optimally compensate the effects of nonlinear friction and is demonstrated in an industrial setting, yielding a significant performance improvement. Compared to conventional time domain methods, the frequency domain approach yields a clear and well defined performance for nonlinear systems, allows for independent tuning of linear and nonlinear controller parameters and yields a high detection sensitivity. Although the frequency domain approach yields a controller design that optimally compensates nonlinearities, it does not necessarily yield optimal tracking behavior, which may require additional control action.

Chapter 6

Conclusions and Recommendations

6.1 Conclusions

The research presented in this thesis deals with the application of frequency domain techniques to nonlinear systems. In particular, frequency domain based modeling, analysis and performance optimization of a class of nonlinear systems is addressed. This is reflected in the research objectives presented in Chapter 1:

O₁ : Investigate the application of frequency domain techniques to the modeling and analysis of nonlinear systems.

O₂ : Develop theoretical concepts and practically applicable methods for performance optimization of nonlinear systems, based on frequency domain analysis.

The first object is mainly addressed in Chapters 2 and 3 by an overview and comparison of frequency domain methods and a novel analysis of systems containing polynomial nonlinearities. The second objective is addressed in Chapters 4 and 5 by the theoretical analysis and practical application of new, frequency domain based techniques for the quantification and optimization of the performance of a class of nonlinear systems. Summarizing, the research presented in this thesis yields the following contributions:

C₁ Overview and comparison of different frequency domain based methods for the modeling and analysis of nonlinear systems (Chapters 2, 3 and in particular Section 2.5).

C₂ Analytical results that allow analysis and numerically efficient computation of the effects of polynomial nonlinearities in the frequency domain (Chapter 3 and in particular Theorem 3.1)

C₃ Theoretical results and practically applicable methodologies that allow optimization of the performance of nonlinear systems by means of novel frequency domain based detection and compensation techniques (Chapters 4, 5 and in particular Theorem 4.1 and Section 5.3).

In general it has been shown that frequency domain methods can be applied to several classes of nonlinear systems and allow to analyze, quantify and optimize the performance of these systems. Specifically, for systems with static nonlinearities this performance optimization has been addressed in detail. In the following, the results discussed in Chapters 2 to 5 are addressed in detail.

Modeling and Analysis of Nonlinear Systems

In Chapter 2, four different frequency domain methods for the modeling and analysis of nonlinear systems are discussed: the Generalized FRF (GFRF), the nonlinear FRF, the describing function approach and linear approximations in the presence of nonlinearities. These methods are compared with respect to the signal and system classes for which they are valid and an overview of the information contained in each model is provided as well. Finally, the type of nonlinear effects captured by each model is compared.

In Chapter 3 new analytical tools and results are presented that allow spectral analysis of the output of a class of nonlinear systems containing polynomial nonlinearities. This provides insight in the dynamics of block structured dynamical systems and allows analytic description and analysis of the corresponding HOSIDFs. Given the systems linear dynamics, the output spectra and Higher Order Sinusoidal Input Describing Functions (HOSIDF) can be described as a simple polynomial function of the parameters defining the nonlinearity. Moreover, using the preceding results, a novel connection is presented between the GFRF and HOSIDF, which both model the dynamics of nonlinear systems in the frequency domain. An explicit analytical relation between these models is derived for polynomial Wiener-Hammerstein systems and necessary and sufficient conditions are derived for this bijective mapping to exist.

Performance Assessment and Optimization of Nonlinear Systems

The second part of this thesis, i.e. Chapters 4 and 5, deals with the frequency domain based analysis and optimization of the performance of a class of nonlinear systems. First of all, in Chapter 4, a frequency domain based method to quantify and optimize the performance of Lur'e-type systems is presented. It is shown that, under mild conditions, a sinusoidal response to a sinusoidal input is necessary and sufficient to show the existence of an equivalent linear and time invariant dynamical model that fully captures the systems dynamics for a well defined set of input signals and initial conditions. This allows to detect and compensate performance degrading nonlinear effects based on output measurements only. Based on this new insight, a frequency domain performance measure is defined which is used to design static nonlinear compensators that optimally compensate performance degrading nonlinear effects.

Secondly, in Chapter 5 the methodology developed in Chapter 4 is adopted and applied to optimize friction compensation in an industrial transmission microscope. The application of frequency domain analysis allows to optimally compensate the ef-

fects of nonlinear friction and is shown to yield a significant performance improvement. Compared to conventional time domain methods, the frequency domain approach allows for independent tuning of linear and nonlinear controller parameters and yields a high detection sensitivity.

Summarizing, the results presented in Chapters 2 - 5 and summarized in contributions \mathbf{C}_1 - \mathbf{C}_3 realize the research objectives \mathbf{O}_1 - \mathbf{O}_2 set for this thesis. With these results in mind, a number of open questions and research topics remain. These recommendations for future research are presented in the following.

6.2 Recommendations

In the following, recommendations for future research are presented. In general, two main recommendations follow from the research presented in this thesis.

- **NONLINEAR THEORY AND ENGINEERING PRACTICE:** Nonlinear effects become increasingly important in high tech applications involving, for example, sensor and actuator nonlinearities, valve systems and magnetic and electric fields. To address these issues it is recommended to connect the large variety of theoretical results in the field of nonlinear dynamics with engineering applications. In particular, a shift from the analytical towards measurable, practically interpretable results would benefit the application of nonlinear theory in practice.
- **APPLICATION OF FREQUENCY DOMAIN METHODS:** Given the widespread acceptance of frequency domain methods in the engineering community and the results presented in Chapters 4 and 5, it is recommended to further explore the application of such methods when applied to nonlinear systems.

In addition to these general recommendations, the following presents detailed suggestions for future research based on the results presented in Chapters 2 to 5.

Modeling and Analysis of Nonlinear Systems

Based on the results in Chapters 2 and 3, the following recommendations are provided:

- **UNIFYING METHODOLOGIES:** Although different frequency domain methods for the analysis and modeling of nonlinear systems exist, a connection between different methodologies is generally missing. It is therefore recommended to further investigate the connections, differences and similarities between different methods to arrive at a more unified framework for the application of frequency domain methods to nonlinear systems.
- **FOCUS ON APPLICABILITY:** When applied to nonlinear systems, frequency domain methods are often viewed from a theoretical point of view. It is recommended to complement these results with tools and methodologies that allow application to identification and control purposes in practice¹.

¹It should be noted that in a number of studies, such steps are already being taken, e.g. see van de Wouw et al. (2008); Nuij et al. (2008a); Pintelon and Schoukens (2012).

- **TRIGONOMETRIC ANALYSIS:** The results presented in Theorem 3.1 provide a novel and numerically efficient way to perform trigonometric analysis. The application of these results to trigonometry has not yet been investigated, but presents an interesting candidate for future research.

Performance Assessment and Optimization of Nonlinear Systems

Both the analysis and the application of the methods presented in Chapters 4 and 5 allow for a number of interesting extensions and additions, which are listed below:

- **EXTENSIONS LUR'E-TYPE SYSTEMS:** The results in Chapter 4 and in particular Theorem 4.1 provide means to assess and optimize the performance of Lur'e-type systems. However, performance optimization is only discussed for the case where the output driving the nonlinearity is known and the control input acts either directly on the input of the nonlinearity or on the same input of the system as the nonlinearity (see Figure 4.2). In general compensation may be based on alternative inputs and outputs which is recommended for future research.
- **EXTENSIONS STATIC NONLINEARITIES:** The class of nonlinear systems considered in this thesis can be extended by considering a more general class of systems containing static nonlinearities. In particular, the static, single input, single output nonlinearity can be extended towards the multiple input, multiple output or the multiple input, single output case. This would, for example, allow for linearization of magnetic drives where nonlinearities depend on both coil-current and position.
- **NON-CONVERGENT SYSTEMS:** The results presented in Chapter 5 indicate that frequency domain based performance analysis is applicable to non-convergent systems as well. It is therefore recommended to consider applications and analysis of non-convergent systems for future research.
- **NON-STATIC NONLINEARITIES:** By considering non-static nonlinearities, the class of systems for which the theory presented in Chapter 4 is valid, can be considerably extended. This would significantly extend the range of applicability and theoretical significance as nonlinearities are rarely truly static in practice.
- **EXCITATION SIGNALS:** The analysis discussed in Chapters 4 and 5 exclusively uses sinusoidal excitation signals. Extensions towards more generalized signal classes such as multisine signals may allow to detect and compensate frequency dependent nonlinear effects and as such extend the applicability of these results.
- **AUTOMATION:** Both in case of uniformly convergent Lur'e-type systems as in case of the friction compensation considered in Chapter 4, automation of the tuning procedure would significantly contribute to practical application of the methodologies. In an extension of the work presented in Chapter 4, it has been observed that the application of extremum seeking algorithms yields promising results. However, alternative studies are required, including stability analysis during online optimization and convexity of the optimization problem.

-
- **COST FUNCTION:** The process of cost function selection as in Chapters 4 and 5 requires further investigation. In particular, the following items are suggested for future research:
 - Optimization of the frequency domain based cost functions (4.3) and (5.4), e.g. the type and number of spectral lines included in the cost function.
 - Design of the shape of the cost function, e.g. the norm taken in (4.3) and (5.4), analysis of convexity of the cost function and analysis of nonzero optimal cost function values and optimality of the corresponding solution.
 - Including tracking information in the frequency domain performance measure, e.g. mixed time and frequency domain cost functions.
 - Including phase information about the nonlinearity in the frequency domain performance measure.
 - **COMPENSATOR ORDER SELECTION AND BASIS FUNCTIONS:** The theory presented in Chapter 4 does not yet include an analysis of the type and order of basis function required. Especially, the trade-off between complexity of the (on-line) optimization problem and the order and type of basis functions used is a recommended subject for future research.

Appendix A

Proofs

A.1 Proofs in Chapter 3

A.1.1 Lemma 3.2

For deterministic spectra $\mathcal{U}(\xi)$, $\mathcal{Y}(\xi)$ and input (3.2), Equation (2.8) yields: $\mathfrak{H}_k(\xi_0, \gamma) = \frac{e^{-ik\varphi_0} \mathcal{Y}(k\xi_0)}{|\mathcal{U}(\xi_0)|^k}$ and hence $H = \Upsilon^{-1}(\gamma)\Phi^{-1}(\varphi_0)Y$. Next, (3.11) yields:

$$H(\xi_0, G_n^\pm) = \Upsilon^{-1}\Phi^{-1}(\varphi_0) \sum_{n=1}^N \Delta(\xi_0)G_n^+(\xi) \Phi(\psi_n) \Omega \Gamma(\gamma_n)\boldsymbol{\alpha}^{[n]}$$

with $\gamma_n = \gamma|G_n^-(\xi_0)|$, $\psi_n = \varphi_0 + \angle G_n^-(\xi_0)$. Finally, $\Phi(\cdot)$ and Δ are diagonal matrices and $\Phi^{-1}(\varphi_0)\Phi(\varphi_0 + \angle G_n^-(\xi_0)) = \Phi(\angle G_n^-(\xi_0))$, which yields (3.12) and completes the proof. \square

A.1.2 Lemma 3.4

The mapping (3.20) follows directly from (3.17) - (4.6) and is bijective if and only if Λ is of full rank. Since Λ is a diagonal matrix, it is of full rank if and only if $|\lambda_p(\varpi_p)| \neq 0 \forall p$. Next, using (4.6), yields $|\lambda_p(\varpi_p)| = 0$, which implies $G^+ \left(\sum_{\ell=1}^p \varpi_p[\ell] \right) = 0$ or $\prod_{\ell=1}^p G^-(\varpi_p[\ell]) = 0$. Hence, $|\lambda_p(\varpi_p)| = 0$ if and only if $\varpi_p \notin \mathbf{W}_p$ and therefore the mapping (3.20) is bijective if and only if $\boldsymbol{\varpi}_P \in \mathbf{W}$. \square

A.1.3 Theorem 3.2

The mapping (3.21) is bijective if and only if $\check{\mathfrak{R}}$ is of full rank. The matrix $\check{\mathfrak{R}}$ is of full rank if and only if all matrices in (3.22) have full rank. Matrices $\check{\Upsilon}$, $\check{\Delta}(\xi_0)G^+(\xi)$, $\check{\Phi}(\angle G^-(\xi_0))$ and $\Gamma(|G^-(\xi_0)|\gamma)$ are diagonal and are defined and of full rank for $\xi_0 \in \mathbb{R}_{>0}$ and $\gamma \neq 0$. Moreover, matrix Λ is of full rank if and only if $\boldsymbol{\varpi}_P \in \mathbf{W}$ (Lemma

3.4). Finally, analysis reveals that $\check{\Omega}$ is upper triangular, see Corollary 3.1. Next, consider an arbitrary row $\check{\Omega}_{\ell_1}$ of $\check{\Omega}$ with its first nonzero element at the k^{th} column in that row. Now, because of the rule according to which $\check{\Omega}$ is generated, any row $\check{\Omega}_{\ell_2}$, $\ell_2 > \ell_1$ has a zero element at the k^{th} position. Hence, there is at least one element $\check{\Omega}_{\ell_1, k} \neq \zeta \check{\Omega}_{\ell_2, k}$, $\zeta \in \mathbb{R} \setminus \{0\}$ and thus $\check{\Omega}_{\ell_1} \neq \zeta \check{\Omega}_{\ell_2}$. Since ℓ_1 and ℓ_2 are arbitrary, this proves that $\check{\Omega}$ has full rank. If $\gamma = 0$ or $\xi_0 \leq 0$ or $\varpi_P \notin \mathbb{W}$, then $\check{\mathfrak{X}}$ is singular or undefined since at least one of the matrices in (3.21) is singular or undefined. Hence, if and only if $\gamma \neq 0$ and $\xi_0 > 0$ and finite and $\varpi_P \in \mathbb{W}$, the mapping (3.21) is defined and is bijective. \square

A.1.4 Lemma 3.5

Consider a linear $\overline{\text{PWIH}}$ system, i.e. $\rho : r(t) = \alpha_1 q(t)$. Then, as an LTI system has a sinusoidal steady state response to a sinusoidal input, $\mathfrak{H}_k = 0 \forall k \neq 1$. Next, using (3.21), the structure of $\check{\Omega}$ and the fact that all other matrices are diagonal yields that $\mathfrak{Z}_p = 0 \forall p \neq 1$. Inversely, if $\mathfrak{Z}_p = 0 \forall p \neq 1$ this implies a linear $\overline{\text{PWIH}}$ system and by the same arguments $\mathfrak{H}_k = 0 \forall k \neq 1$. \square

A.2 Proofs in Chapter 4

A.2.1 Theorem 4.1

Consider a Lur'e-type system as in Definition 4.1 and assume assumptions A₁-A₃ in Theorem 4.1 are satisfied. Next, consider the single sided spectra of the steady state signals $w(t)$, $\bar{u}_w(t)$ and $\bar{y}_{\ell, w}(t)$, $\ell = 1, 2$, denote these by $\mathcal{W}(\xi)$, $\mathcal{U}_w(\xi)$, $\mathcal{Y}_{\ell, w}(\xi) \in \mathbb{C}$ and consider the relation between the input and steady state output as follows from (4.1):

$$\begin{aligned} \begin{bmatrix} \mathcal{Y}_{1, w}(\xi) \\ \mathcal{Y}_{2, w}(\xi) \end{bmatrix} &= \begin{bmatrix} G_{1, w}(\xi) & G_{1, u}(\xi) \\ G_{2, w}(\xi) & G_{2, u}(\xi) \end{bmatrix} \begin{bmatrix} \mathcal{W}(\xi) \\ \mathcal{U}_w(\xi) \end{bmatrix} \\ &= \left(\begin{bmatrix} C_1 \\ C_2 \end{bmatrix} (i2\pi\xi I - A)^{-1} \begin{bmatrix} B_w & B_u \end{bmatrix} + \begin{bmatrix} D_{1, w} & D_{1, u} \\ D_{2, w} & D_{2, u} \end{bmatrix} \right) \begin{bmatrix} \mathcal{W}(\xi) \\ \mathcal{U}_w(\xi) \end{bmatrix} \end{aligned} \quad (\text{A.1})$$

The proof of equivalency of S₁-S₃ is based on the following well known property of LTI systems:

Property A.1. *If a system (4.2) is subject to a sinusoidal input $w \in \mathcal{S}_{\xi_0}$, then all nonzero steady state outputs are sinusoidal, i.e. $\bar{y}_{\ell, w} \in \mathcal{S}_{\xi_0} \forall \ell = 1, 2$.*

Now let $v \in \mathbb{R}_{>0}$ and define:

$$\mathfrak{J} = \{(x_0, w) \in \mathbb{R}^n \times \mathbb{B}_p \mid \|y_2(t)\|_{\infty} \leq v\}$$

Next, let $w \in \mathcal{S}_{\xi_0}$ be sinusoidal with frequency ξ_0 and consider the following intermediate results:

1. ($S_1 : \text{TRUE} \rightarrow S_2 : \text{TRUE}$) : According to assumption A₃, $|G_{1,u}(\xi)| \neq 0 \forall \xi \in \mathbb{R}$. Using (A.1), this implies that if $\bar{y}_{1,w} \in \mathbf{S}_{\xi_0}$, then $\bar{u}_w \in \mathbf{S}_{\xi_0}$ or $\bar{u}_w = 0$. Next, as $\bar{y}_{2,w}$ is nonzero according assumption A₂, (A.1) implies that $\bar{y}_{2,w} \in \mathbf{S}_{\xi_0}$. Hence, S_2 is true, which completes this part of the proof.
2. ($S_1 : \text{TRUE} \rightarrow S_3 : \text{TRUE}$) : From 1 it follows that if S_1 is true, then $\bar{y}_{2,w} \in \mathbf{S}_{\xi_0}$ and $\bar{u}_w \in \mathbf{S}_{\xi_0}$ or $\bar{u}_w = 0$, which, as $\phi : \mathbb{R} \mapsto \mathbb{R}$, implies:

$$\phi(y_2(t)) = \alpha y_2(t) \quad \alpha \in \mathbb{R}, \|y_2(t)\|_\infty \leq v$$

where $v = \|\bar{y}_{2,w}\|_\infty$. Hence, for all $(x_0, w) \in \mathfrak{J}$ the nonlinear feedback in Figure 4.1 reduces to a linear feedback. As the system is uniformly convergent according to A₁, this implies there exists a representation (4.2) such that $x(t) = \tilde{x}(t)$ and $y(t) = \tilde{y}(t)$ for all $t \in \mathbb{R}$ and $(x_0, w) \in \mathfrak{J}$. Hence, S_3 is true, which concludes this part of the proof.

3. ($S_2 : \text{TRUE} \rightarrow S_3 : \text{TRUE}$) : This follows from 2.
4. ($S_1 : \text{FALSE} \rightarrow S_3 : \text{FALSE}$) : If $w \in \mathbf{S}_{\xi_0}$, but $\bar{y}_{1,w} \notin \mathbf{S}_{\xi_0}$, Property A.1 is violated which implies that a representation (4.2) does not exist. Hence, S_3 is false, which completes this part of the proof.
5. ($S_1 : \text{FALSE} \rightarrow S_2 : \text{FALSE}$) : According to A₃, $|G_{2,u}(\xi)| \neq 0 \forall \xi \in \mathbb{R}$. As $w \in \mathbf{S}_{\xi_0}$, but $\bar{y}_{1,w} \notin \mathbf{S}_{\xi_0}$, (A.1) implies $\bar{u}_w \notin \mathbf{S}_{\xi_0}$. However, if $y_{2,w} \in \mathbf{S}_{\xi_0}$, then, according to (A.1), $u_w(t) \in \mathbf{S}_{\xi_0}$, which contradicts the previous statement and hence $y_{2,w} \notin \mathbf{S}_{\xi_0}$. This implies that S_2 is false, which completes this part of the proof.
6. ($S_2 : \text{FALSE} \rightarrow S_3 : \text{FALSE}$) : This proof is identical to the proof in 4.

Hence, the proofs in 1-6 yield that $S_1 \leftrightarrow S_2$, $S_1 \leftrightarrow S_3$ and $S_2 \leftrightarrow S_3$, i.e. it is shown that S_1 - S_3 are equivalent which completes the proof. \square

A.2.2 Results in Table 4.1

Consider the Chebyshev based compensator as in (4.5) and note that:

$$\chi(\nu) = \lambda\nu + f_\chi(\nu)$$

with λ as in (4.6) and $\partial f_\chi / \partial \nu|_{\nu=0} = 0$. Furthermore, note that the nonlinearity ϕ in Figure 4.2 can always be written as $\phi(\nu) = \rho\nu + f_\phi(\nu)$, $\rho \in \mathbb{R}$, with $\partial f_\phi / \partial \nu|_{\nu=0} = 0$. Now, consider two cases:

cascade compensator In case of a cascade compensator configuration as in Figure 4.2a, the output of the compensated nonlinearity equals:

$$-\phi(\chi(\nu)) = -\lambda\rho\nu + f_{\chi\phi}^\times(\nu)$$

with $\partial f_{\chi\phi}^{\times}/\partial\nu|_{\nu=0} = 0$. As $f^{\times}(\nu)$ does not contain a linear term in its Taylor expansion, optimization of the performance in the sense of Definition 4.2 yields $f^{\times}(\nu) \rightarrow 0$ as $\aleph \rightarrow 0$ in (4.3). Hence, if optimal performance is attained such that $\aleph = 0$, then if $\lambda = \alpha$, the linear feedthrough equals $\lambda = -\alpha\rho$.

parallel compensator In case of a parallel compensator configuration as in Figure 4.2b, the output of the compensated nonlinearity equals:

$$\chi(\nu) - \phi(\nu) = (\lambda - \rho)\nu + f_{\chi\phi}^+(\nu)$$

with $\partial f_{\chi\phi}^+/\partial\nu|_{\nu=0} = 0$. As $f^+(\nu)$ does not contain a linear term in its Taylor expansion, by the same reasoning for in the cascade compensator case, $f^+(\nu) \rightarrow 0$ as $\aleph \rightarrow 0$. Hence, if optimal performance is attained such that $\aleph = 0$, then if $\lambda = \alpha$, the linear feedthrough equals $\lambda = \alpha - \rho$.

This yields the results presented in Table 4.1.

Appendix B

Additional Results

B.1 Computation of the BLA and Signal Processing

Consider the following subclass of Gaussian Riemann equivalent signals.

Definition B.1 (Odd random phase multisine).

A signal $u^{[m]}(t)$ is the m^{th} realization of an odd random phase multisine if it is harmonic according to Definition 1.4 and $\xi_n \in \{(2n-1)\xi_0 \mid n \in \mathbb{N}_{\geq 1}\}$ for some $\xi_0 \in \mathbb{R}_{>0}$. Moreover, A_k and φ_k are mutually independent, $\mathbb{E}\{e^{i\varphi_k^{[m]}}\} = 0$ and $A_k^2 = f_A^2(\xi_k)$ with $f_A(\xi)$ a user defined piecewise continuous function with a finite number of discontinuities.

The odd random phase multisine is particularly useful for detection of nonlinear effects when a frequency line is removed approximately every 5 odd frequency lines (Pintelon et al., 2004b). For convenience the same lines are removed for all realizations.

Next, consider an experiment with M realizations of the signal defined in Definition B.1. Furthermore, P periods of the input signal $u^{[m]}(t)$ and output signal $y^{[m]}(t)$ are measured. This yields $P \times M$ periodic responses and the same number of estimates of the Fourier spectra of the output $\mathcal{Y}_F^{[m]}$. Averaging over multiple periods of the same realization yields the variance originating from stochastic distortions (noise), but does not yield nonlinear effects.

$$\hat{\mathcal{Y}}_F^{[m]} = \frac{1}{P} \sum_{p=1}^P \mathcal{Y}_F^{[m]}_p \quad (\text{B.1})$$

$$\sigma_{\mathcal{N}}^{2[m]} = \frac{1}{P(P-1)} \sum_{p=1}^P \left| \mathcal{Y}_F^{[m]}_p - \hat{\mathcal{Y}}_F^{[m]} \right|^2 \quad (\text{B.2})$$

The average spectra $\hat{\mathcal{Y}}_F^{[m]}$ consist both of the excited spectral lines and a possible response on non-excited spectral lines. Therefore, the analysis splits into two parts.

First, the response on the excited lines will be analyzed and second, the computation of the response measured on non-excited lines will be discussed.

For frequency lines where the system was originally excited, the part of the output spectrum that is generated by the BLA of the system and the corresponding variance are calculated as follows:

$$\check{\mathcal{Y}}_F = \frac{1}{M} \sum_{m=1}^M \left[\frac{\mathcal{W}_F^{[m]}}{|\mathcal{W}_F^{[m]}|} \right]^{-1} \hat{\mathcal{Y}}_F^{[m]} \quad (\text{B.3})$$

$$M\sigma_{\mathcal{F}}^2 + \sigma_{\mathcal{N}}^2 = \frac{1}{M-1} \sum_{m=1}^M \left| \check{\mathcal{Y}}_F^{[m]} - \check{\mathcal{Y}}_F \right|^2 \quad (\text{B.4})$$

where $\sigma_{\mathcal{N}}^2$ is the variance estimate of the disturbing noise (B.2) of the spectrum, averaged over P periods as computed from. Next, $\sigma_{\mathcal{F}}^2$ is the variance estimate of the nonlinear noise source on the average over M realizations. This variance is calculated by analyzing the variance over different realizations since the nonlinearities are excited differently for different realizations of the multisine. The calculations above yield an equivalent system in the sense of Figure 2.6 and allow to compute the BLA as in (2.10) (Lemma 2.1).

The response at non-excited lines is obtained by calculating the variance of the power in the output spectra, measured at the non-excited lines. A distinction is made between energy occurring at odd and even lines for classification of the nonlinearities:

$$\mathcal{P}^2(\ell_{o/e}) = \frac{1}{M-1} \sum_{m=1}^M \left| \varepsilon - \hat{\mathcal{Y}}_F^{[m]}(\ell_{o/e}) \right|^2 \quad (\text{B.5})$$

where $\ell_{o/e}$ denotes the odd and even non-excited frequency lines respectively. The average value ε is small, since the phases of $\hat{\mathcal{Y}}_F^{[m]}(\ell_{o/e})$ are randomly distributed in the interval $[-\pi, \pi)$ and the average therefore tends to zero.

Summarizing, by conducting measurements with P periods of M realizations of the random multisine (Definition B.1), the BLA is obtained using (B.1)-(B.4). Furthermore, the variance on this BLA due to stochastic disturbances is computed according to (B.2). The influence of nonlinearities can be computed as a variance of the output spectrum or FRF by (B.4). Finally, an estimate of nonlinear effects as well as a classification of these effects is obtained from (B.5).

B.2 Statistics

Consider the output $y(t)$ of the system as in Figure 5.1 subject to N periods of a sinusoidal input signal $w \in \mathbf{S}$, after transient effects have vanished. The measured stochastic variable $y_n(t) \in \mathbb{R}$, $n = 1, 2, \dots, N$ is a deterministic signal, distorted by stationary (colored) noise which implies that the corresponding spectra $\mathcal{Y}_n(\xi) \in \mathbb{C}$ are asymptotically circular complex normally (c.c.n) distributed. Next, consider sample

mean $\hat{\mathcal{Y}}$ (B.6), the variance on the sample mean $\sigma_{\hat{\mathcal{Y}}}^2$ (B.7) and the sample variance $\sigma_{\hat{\mathcal{Y}}}^2 = N\sigma_{\mathcal{Y}}^2$.

$$\hat{\mathcal{Y}}(k\xi_0) = \frac{1}{N} \sum_{n=1}^N \mathcal{Y}_n(k\xi_0) \quad (\text{B.6})$$

$$\sigma_{\hat{\mathcal{Y}}}^2(k\xi_0) = \frac{1}{N(N-1)} \sum_{n=1}^N \left| \mathcal{Y}_n(k\xi_0) - \hat{\mathcal{Y}}(k\xi_0) \right|^2 \quad (\text{B.7})$$

Then, denote the corresponding (unknown) true variances by ς^2 and note that as \mathcal{Y}_n is c.c.n. distributed the true sample variance is related to the estimated sample variance by:

$$\mathbf{E} \{ \sigma_{\hat{\mathcal{Y}}}^2 \} = \varsigma_{\mathcal{Y}}^2 = 2\varsigma_{\Re\{\mathcal{Y}\}}^2 = 2\varsigma_{\Im\{\mathcal{Y}\}}^2$$

Since \mathcal{Y}_n is c.c.n. distributed, the normalized estimate of the square of the absolute value of the sample mean is non central $\chi_{2,\text{noncentral}}^2$ distributed if $\mathbf{E} \{ \hat{\mathcal{Y}} \} \neq 0$. Moreover, the normalized estimate of the variance on the sample mean is central χ_2^2 distributed. Hence, the ratio of the normalized estimates of the square of the absolute value and variance of the sample mean is simply noncentral $F_{2,2(N-1)}$ distributed, i.e.

$$\frac{\frac{|\hat{\mathcal{Y}}|^2}{\varsigma_{\hat{\mathcal{Y}}}^2/(2N)}}{\frac{\sigma_{\hat{\mathcal{Y}}}^2}{\varsigma_{\hat{\mathcal{Y}}}^2/2}} \sim \frac{\chi_{2,\text{noncentral}}^2}{\chi_{2(N-1)}^2} \Rightarrow N \frac{|\hat{\mathcal{Y}}|^2}{\sigma_{\hat{\mathcal{Y}}}^2} = \frac{|\hat{\mathcal{Y}}|^2}{\sigma_{\hat{\mathcal{Y}}}^2} \sim F_{2,2(N-1),\text{simply noncentral}}$$

However, if $\mathbf{E} \{ \hat{\mathcal{Y}} \} = 0$, the normalized square of the absolute value of the sample mean is central χ_2^2 distributed. Hence, the corresponding ratio of the normalized estimates of the square of the absolute value and variance of the sample mean is **central** $F_{2,2(N-1)}$ distributed, i.e.

$$\frac{|\hat{\mathcal{Y}}|^2}{\sigma_{\hat{\mathcal{Y}}}^2} \sim F_{2,2(N-1)} \quad (\text{B.8})$$

Hence, to test if $\mathbf{E} \{ \hat{\mathcal{Y}}(k\xi_0) \}$ is significantly different from 0 with a confidence level η , it suffices to test if $|\hat{\mathcal{Y}}(k\xi_0)|^2/\sigma_{\hat{\mathcal{Y}}}^2(k\xi_0)$ is not $F_{2,2(N-1)}$ distributed with the same confidence level η . This is formalized in Definition 5.3.

Bibliography

- F. Al-Bender, V. Lampaert and J. Swevers. The generalized maxwell-slip model: A novel model for friction simulation and compensation. *IEEE T Automat Contr*, 50(11):1883–1887, 2005.
- E. Alcorta-García, L. Rodríguez-Alfaro, D. Diaz-Romero and C. Posadas-Castillo. Characterization of frequency response functions for nonlinear convergent systems. In *Proc Conference on Control and Fault-Tolerant Systems*, pages 630–635, 2010.
- B. Armstrong-H'elouvry. *Control of machines with friction*. Kluwer, 1991.
- B. Armstrong-H'elouvry, P. Dupont and C. Canudas de Wit. A survey of models, analysis tools and compensation methods for the control of machines with friction. *Automatica*, 30:1083–1138, 1994.
- E. Bedrosian and S. Rice. Output properties of Volterra systems (nonlinear systems with memory) driven by harmonic and Gaussian inputs. *Proc IEEE*, 59(12):1688–1707, 1971.
- S. Billings and Z.-Q. Lang. A bound for the magnitude characteristics of nonlinear output frequency response functions: Part 1. analysis and computation. *Int J Control*, 65(2):309–328, 1996a.
- S. Billings and Z.-Q. Lang. A bound for the magnitude characteristics of nonlinear output frequency response functions: Part 2. practical computation of the bound for systems described by the nonlinear autoregressive model with exogenous input. *Int J Control*, 65(3):365–384, 1996b.
- S. Billings and J. C. Peyton Jones. Mapping non-linear integro-differential equations into the frequency domain. *Int J Control*, 52:863–879, 1990.
- S. Billings and K. Tsang. Spectral analysis for non-linear systems, part i: Parametric non-linear spectral analysis. *Mech Syst Signal Pr*, 3(4):319–339, 1989a.
- S. Billings and K. Tsang. Spectral analysis for non-linear systems, part ii: Interpretation of non-linear frequency response functions. *Mech Syst Signal Pr*, 3(4):341–359, 1989b.
- S. Billings, K. Tsang and G. Tomlinson. Spectral analysis for non-linear systems, part iii: Case study examples. *Mech Syst Signal Pr*, 4(1):3–21, 1990.
- H. Bode. *Network analysis and feedback amplifier design*. Van Nostrand, 1945.

- S. Boyd and L. O. Chua. Fading memory and the problem of approximating nonlinear operators with volterra series. *IEEE T Circuits Syst*, CAS-32(11):1150–1161, 1985.
- S. Boyd, Y. Tang and L. O. Chua. Measuring volterra kernels. *IEEE T Circuits Syst*, CAS-30(8):571–577, 1983.
- P. van Bree, C. van Lierop and P. van den Bosch. Feed forward initialization of hysteretic systems. In *Proc Conference on Decision and Control*, pages 3505–3510, 2010a.
- P. van Bree, C. van Lierop and P. van den Bosch. Electron microscopy experiments concerning hysteresis in the magnetic lens system. In *Proc Conference on Control Applications*, pages 956–961, 2010b.
- W. van den Broek, S. van Aert and D. van Dyck. A model based reconstruction technique for depth sectioning with scanning transmission electron microscopy. *Ultramicroscopy*, 110(5):548–554, 2010.
- W. van den Broek, S. van Aert, P. Goos and D. van Dyck. Throughput maximization of particle radius measurements through balancing size versus current of the electron probe. *Ultramicroscopy*, 111(7):940–947, 2011.
- J. de Bruin, A. Doris, N. van de Wouw, W. Heemels and H. Nijmeijer. Control of mechanical motion systems with non-collocation of actuation and friction: a popov criterion approach for input-to-state stability and set-valued nonlinearities. *Automatica*, 45:405–415, 2009.
- C. Canudas de Wit, H. Olsson, K. Astrom and P. Lischinsky. New model for control of systems with friction. *IEEE T Automat Contr*, 40(3):419–425, 1995.
- C. Coulomb. Theory des machines implique, en ayant egard au frottement de leurs parties, et a la roideur deus cordages. *Mem Math Phy*, 1785.
- P. Dahl. A solid friction model. *The Aerospace Corporation Technical Report*, 1968.
- B. Demidovich. Lectures on stability theory. Nauka, Moscow (in Russian), 1967.
- T. D’haene, R. Pintelon, J. Schoukens and E. Van Gheem. Variance analysis of frequency response function measurements using periodic excitations. *IEEE T Instrum Meas*, 54(4):1452–1456, 2005.
- T. Dobrowiecki and J. Schoukens. Measuring a linear approximation to weakly nonlinear mimo systems. *Automatica*, 43(10):1737–1751, 2007.
- M. Enqvist and L. Ljung. Linear approximations of nonlinear fir systems for separable input processes. *Automatica*, 41(3):459–473, 2005.
- P. Eykhoff. *System identification - parameter and state estimation*. John Wiley & Sons, 1974.
- A. Gelb and W. Vander Velde. *Multiple input describing functions and nonlinear system design*. McGraw Hill, 1968.
- D. George. Continuous nonlinear systems. *Technical Report MIT, USA*, 1959.
- F. Giri and E.-W. Bai, editors. *Block-oriented nonlinear system identification*. Springer, 1st edition, 2010.
- K. Godfrey, editor. *Perturbation signals for system identification*. Prentice Hall, 1993.

- I. Gradshteyn and I. Ryzhik. *Table of Integrals, Series and Products*. Academic Press, 6st edition, 2000.
- P. Guillaume, J. Schoukens, R. Pintelon and I. Kollár. Chrest-factor minimization using nonlinear Chebyshev approximation methods. *IEEE T Instrum Meas*, 40(6): 982–989, 1991.
- M. Heertjes, D. Hennekens and M. Steinbuch. Mimo feed-forward design in wafer scanners using a gradient approximation-based algorithm. *Control Eng Pract*, 18: 495–506, 2010.
- X. Jing. Frequency domain analysis and identification of block-oriented nonlinear systems. *J Sound Vib*, 330(22):5427–5442, 2011.
- X. Jing, Z. Lang, S. Billings and G. Tomlinson. The parametric characteristic of frequency response functions for nonlinear systems. *Int J Control*, 79(12):1552–1564, 2006.
- X. Jing, Z. Lang and S. Billings. Mapping from parametric characteristics to generalized frequency response functions of non-linear systems. *Int J Control*, 81(7):1071–1088, 2008a.
- X. Jing, Z. Lang and S. Billings. Output frequency response function-based analysis for nonlinear volterra systems. *Mech Syst Signal Pr*, 22(1):102–120, 2008b.
- X. Jing, Z. Lang, S. Billings and G. Tomlinson. Frequency domain analysis for suppression of output vibration from periodic disturbance using nonlinearities. *J Sound Vib*, 314(3-5):536–557, 2008c.
- X. Jing, Z. Lang and S. Billings. Parametric characteristic analysis for generalized frequency response functions of nonlinear systems. *Circ Syst Signal Process*, 28(5): 699–733, 2009a.
- X. Jing, Z. Lang and S. Billings. Determination of the analytical parametric relationship for output spectrum of volterra systems based on its parametric characteristics. *J Math Anal Appl*, 351(2):694–706, 2009b.
- X. Jing, Z. Lang and S. Billings. Output frequency properties of nonlinear systems. *Int J Nonlinear Mech*, 45(7):681–690, 2010.
- C. Johnson and R. Lorenz. Experimental identification of friction and its compensation in precise, position controlled mechanisms. *IEEE T Ind Applic*, 28(6):1392–1398, 1992.
- H. Khalil. *Nonlinear systems*. Prentice Hall, 2002.
- V. Lampaert, J. Swevers and F. Al-Bender. Modification of the leuven integrated friction model structure. *IEEE T Automat Contr*, 47(4):683–687, 2002.
- V. Lampaert, J. Swevers and F. Al-Bender. Comparison of model and non-model based friction compensation techniques in the neighbourhood of pre-sliding friction. In *Proc American Control Conference*, volume 2, pages 1121–1126, 2004.
- Z. Lang, S. Billings, R. Yue and J. Li. Output frequency response function of nonlinear Volterra systems. *Automatica*, 43(5):805–816, 2007.

- Z.-Q. Lang and S. Billings. Output frequency characteristics of nonlinear systems. *Int J Control*, 64(6):1049–1067, 1996.
- Z.-Q. Lang and S. Billings. Output frequencies of nonlinear systems. *Int J Control*, 67(5):713–730, 1997.
- Z.-Q. Lang and S. Billings. Evaluation of output frequency responses of nonlinear systems under multiple inputs. *IEEE T Circuits II*, 47(1):28–38, 2000.
- D. Langswierdt, N. Bouck and Y. Berbers. Architecture-driven development of embedded systems with acol. In *Proc IEEE International Symposium on Object/Component/Service-Oriented Real-Time Distributed Computing Workshops*, volume 2, pages 138–144, 2010.
- C. Lesiak and A. J. Krener. Existence and uniqueness of volterra series for nonlinear systems. *IEEE T Automat Contr*, AC-23(6):1090–1095, 1978.
- L. Li and S. Billings. Estimation of generalized frequency response functions for quadratically and cubically nonlinear systems. *J Sound Vib*, 330(3):461–470, 2011a.
- L. Li and S. Billings. Analysis of nonlinear oscillators using volterra series in the frequency domain. *J Sound Vib*, 330:337–355, 2011b.
- L. Li and S. Billings. Piecewise volterra modeling of the duffing oscillator in the frequency-domain. *Mech Syst Signal Pr*, 26(1):117–127, 2012.
- L. Ljung. *System identification, theory for the user*. Prentice Hall, 1999.
- N. Muhammad, Y. Vandewoude, B. Y. and S. van Loo. *New Advanced Technologies*, chapter Modelling Embedded Systems with AADL: A Practical Study. InTech, 2010.
- P. Nuij, O. Bosgra and M. Steinbuch. Higher-order sinusoidal input describing functions for the analysis of non-linear systems with harmonic responses. *Mech Syst Signal Pr*, 20(8):1883–1904, 2006.
- P. Nuij, M. Steinbuch and O. Bosgra. Experimental characterization of the stick/sliding transition in a precision mechanical system using the third order sinusoidal input describing function. *Mechatronics*, 18(2):100–110, 2008a.
- P. Nuij, M. Steinbuch and O. Bosgra. Measuring the higher order sinusoidal input describing functions of a non-linear plant operating in feedback. *Control Eng Pract*, 16(1):101–113, 2008b.
- P. Nuij, M. Steinbuch and O. Bosgra. Non-parametric identification of higher order sinusoidal output describing functions. In *Proc International Conference on Noise and Vibration Engineering*, pages 2361–2371, 2008c.
- A. Pavlov and N. van de Wouw. Fast computation of frequency response functions for a class of nonlinear systems. In *Proc Conference on Decision and Control*, pages 1180–1186, 2008.
- A. Pavlov, A. Pogromsky, N. van de Wouw and H. Nijmeijer. Convergent dynamics, a tribute to Boris Pavlovich Demidovich. *Syst Control Lett*, 52(3-4):257–261, 2004.
- A. Pavlov, N. van De Wouw and H. Nijmeijer. Convergent systems: analysis and synthesis. In *Lect Notes Control Inf Sci*, volume 322, pages 131–146, 2005.
- A. Pavlov, N. van de Wouw and H. Nijmeijer. *Uniform output regulation of nonlinear*

- systems - a convergent dynamics approach*. Systems and control: foundations & applications. Birkhauser, 2006.
- A. Pavlov, A. Pogromsky, N. van de Wouw and H. Nijmeijer. On convergence properties of piecewise affine systems. *Int J Control*, 80(8):1233–1247, 2007a.
- A. Pavlov, N. van de Wouw and H. Nijmeijer. Frequency response functions for nonlinear convergent systems. *IEEE T Autom Control*, 52(6):1159–1165, 2007b.
- A. Pavlov, N. Van De Wouw, A. Pogromsky, M. Heertjes and H. Nijmeijer. Frequency domain performance analysis of nonlinearly controlled motion systems. In *Proc. CDC*, pages 1621–1627, 2007c.
- J. Peyton Jones and S. Billings. Recursive algorithm for computing the frequency response of a class of non-linear difference equation models. *Int J Contr*, 50(5):1925–40, 1989.
- J. Peyton Jones and S. Billings. Interpretation of non-linear frequency response functions. *Int J Contr*, 52(2):319–46, 1990.
- J. Peyton Jones and S. Billings. Describing functions, volterra series and the analysis of non-linear systems in the frequency domain. *Int J Control*, 53(4):871–87, 1991.
- C. Philips, J. Parr and E. Riskin. *Signals, systems and transforms*. Prentice Hall, 2008.
- R. Pintelon and J. Schoukens. Measurement and modelling of linear systems in the presence of non-linear distortions. *Mech Syst Signal Pr*, 16(5):785–801, 2002.
- R. Pintelon, Y. Rolain, G. Vandersteen and J. Schoukens. Experimental characterization of operational amplifiers: A system identification approach - ii: Calibration and measurements. *IEEE T Instrum Meas*, 53(3):863–876, 2004a.
- R. Pintelon, G. Vandersteen, L. De Locht, Y. Rolain and J. Schoukens. Experimental characterization of operational amplifiers: A system identification approach - i: Theory and simulations. *IEEE T Instrum Meas*, 53(3):854–862, 2004b.
- R. Pintelon, J. Schoukens, G. Vandersteen and K. Barbe. Estimation of nonparametric noise and frf models for multivariable systems-part i: Theory. *Mech Syst Signal Pr*, 24(3):573–595, 2010a.
- R. Pintelon, J. Schoukens, G. Vandersteen and K. Barbe. Estimation of nonparametric noise and frf models for multivariable systems-part ii: Extensions, applications. *Mech Syst Signal Pr*, 24(3):596–616, 2010b.
- R. Pintelon, K. Barbé, G. Vandersteen and J. Schoukens. Improved (non-)parametric identification of dynamic systems excited by periodic signals. *Mech Syst Signal Pr*, 25(7):2683–2704, 2011a.
- R. Pintelon, G. Vandersteen, J. Schoukens and Y. Rolain. Improved (non-)parametric identification of dynamic systems excited by periodic signals, the multivariate case. *Mech Syst Signal Pr*, 25(8):2892–2922, 2011b.
- R. Pintelon and J. Schoukens. *System identification: a frequency domain approach*. Wiley-Blackwell, 2012.
- D. Rabijns, G. Vandersteen and W. Moer. An automatic detection scheme for periodic

- signals based on spectrum analyzer measurements. *IEEE T Instrum Meas*, 53:1433–1440, 2004.
- A. Ramasubramanian and L. Ray. Stability and performance analysis for non-model-based friction estimators. In *Proc American Control Conference*, pages 2929–2935, 2001.
- D. Rijlaarsdam, S. van Loon, P. Nuij and M. Steinbuch. Nonlinearities in industrial motion stages - detection and classification. In *Proc American Control Conference*, pages 6644–6649, 2010.
- D. Rijlaarsdam, P. Nuij, J. Schoukens and M. Steinbuch. Spectral analysis of block structured nonlinear systems and higher order sinusoidal input describing functions. *Automatica*, 47(12):2684–2688, 2011.
- D. Rijlaarsdam, P. Nuij, J. Schoukens and M. Steinbuch. Frequency domain based nonlinear feed forward control design for friction compensation. *Mech Syst Signal Pr*, 27(2):551–562, 2012a.
- D. Rijlaarsdam, T. Oomen, P. Nuij, J. Schoukens and M. Steinbuch. Uniquely connecting frequency domain representations of given order polynomial Wiener-Hammerstein systems. *provisionally accepted*, 2012b.
- M. Rudnaya, R. Mattheij and J. Maubach. Evaluating sharpness functions for automated scanning electron microscopy. *J Microscopy*, 240(1):38–49, 2010.
- M. Rudnaya, W. Van den Broek, R. Doornbos, R. Mattheij and J. Maubach. Defocus and twofold astigmatism correction in haadf-stem. *Ultramicroscopy*, 111(8):1043–1054, 2011.
- W. Rugh. *Nonlinear system theory: the Volterra / Wiener approach*. Johns Hopkins University Press, 1981.
- I. Sandberg. Mathematical foundation of associated expansions for mildly nonlinear systems. *IEEE T Circuits Syst*, CAS-30(7):441–455, 1983.
- M. Schetzen. *The Volterra and Wiener theories of nonlinear systems*. John Wiley & Sons, Inc., 1980.
- J. Schoukens and T. Dobrowiecki. Design of broadband excitation signals with a user imposed power spectrum and amplitude distribution. In *Proc IEEE Instrumentation and Measurement Technologie Conference*, volume 2, pages 1002–1005, 1998.
- J. Schoukens, T. Dobrowiecki and R. Pintelon. Parametric and nonparametric identification of linear systems in the presence of nonlinear distortions, a frequency domain approach. *IEEE T Automatic Contr*, 43(2):176–190, 1998.
- J. Schoukens, R. Pintelon, T. Dobrowiecki and Y. Rolain. Identification of linear systems with nonlinear distortions. *Automatica*, 41(3):491–504, 2005.
- J. Schoukens, Y. Rolain and R. Pintelon. Analysis of windowing/leakage effects in frequency response function measurements. *Automatica*, 42(1):27–38, 2006.
- J. Schoukens, J. Lataire, R. Pintelon, G. Vandersteen and T. Dobrowiecki. Robustness issues of the best linear approximation of a nonlinear system. *IEEE Trans Instrum Meas*, 58(5):1737–1745, 2009.

- J. Schoukens, R. Pintelon, G. Vandersteen and Y. Rolain. Design of excitation signals for nonparametric measurements on mimo-systems in the presence of nonlinear distortions. In *Proc International Instrumentation and Measurement Technology Conference*, pages 1–5, 2010.
- M. Schoukens, R. Pintelon and Y. Rolain. Parametric identification of parallel hammerstein systems. *IEEE T Instrum Meas Meas*, 60(12):3931–3938, 2011.
- K. Shanmugam and M. T. Jong. Identification of nonlinear systems in frequency domain. *IEEE T Aerosp*, 11(6):1218–1225, 1975.
- S. Skogestad and I. Postlethwaite. *Multivariable feedback control*. John Wiley & Sons, 2005.
- M. Stone. The generalized weierstrass approximation theorem. *Math Mag*, 21(4):167–184, 1948a.
- M. Stone. The generalized weierstrass approximation theorem. *Math Mag*, 21(5):237–254, 1948b.
- J. Swevers, F. Al-Bender, C. Ganseman and T. Prajogo. An integrated friction model structure with improved presliding behavior for accurate friction compensation. *IEEE T Automat Contr*, 45(4):675–686, 2000.
- A. Tejada and A. den Dekker. The role of poisson’s binomial distribution in the analysis of tem images. *Ultramicroscopy*, 111(11):1553–1556, 2011.
- A. Tejada, A. den Dekker and W. Van den Broek. Introducing measure-by-wire, the systematic use of systems and control theory in transmission electron microscopy. *Ultramicroscopy*, 111(11):1581–1591, 2011.
- T. Tjahjowidodo, F. Al-Bender, H. Van Brussel and W. Symens. Friction characterization and compensation in electro-mechanical systems. *J Sound Vib*, 308(3-5):632–646, 2007.
- D. Torfs, R. Vuerinckx, J. Swevers and J. Schoukens. Comparison of two feedforward design methods aiming at accurate trajectory tracking of the end point of a flexible robot arm. *IEEE T Contr Syst Tech*, 6(1):2–14, 1998.
- M. Tsai, I. Chiu and M. Cheng. Design and implementation of command and friction feedforward control for cnc motion controllers. *IEE Proc-D*, 151(1):13–20, 2004.
- K. Vanhoenacker, T. Dobrowiecki and J. Schoukens. Design of multisine excitations to characterize the nonlinear distortions during frf-measurements. *IEEE T Instr Meas*, 50(5):1097 – 1102, 2001.
- K. Vanhoenacker, J. Schoukens, J. Swevers and D. Vaes. Summary and comparing overview of techniques for the detection of non-linear distortions. In *Proce ISMA*, pages 1241–1255, 2002.
- V. Volterra. Sopra le funzioni che dipendono de altre funzioni. *Rend. R. Accademia dei Lincei 2 Sem*, pages 141–146 and 153–158, 1887.
- V. Volterra. *Theory of functionals and of integral and integro-differential equations*. Dover Publications Inc, 1959.
- K. Weierstrass. Über die analytische darstellbarkeit sogenannter willkürlicher func-

- tionen einer reellen veränderlichen. *Sitzungsberichte der Königlich Preussischen Akademie der Wissenschaften zu Berlin*, II:633 – 639 and 789 – 805, 1985.
- N. Wiener. Response of a nonlinear system to noise. Technical report, Radiation Lab MIT (restricted, declassified July 1946, no. PB-1-58087), 1942.
- N. van de Wouw and A. Pavlov. Tracking and synchronisation for a class of pwa systems. *Automatica*, 44(11):2909–2915, 2008.
- N. van de Wouw, H. Pastink, M. Heertjes, A. Pavlov and H. Nijmeijer. Performance of convergence-based variable-gain control of optical storage drives. *Automatica*, 44(1):15–27, 2008.
- V. Yakubovich. The matrix-inequality method in the theory of the stability of nonlinear control systems. *Avtomatika i Telemekhanika*, 25(7):1017–1029, 1964.
- R. Yue, S. Billings and Z.-Q. Lang. An investigation into the characteristics of nonlinear frequency response functions. part 1: Understanding the higher dimensional frequency spaces. *Int J Control*, 78(13):1031–1044, 2005a.
- R. Yue, S. Billings and Z.-Q. Lang. An investigation into the characteristics of nonlinear frequency response functions. part 2: New analysis methods based on symbolic expansions and graphical techniques. *Int J Control*, 78(14):1130–1149, 2005b.
- H. Zhang, S. Billings and Q. Zhu. Frequency response functions for nonlinear rational models. *Int J Control*, 61(5):1073–1097, 1995.
- Y. Zhang, G. Liu and A. Goldenberg. Friction compensation with estimated velocity. In *Proc IEEE ICRA*, volume 3, pages 2650–2655, 2002.
- K. Zhou, J. Doyle and K. Glover. *Robust and optimal control*. Prentice Hall, 1996.

Summary

Frequency Domain Based Performance Optimization of Systems with Static Nonlinearities

The widespread acceptance and applicability of frequency domain techniques for linear and time invariant systems has been an impetus for the extension of these methodologies towards nonlinear systems. However, although the application of frequency domain methods for the analysis, modeling and control of nonlinear systems can be advantageous it is generally not straightforward. This work contributes to this field by providing connections between different frequency domain methods for nonlinear systems using new analytical results with an application to spectral analysis of block structured systems. Furthermore, practically applicable results that allow frequency domain based performance optimization of nonlinear systems are presented.

The first part of the thesis deals with the analysis of nonlinear effects in the frequency domain. The contribution of this part is twofold: First, a comparative literature review and new analytical results are used to connect different, existing frequency domain methods for nonlinear systems. Second, new analytical results are presented that allow spectral analysis of parallel polynomial Wiener-Hammerstein systems. This yields insight in the mechanism that generates nonlinear effects in the frequency domain and provides a numerically efficient method to compute these effects.

In the second part of the thesis, a novel frequency domain based approach for detection, quantification and optimal compensation of performance degrading nonlinear effects is presented. It is shown that a frequency domain representation of the input-output dynamics yields a well defined notion of performance for a class of nonlinear systems. This allows to detect nonlinear effects and optimally design static nonlinear compensators minimizing the effects of performance degrading nonlinearities, based on output measurements only, without requiring models of the nonlinearity and other system dynamics. For Lur'e systems, necessary and sufficient conditions for optimal performance are provided, based on a spectral representation of the systems output. Finally, the approach is shown to be effective in an industrial case study of frequency domain based optimal friction compensation in a transmission electron microscope.

Samenvatting

Frequency Domain Based Performance Optimization of Systems with Static Nonlinearities

Frequentie domein methoden zijn populair voor de analyse van linear en tijds-invariante systemen. De toepasbaarheid en brede acceptatie van deze methoden in de praktijk is een drijvende kracht voor het toepassen van dergelijke methoden op niet lineaire systemen. Hoewel het gebruik van frequentie domein methoden voor niet lineaire systemen voordelig kan zijn is een dergelijke uitbreiding niet triviaal. Dit werk draagt hieraan op twee manieren bij. Ten eerste wordt een vergelijkend overzicht gegeven van bestaande technieken en wordt een frequentie domein analyse van systemen met polynomiale niet lineariteiten gepresenteerd. Ten tweede wordt een praktisch georiënteerde methode geïntroduceerd waarmee de prestatie van niet lineaire systemen in het frequentie domein in kaart gebracht en geoptimaliseerd kan worden.

In het eerste deel van het proefschrift wordt de analyse van niet lineariteiten in het frequentie domain besproken. Deze bijdrage bestaat uit een vergelijkend overzicht van bestaande methoden en een analyse van polynomiale niet lineariteiten in het frequentie domein. Ten eerste worden bestaande methoden in een consistente notatie geïntroduceerd wat een onderling vergelijk mogelijk maakt. Daarnaast wordt een frequentie domein analyse van Wiener-Hammerstein systemen met polynomiale niet lineariteiten gepresenteerd. Hieruit volgt hoe deze niet lineariteiten zich manifesteren in het frequentie domein wat leidt tot numerieke methoden om deze effecten te berekenen.

Het tweede deel van het proefschrift behelst de prestatie van niet lineaire systemen. Het wordt duidelijk dat frequentie domein methoden het mogelijk maken om prestatieverminderende niet lineaire effecten te detecteren, quantificeren en te compenseren. Dit leidt tot de definitie van een nieuwe prestatie maat en het ontwerp van niet lineaire compensatoren die deze optimaliseren. Voor Lur'e systemen wordt tevens aangetoond dat frequentie domein analyse een meetbare, noodzakelijke en voldoende voorwaarde levert voor optimale prestatie. Tenslotte wordt in een experimentele studie van een elektronen microscoop aangetoond dat deze technieken effectief zijn voor optimale compensatie van prestatieverminderende effecten (wrijving) in de praktijk.

Dankwoord

Aan het tot stand komen van een proefschrift dragen veel mensen bij. Gedurende de afgelopen vier jaar heb ik met veel inspirerende mensen aan twee verschillende universiteiten mogen werken en heb ik me altijd gesteund geweten door vrienden en familie. Daarom zou ik op deze plek graag een aantal mensen speciaal willen bedanken.

Allereerst mijn promotoren en copromotor. Maarten, bedankt voor alle vrijheid en mogelijkheden die je binnen jouw groep biedt. Zowel de vrijheid in het onderzoek als de mogelijkheden om veel te reizen en een jaar in Brussel door te brengen, zijn mijn promotietraject zeker ten goede gekomen. Daarnaast aan Johan veel dank voor de mooie tijd in Brussel en je kritische en inhoudelijke blik. De kans om de kennis en ervaring bij ELEC te mogen combineren met de kennis en kunde in Eindhoven heeft in belangrijke mate bijgedragen aan dit proefschrift. Als laatste dank aan Pieter voor je enthousiasme, realistische visie en leerzame input op experimenteel gebied.

Dank voor alle gezelligheid en de boeiende discussies aan mijn collega's in Eindhoven en Brussel en speciaal aan mijn kamergenoten: Wojtek, Ebrahim, Anna, Diane, Ludwig, John, Maarten, Sinan, Tom en Rik. Dank aan Nathan voor de leerzame discussies, aan Simon voor de gezellige lunches en aan Tom voor de samenwerking en de L^AT_EX-stijl die aan dit proefschrift ten grondslag ligt. Dank ook aan de partners binnen het Condor project en aan FEI Company voor de experimentele opstelling. Furthermore, I would like to thank my students: Bas, Vincent, Andrei and Chris for our collaboration and their contribution to the results presented in this thesis. Finally, I would like to thank Alina, for her contribution to the results presented in Chapter 5.

Als laatste dank aan mijn familie. Aan mijn ouders, Anne en Henriëtte, voor jullie steun, vertrouwen, interesse en het creëren van de mogelijkheden die tot dit promotietraject hebben geleid. Aan mijn grootouders, Jan en Tan voor alle gastvrijheid en gezelligheid sinds wij in Eindhoven wonen. Dank ook aan mijn paranimfen, Martin en Anne Fleur, voor alle mooie momenten en de bijdrage aan de voorbereiding van de verdediging. Daarnaast dank aan Sonja en Djoya voor het omslagontwerp. Als laatste veel dank aan Sonja voor alle steun, liefde, interesse en het lezen van alle artikelen en het proefschrift. Als er een tweede auteur op dit proefschrift mocht staan, was jij het.

David Rijlaarsdam, juni 2012

List of Publications

Book Chapters

- A. Pogromski, D. Rijlaarsdam and H. Nijmeijer, Experimental Huygens synchronization of oscillators, in *Nonlinear dynamics and chaos: advances and perspectives*, Editors: M. Thiel, J. Kurths, M. Carmen Romano, A. Moura, G. Karolyi, 195-209, Springer, Book chapter, 2010
- D. Rijlaarsdam, A. Pogromski and H. Nijmeijer, Synchronization between coupled oscillators: an experimental approach, in *Dynamics and Control of Hybrid Dynamical Systems*, Editors: G. Leonov, H. Nijmeijer, A. Pogromsky, A. Fradkov, 153-164, World Scientific Publishing Company, Book chapter, 2010

Refereed Journal Publications

- A. Setiadi, D. Rijlaarsdam, P. Nuij and M. Steinbuch, Frequency domain based real-time performance optimization of Lur'e systems, *submitted, under review*
- D. Rijlaarsdam, A. Setiadi, P. Nuij, J. Schoukens and M. Steinbuch, Frequency domain based nonlinearity detection and compensation in Lur'e systems, *submitted, under review*
- M. Rijlaarsdam, D. Rijlaarsdam, L. Dorssers, A. Gillis and L. Looijenga, miMsg: an unbiased target enrichment algorithm for predicted miR-mRNA interactions based on matched expression data, *submitted, under review*
- D. Rijlaarsdam, T. Oomen, P. Nuij, J. Schoukens and M. Steinbuch, Uniquely connecting frequency domain representations of given order polynomial Wiener Hammerstein systems, *provisionally accepted*
- D. Rijlaarsdam, P. Nuij, J. Schoukens and M. Steinbuch, Frequency domain based nonlinear feed forward control design for friction compensation, *Mechanical Systems and Signal Processing*, 27(2):551-562, 2012
- D. Rijlaarsdam, P. Nuij, J. Schoukens and M. Steinbuch, Spectral analysis of block structured nonlinear systems and higher order sinusoidal input describing functions, *Automatica*, 47(12):2684-2688, 2011

Refereed Proceedings

- D. Rijlaarsdam, P. Nuij, J. Schoukens and M. Steinbuch, New connections between frequency response functions for a class of nonlinear systems, In *Proc IFAC Symposium on System Identification*, Brussels, Belgium, 2012
- D. Rijlaarsdam, P. Nuij, J. Schoukens and M. Steinbuch, Spectral analysis of block structured nonlinear systems, In *Proc IFAC World Congress*, Milan, Italy, page 4416-4421, 2011
- D. Rijlaarsdam, P. Nuij, J. Schoukens and M. Steinbuch, Frequency domain based friction compensation, industrial application to transmission electron microscopes, In *Proc American Control Conference*, San Francisco, United States, page 4093-4098, 2011
- D. Rijlaarsdam, S. van Loon, P. Nuij and M. Steinbuch, Nonlinearities in industrial motion stages - detection and classification, In *Proc American Control Conference*, Baltimore, United States, page 6644-6649, 2010
- D. Rijlaarsdam, V. van Geffen, P. Nuij, J. Schoukens and M. Steinbuch, Frequency domain based feed forward tuning for friction compensation, In *Proc ASPE Spring Topical Meeting*, Boston, United States, page 129-134, 2010
- D. Rijlaarsdam, A. Pogromski and H. Nijmeijer, Synchronization between coupled oscillators: a uniform experimental approach, In *Proc EUROMECH Non-linear Dynamics Conference*, St. Petersburg, Russian Federation, digital copy, 2008
- D. Rijlaarsdam, I. Tyukin, H. Nijmeijer, A. Semyanov and C. van Leeuwen, Qualitative modeling of neuronal behavior effects of diffusion, In *Proc International Scientific Conference on Physics and Control*, Potsdam, Germany, digital copy, 2007
- D. Rijlaarsdam and V. Mladenov, Synchronization of chaotic cellular neural networks based on Rössler cells, In *Proc Seminar on Neural Network Applications in Electrical Engineering*, Belgrade, Serbia, page 41-43, 2006

Curriculum Vitae

David Rijlaarsdam was born on December 31st, 1982 in Leiden, The Netherlands.

- 1995 - 2002 Secondary school, Northgo College, Noordwijk.
- 2002 - 2008 Master of Science in Mechanical Engineering, Eindhoven University of Technology, graduated *cum laude*, including
 - 2006 Internship at RIKEN Brain Science Institute, Tokyo, Japan;
 - 2008 Graduation project on 'Huygens synchronization in various dynamical systems'.
- 2008 - 2012 Ph.D. candidate at the Eindhoven University of Technology, department of Mechanical Engineering, Control Systems Technology group and at the Vrije Universiteit Brussel, department of Fundamental Electricity and Instrumentation.